EPFL

Thèse n° 8487

Capacitive sensor to monitor the level of drug inside an injector pen

Présentée le 19 novembre 2021

Faculté des sciences et techniques de l'ingénieur
Groupe SCI STI CD
Programme doctoral en microsystèmes et microélectronique

pour l'obtention du grade de Docteur ès Sciences

par

Sylvain Paul Fernand JOLY

Acceptée sur proposition du jury

Dr J.-M. Sallese, président du jury
Prof. C. Dehollain, Dr A. P. G. Lepple-Wienhues, directeurs de thèse
Dr N. Butterlin, rapporteuse
Prof. M. Green, rapporteur
Dr J.-M. Vesin, rapporteur

École polytechnique fédérale de Lausanne

2021

Acknowledgements

I want to thank Prof. Catherine Dehollain and Dr Albrecht Lepple-Wienhues who, firstly, encouraged me to engage in doctoral study and gave me the opportunity to do this thesis work between the industrial and research worlds. Then, for their advice, their support, and the time they spent helping me. It was a real pleasure to exchange and develop the smart pen cap together. I want also to thank the members of the jury, the Committee president Prof. Jean-Michel Sallèse, the internal reporter Dr Jean-Marc Vesin, and the external reporters Dr Nadia Butterlin and Prof. Michael M. Green for the times they spent to read and evaluate this document and this PhD work. I would like to thank Rainer Platz, Gaëtan Boulard and Christine Aubert for their help and having allowed this great experience of doing this doctorate in Valtronic Technologies.

I would like to thank my colleagues and former colleagues who worked on this project: Dr Matteo Simonicini, Dr Jean Baptiste Orhan, Alexis Pokorny, Younouss Faye, Julien Magnin Feysot, Antoine Genouel, Brice Marty and Dr Thomas Glanzmann, who shared a part of this adventure to develop this innovative device. This work would not be possible without them. To Guillaume Marceau, Thimotée Guillemot, Jeremy Bir, Alexandre Klaey, Jean Marc Marmy, Sylvain Huguenin and all other colleagues, discussion and work together on other interesting projects gave me some insight for this work and allowed me to develop my knowledge and methodology on other topics.

I would like to thank my friends, the “Belfort” and “Le Russey” teams who encouraged me and for the good time that we had together. Finally, I thank my parents, Robert Joly, Arielle Bron-Joly, my sister Angie Joly, my brother-in-law Lucas Joyeux and my parents-in-law Fabienne Richter and Olivier Schneider for their support, the trust they have on me and the time they babysitted my daughter to allow me focusing on the thesis redaction.

I finally dedicated my thesis to my beloved wife Adèle Richter-Joly who supported me at any time, encouraged me during instants of doubt and for her patience. To my daughter Margot Joly who illuminated my days and motivated me to go to the end of this project during challenging moments.

Lausanne, the 26th July 2021

Abstract

Diabete is a disease which is spreading faster than ever, impacting now a larger population. Patients suffering from this disease need the injection of insulin to control extracellular sugar levels. Pharmaceutical companies developed injector pens to allow patients to inject themself the right amount of drug. But the dosage depends on many parameters as the previous meal, current blood sugar level… and a wrong dosage can lead to health problem e.g., loss of conciousness at short terms and severe diseases like cardiac pathologies at long terms… To prevent these situations, a smart pen cap has been developed at Valtronic Technologies to follow and log the individual injections by measuring the level of drug in the pen, the temperature, and the relative humidity to allow the patient and the medical staff to have an history of the injections and the climatic conditions.

Injector pen and smart pen cap have been firstly presented with a non-exhaustive list of different physics which can be used to measure a level of liquid. For need of precision, the capacitance technique is the best technology choice. Therefore, the smart pen cap is based on a capacitive sensor. Different capacitance converter topologies have been compared through a bibliographic study. It appears that the Lock-in converter gives the best sensitivity and Charge Sensitivity Amplifier has the lowest power consumption. A trade-of was to use a capacitance-to-digital-converter with ΣΔ topology. A chip from Analog device® has been selected due to its high resolution below the femto-farad level, its simple interface and its availability on the market which allows a fast development and industrialisation. Then, switch and electronic structure are presented. First tests with an empty device have been conducted to find the noise floor, which is below 0.1fF.

Subsequently, a study of different electrodes configuration has been performed. Firstly, an analysis on two parallel flat electrodes has been conducted using theoretical and simulation approaches. Then, two semi-cylindrical electrodes have been analysed. A comparison has been made between two theoretical methods which are: considering an infinite number of parallel flat electrodes following the shape of the semi-cylindrical electrodes and the conformal mapping methods. This last method gives coherent results when comparing real measurements and simulation. The device is equipped with semi-cylindrical electrodes which allow for a small package and a good correlation between capacitance and drug level with a convertion slope of 0.5fF/µL. Tests have been performed which give an error of ± 1 IU and ± 4 IU for large injection (set point equal to 72 IU).

Finally, the study of some parasitic effects is presented in the last section. An important effect is the climatic effect which affects the capacitance due to variation of electric permittivity linked to temperature change and water absorption of certain materials as plastics. To compensate for this effect, reference electrodes and a climatic sensor have been implemented. Another important effect comes from the cartridge position in the non-uniform electric field of the smart pen cap. A four electrodes device has been realized to allow a perpendicular rotation of the electric field to obtain a more constant averaged electric field. As a consequence, the position impact of the cartridge has been reduced. Other effects like external perturbation on the electric field, bubbles, discrepancy between the injected and remaining volume and manufacturing tolerance have been considered. Considering these parasitic effects, the device can detect a minimum injection of 52µL.

Keywords

Capacitive sensor, injector pen, diabetes, smart pen cap, capacitance, electrodes, parasitic effects, conformal mapping

Résumé

Le diabète est une maladie en forte progression touchant dorénavant un plus large public. Les patients souffrant de cette pathologie doivent s'injecter de l'insuline afin d'être capable d'absorber le sucre. Afin de faciliter les injections d'insuline, les compagnies pharmaceutiques ont développé des stylos auto-injecteurs avec des doses prédifinies. Malheureusement, la quantité d'insuline dépend de nombreux paramètres, comme par exemple, le type d'aliments ingérés, le temps ecoulé depuis leur ingestion et le niveau de sucre dans le sang… Un mauvais dosage peut conduire à des problèmes de santé variés : à court terme, des évanouissements et à long terme, des pathologies plus lourdes comme des problèmes cardiaques ou de circulation sanguine. Un capuchon de stylo injecteur a donc été développé afin de suivre et enregister le niveau d'insuline restant au sein du stylo injecteur. Il enregistre également les conditions climatiques que ce dernier subit. Tout cela afin de faciliter le suivi du traitement médical par le patient et le personnel soignant.

Ce capuchon de stylo intelligent est doté d'un capteur capacitif. Une étude bibliographique étudiant plusieurs topologies de convertisseur de capacité electrique a été réalisé. Les meilleures résolutions peuvent être obtenues via un convertisseur à topologie « lock-in detection ». À l'opposé, les convertisseurs ayant les meilleures performances en termes de consommation d'énergie sont les convertisseurs basés sur une topologie de « Charge Sensitivity Amplifier ». Un convertisseur capacitance vers digital de type ΣΔ fabriqué par Analog Device® permet une haute résolution, en dessous du femto-farad, est facilement interfaçable et avec une grande disponibilité sur le marché. Cela permet un développement et une industrialisation rapide. Pour finir, des interrupteurs pilotables et la structure électronique sont présentés. Des premiers tests ont été réalisés avec un dispositif à vide afin d'obtenir le plus bas niveau de bruit possible, ce dernier étant inférieur à 0.1fF.

Ensuite, une étude sur les différentes configurations d'électrodes a été menée. Une premiere approche theorique et de simulation a été réalisée avec deux électrodes plates parallèles. Puis une seconde étude a été menée sur deux électrodes semi-cylindriques qui permettent d'atteindre de meilleure performance. Deux méthodes theoriques ont été comparées. La première considére que la capacité totale est égale à la somme d'une infinité de capacités parallèles dont les électrodes plates suivent la forme cylindrique du capuchon. L'autre méthode s'appuie sur une méthode mathématique permettant de transformer les électrodes incurvées en électrodes plates en utilisant des transformées conformes. Cette dernière methode donne des résultats équivalent aux simulations et aux tests. Finalement, le dispositif est equipé d'électrodes semi-cylindriques qui permettent de développer un système avec un faible encombrement et une bonne intéraction entre la variation de capacité et le niveau d'insuline. Le facteur de conversion relevé est de 0.5fF/µL. Des tests ont été réalisés donnant une erreur moyenne de ± 1 IU et ± 4 IU pour les grandes injections (injection de 72 IU).

Une étude de plusieurs effets parasites est présentée dans le dernier chapitre. L'un des plus important étant l'impact des variations climatiques sur la capacité. Des électrodes de référence ainsi qu'un capteur climatique ont été implémentés afin de compenser les variations de températures et d'humidité relative. Un autre effet indésirable important est la position de l'ampoule d'insuline dans le champ électrique du capuchon de stylo inteligent. Pour compenser cet effet, un dispositif avec quatre électrodes permet un changement d'orientation du champ electrique. Cela crée un champ electrique moyen plus constant et permet d'atténuer les effets dus à la position de l'ampoule dans le capuchon. D'autres effets ont été considérés comme l'effet du champ électrique extérieur au dispositif sur la capacité et l'utilité d'un blindage. L'effet des bulles, l'erreur entre le volume injecté et le volume restant dans le stylo, et l'impact des tolérances de fabrication ont également été présentés. En considérant ces effets parasites, le dispositif est capable de détecter une injection minimale de 52µL.

Mots-clés

Capteur capacitif, stylo injecteur, diabètes, capuchon de stylo intelligent, capacitance, électrodes, effets parasites, transformé conforme

Contents

List of Figures

List of Tables

List of symbols

AC: Alternating Current

ASIC: Application Specific Integration Circuit

BLE: Bluetooth Low Energy

CDC: Capacitance to Digital Converter

CSA: Charge Sensitivity Amplifier

CTI: Commission pour la Technologie et l'Innovation

DC: Direct Current

ENOB: Effective Number Of Bits

EPFL : Ecole Polytechnique Fédérale de Lausanne

ESD: Electro-Static Discharge

FOM: Figure Of Merit

I^2C: Inter-Integrated Circuit

IU: International Unit (of Insulin: equivalent to 10µL of water volume)

LDO: Low Drop Out (voltage regulator)

LID: Lock-In Demodulator

MCU: Micro-Controller Unit

MEMS: MicroElectroMechanical Systems

PCB: Printed Circuit Board

PCBA: Printed Circuit Board Assembled

PWM: Pulse Width Modulation

RF: Radio-Frequency

RFID: Radio-Frequency IDentification

SAR: Successive Approximation Recursive (Converter)

SNR: Signal Noise Ratio

SPDT: Single Pole, Double Throw

SPICE: Simulation Program with Integrated Circuit Emphasis

TIA: Trans-Impedance Amplifier

UART: Universal Asynchronous Receiver Transmitter

UV: Ultra-Violet

Introduction

Some diseases need treatments with daily injections, and sometimes, multiple injections per day. This is restrictive for the patient, who needs to pay attention to inject the right amount of drug at the right time. This thesis will focus on diabetes because this is an important disease. In 2014, 422 million people had diabetes in the world [1]. This is 108 million people more than in 1980, indicating that this disease is getting more and more frequent. In 2012, 1.5 million people directly died due to this pathology and another 2.2 million people died due to the consequences of too high blood glucose concentration. The cost of diabetes for the society is estimated in 2016 at 833 Billion $US/ year and that figure has tripled between 2003 to 2013. According to estimation of the International Diabetes Federation (IDF), the number of adults who suffer from diabetes will increase by 51% from today to 2045 with a large impact in Africa and middle east areas. The World Health Organization estimates the cost of diabetes at 1.7 trillion $US in 2030 [1]. So, it is important to create device to limit the impact of this disease and facilitate the life of patients.

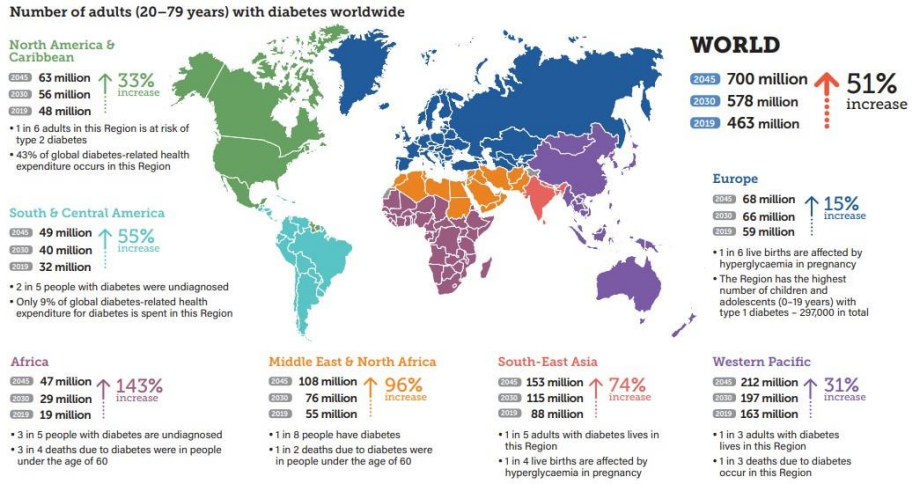

Figure 1: Prevalence of diabetes [2]

People who suffer from diabetes have difficulties to regulate blood glucose concentration due to metabolic problems caused by insulin which is the sugar's regulatory hormone. Two main types of diabetes exist [3]:

- Type 1 diabete is an autoimmune disease where the immune system attacks beta cells in the pancreas causing the loss of insulin production in the body. This often occurs already at young age and, if not treated with insulin, leads to death. People with type 1 diabetes need daily insulin injections to keep their blood glucose levels in a survivable range. Together with the related latent autoimmune diabetes in adults this represents about 15-20 % of diabetes cases [4, 5].
- Type 2 diabete is an insulin resistance developed by the body, which is closely linked to obesity. The insulin production in the pancreas' beta cells cannot keep up with the demand of a large volume of fat tissue. Type 2 diabetes is most commonly seen in older adults but is increasingly seen in children and younger adults owing

to rising levels of obesity, physical inactivity and inappropriate diet. The treatment starts generally with oral drugs and as the disease progresses, people need to inject GLP-1 or insulin or both.

To compensate this lack of insulin, patients need to inject themselves synthetic insulin. Thanks to injection pens, this task has become easier and people can live in a more normal manner. They just need to take with them the injector pen [6].

But some problems still exist with these injector pens. The main issue is that it is difficult to calculate the correct dose because this depends on many parameters [7]:

- Past parameters
  - When was the time of the last lunch? And what was the type of food?
  - When was the last injection? What dose was injected? What type of insulin was injected (fast or slow insulin)?
- Present parameter
  - Using a glucometer, what is the blood sugar level?
- Future parameter
  - What will be planned after the injection (e.g., staying at home or doing some sport)?

Many patients frequently fail to administer their required correct doses. Reasons given include: too busy (19%), travelling (16%), skipped meal (15%), stress or emotional problems (12%), embarrassing to inject in public (10%), challenging to take it at the same time every day (9%), forgot (7%), too many injections (6%), avoid weight gain (4%), regimen is too complicated (3.8%), and injections are painful (3%) [8]. Patients are routinely overwhelmed with this complicated self-therapy [9]

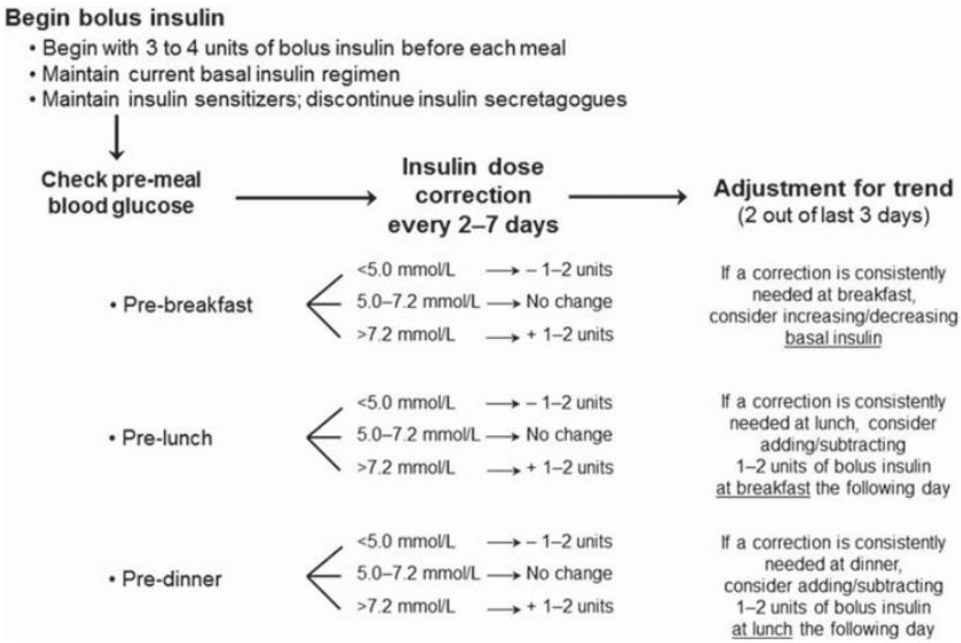

Figure 2: Exemple of the complex process to determine insulin dose [10]

If the patient performs a mistake when injecting the insulin, he can suffer from:

- Hyperglycemia: If the insulin dose is too low, the elevated blood sugar is poisoning the body. Causes include under-dosing, omitted shots, injector pen malfunction (bubbles or clogged needles…), excessive carbohydrate

intake, lack of exercise etc. This condition results in long-term vascular damage and long-term injuries. If the blood sugar runs extremely high, patients may enter a potentially deadly ketoacidotic coma [11]

- Hypoglycemia: This can be caused by too high dose, wrong insulin used, too little carbohydrate eating, etc. The potential life-threatening situation causes seizures, unconsciousness, and accidents. Many hypoglycemia events may not be correctly recognized. 100'000 admissions per year to emergency services are due to insulin-induced hypoglycemia in the US only, a potentially deadly effect of self-injection errors [12].

To respond at these different challenges, a device has been developed in the frame of this PhD thesis to follow the quantity of drug inside the injector pen, the timestamp of each injection and the ambient temperature and relative humidity. Utilizing these data, the patient and the medical staff can know if the right drug amount has been ejected at the right times and if the drug has been stored in appropriate condition. This device is presented in Figure 3, it is the white part which is called "Smart pen Cap" [13].

Figure 3: Insulin pen and Smart pen cap (white part)

In this thesis, the first part in Chapter 1 will focus on the device and the technics to measure the level of drug inside the injector pen, with a special focus on the capacitive measurement technics. The second part, Chapter 2, will deal with the shape of the electric field to find the best compromise between the electrode shape and the interaction between the electric field and the liquid level. The last part, Chapter 3, will focus on different parasitic effects and their impact on the measurement. Then the thesis conclusion and some improvement idea for future iteration of prototypes will be presented.

Chapter 1. Device and Measurement methods

1.1 Chapter introduction

In this chapter, the principle to measure the volume of drug will be discussed and the electronic design used in the current prototype will be presented. The user requirements for this device are that it shall have a small footprint to be easily transportable, low power consumption to have a long lifetime before replacing batteries, able to measure an injection of a single dose of drug and connectable easily with a smartphone. It is possible to imagine that in the future the data acquired by the smart pen cap can be used with glucometer, smartwatch… to provide a personalized and preventive healthcare by adapting the best posology to the different physiological variables.

Firstly, the injector pen will be presented with a focus on its functional blocks and a quick description of the different parts. This work will be done especially on the insulin injector pen which is able to inject 1 International Unit (IU) of insulin which corresponds to 10 µL of drug. Secondly, the smart pen cap device will be presented, with an overview of three main electronic blocks. After that, a discussion on the chosen technology to measure a level of liquid will be addressed by comparing different physical principles. The following section will deal with a non-exhaustive bibliographic study on capacitance measurement techniques with a comparison of ten different mainstream topologies. Then, a quick overview of the different electronic switches used during the prototype development will be done. Finally, measurement of the empty device will be presented to observe the steady-state noise.

1.2 Injector pen presentation

There are different injector pens manufactured by several pharmaceutical companies containing various drugs (Insulin, Growth hormones…). The drug is contained in a glass cartridge and should be stored generally in a fridge to preserve the drug efficiency. Different types of injector pen exist:

- single injection pen as adrenalin injector,
- cartridge replaceable single injection pen,
- multi-injection pen typical for insulin pens [14]
- replaceable-cartridge multi-injection pen also currently used for insulin pen [15].

In [16], an ensemble of different insulin injector pens is presented. The injection pen used in this work is a multi-injection prefilled insulin pen. An overview of the parts composing an injector pen is presented in Figure 4. By considering that 1 IU of insulin corresponds to 0.0347mg of human insulin [17, 18], the dilution factors commonly used in injector pen is U100, therefore 1 IU correspond to 10 µL of drug. The studied injector pen has these following physical characteristics:

- Inner diameter of the cartridge: 10 mm
- Water column length in the full cartridge: 23 mm
- Volume of water / drug solution: 3 mL

The volume of drug is larger than the possible injection volume because the plunger will not go to the end of the cartridge. The cartridge has in one side a septum which allow a part of the needle to penetrate inside the cartridge. At the opposite end of the cartridge, a plunger seals the drug compartment. This cartridge is maintained in position inside a cartridge holder, one side by holding the edge of the septum and in the other end, the plunger is maintained compressed by a spindle which is mechanically connected to the dose set knob.

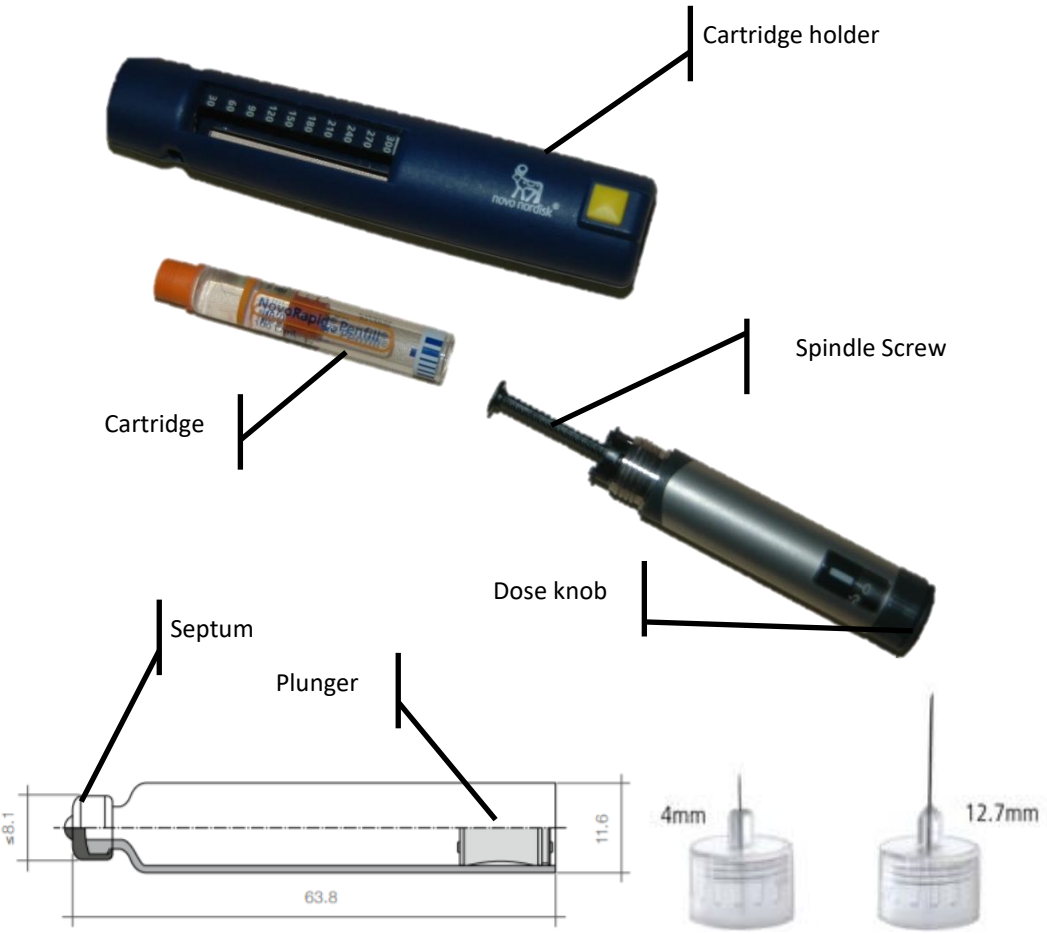

Figure 4: Injector pen [19], cartridge [14] and needle [20] example

The patient must follow certain steps when he uses the pen. Firstly, removing the injector pen from the fridge 30 minutes before injection to let the drug to reach the ambient temperature to prevent injection pain. Then, a priming step shall be done by snapping the pen with the septum up to move bubbles at the needle end. Then pressurize the cartridge by setting one dose on the knob and finally inserting gently the needle to remove air bubbles inside the cartridge. Finally, the patient can set the right dose and inject himself by changing at each injection the body area of injection to prevent pain and injury by multiple injections at the same place.

1.3 Technologies choices

Figure 5: Nilomètre [Source : Réjean Jobin]

Measuring a level of liquid is an ancient problem. Already in antiquity the level of the rivers was followed to know the water resources availables by visualising the level of known reservoirs near the river as presented in Figure 5. In the modern age, in 1831, Henry Palmer developed the first automatic level logger on paper for the Tamise [21]. Nowaday, different technologies exist, and the technical choice will be led by the application requirement which are:

- Embedded: The device shall have a low footprint and low power consumption to be portable
- No contact with liquid: the device shall prevent any contamination of the sterile drug
- Orientation independence: the device shall be able to precisely measure a volume of liquid inside the injector pen in any direction compared to gravity
- Low cost: The device should be not expensive to easily distribute it and be reusable many times
- Type of liquid: The device shall be able to detect the type of liquid by a physical property of the liquid as the volumic mass or electric permittivity.

In Table 1, different volume measurement technics have been compared by using the previous criteria needed for the Smart Pen Cap. Here is a small description of each technic

- Weight: it measures the mass of known container using the gravity, and by knowing the volumic mass of the liquid, it is possible to precisely know the quantity of liquid. It will be chosen as a gold standard method by using a pharmaceutical precision scale with a precision at 0.1 mg.
- Hydrostatic: it uses the pressure applied on an immerged device at a known level. The pressure measured by this kind of device will be directly impacted by the height of the liquid above the device.
- Plunger: it consists to measure a level of liquid by placing a device floating at the surface of the liquid and measuring the distance between the plunger and a fixed reference. This technic has been used by Henry Palmer.
- Waves: it consists to send a wave (acoustic or light) and observe the reflection area, which can be done by interferometers or counting the flying time of the wave.
- Capacitance: it uses the variation of capacitance which depends on the electrode areas and the relative electric permittivity ratio between air, which is equal to 1, and the liquid, here considered as water, which is close to 80 (depending on the temperature). This method seems best suited to the requirement, for its orientation independence and permeation of pen and drug container by the electric field without contacting the drug.

Table 1 : Liquid level measurement technics comparison

	Weight	*Hydrostatic*	*Plunger*	*Waves*	*Capacitance*
Embedded	No	No	No	Yes	Yes
No Contact	Yes	No	No	Yes	Yes
Orientation independence	No	No	No	Yes	Yes
Low cost	Yes	Yes	Yes	No	Yes
Type of liquid	No	No	No	Yes	Yes

.

1.4 Smart pen cap overview

The smart pen cap can be split in three functioning main parts which are:

- **The measurement unit**, which can be split in two sub-parts.
  - The circuitry, which consists to a Capacimeter, switches and climatic sensor will be presented in the next sub-sections.
  - The electrode geometry and the electric field shape will be introduced in section Chapter 2. The third chapter will deal with parasitic effects and solutions to compensate them will be presented.
- **The control and wireless communication unit** drives the device and provides information to the user. A Cypress Semiconductor® System On chip Micro-Controller Unit (MCU) combined with Bluetooth low energy (V4.2) has been used to communicate wirelessly with the smartphone. It drives the capacitance to digital converter (CDC), switch and climatic sensor using Inter-Integrated Circuit (I^2C) protocol. It can optimize power consumption by switching the device in low power when required. An autonomy of 6 months can be reached using that device.
- **The power unit** is composed by two 3 V cells coin CR2032 in series, then a 3.3 V low drop-out voltage regulator (LDO) controls the voltage and prevent Electro-Magnetic Interference perturbation compared to the use of a Buck oscillator regulator.

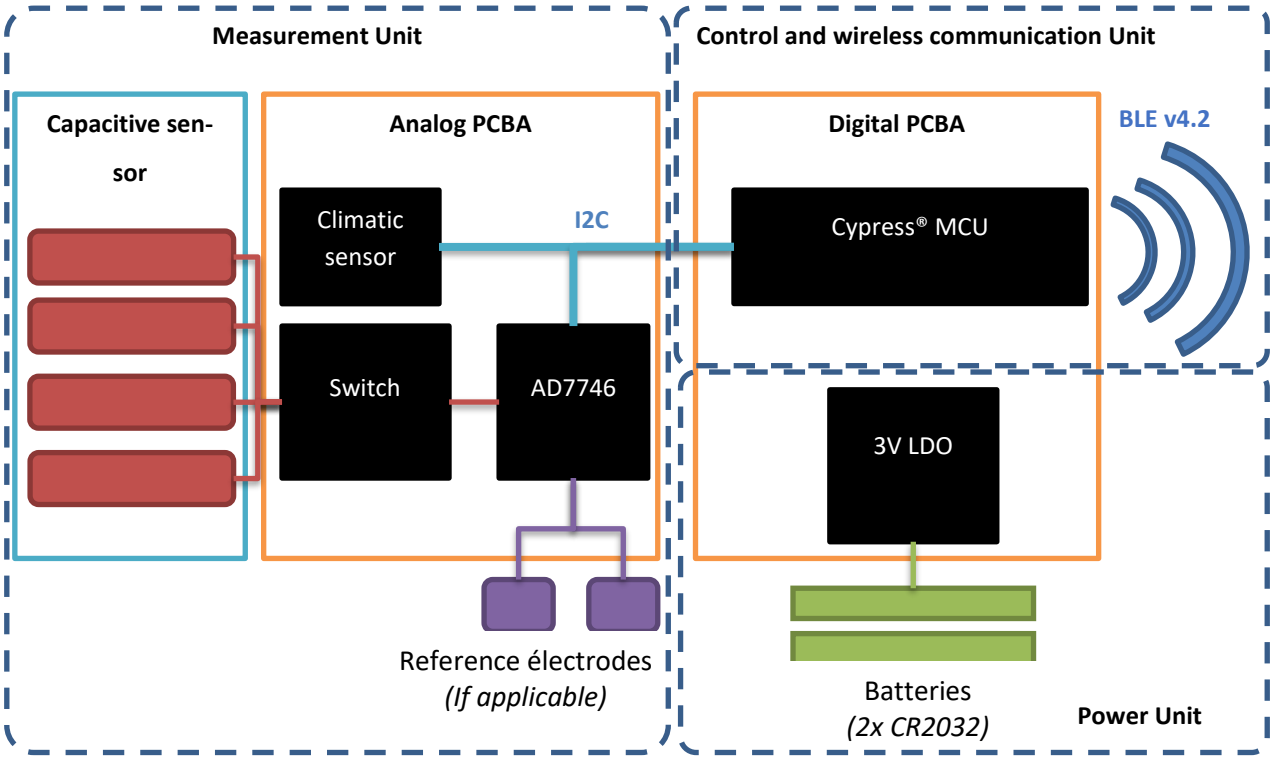

Figure 6: Schema block of the smart pen cap device

The current device has a temperature and humidity sensors SHT35 from Sensirion® mounted on the analogic PCBA and oriented towards the electrode. This sensor allows following the variation of temperature and relative humidity occurring on the device. Therefore, it is possible to send a warning when the smart pen cap, with a pen inside, detects that

the temperature is too high or if the injector pen stayed too long outside the fridge. It shall be also possible to detect if the pen has not reached its stable temperature after leaving the fridge.

By using the Bluetooth low energy wireless communication, a Cypress Semiconductor® dongle has been programmed to collect the data (capacitances, temperature, relative humidity, and battery level) and send them using a Universal Asynchronous Receiver Transmitter (UART) communication canal to a computer. On the computer a Python application reads the communication port and logs the information in .csv to be able to do post-treatment using spreadsheet Software. On Figure 7, an exploded view of the smart pen cap is presented. The electrodes are presented in blue, the shielding is the yellow part. In “A”, is the plastic part which hold electrode at the inner surface, by dispensing glue inside the holes. At the outside of this plastic part the shielding is placed. The part “B” is the mechanical cover which protect the shielding and give the final aspect of the device. In “C” are the digital and analogic PCBA. Finally, “D” corresponds to the batteries and batteries holder.

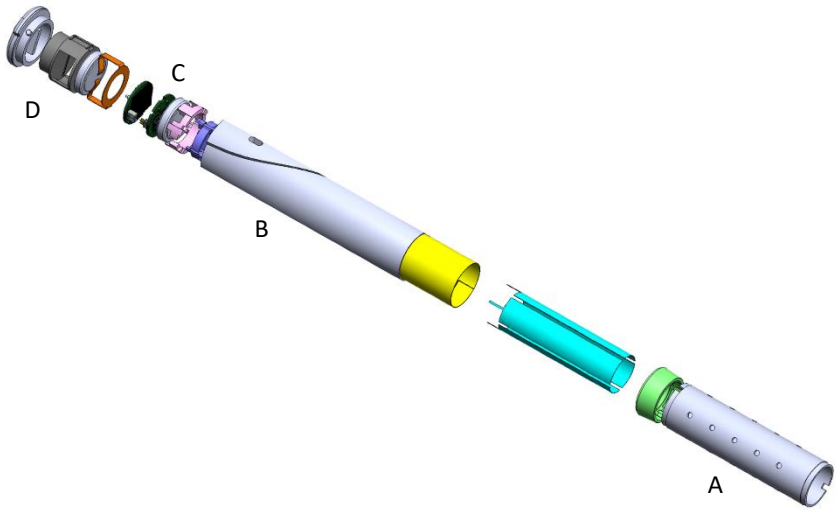

Figure 7: Exploded view of the smart pen cap

1.5 Capacitance measurement technics

1.5.1 Introduction

As presented in the section 1.3, a capacitive sensor has been selected to monitor the level of drug inside the injector pens. According to the user requirements, the device needs to be discreet and ease of use. This implies that the electronic shall be:

- As low power as possible to save power and increase the batteries lifetime.
- A small footprint to design tiny PCBA, thus allow to design a small device to be easily transportable
- Able to detect a change of 10µL, which can be converted to a change below 5fF according Chapter 2
- Measurement speed is not critical because the injection timing is at the hours level

In this section, different capacitive sensors will be presented with their advantages and their drawbacks [22, 23, 24]. Finally, a comparative discussion will select which technology fits best to the requirements.

1.5.2 Capacitance to Voltage converter (C2V)

These converters are based on the conversion of a capacitance variation into a voltage change. This technic is widely used according the treatment simplicity of the output. Different technics exist and they are presented hereafter.

1.5.2.1 De Sauty bridge

The origin of this technic is quite old, and it has been used at the beginning of the $\overline{XX}$century [25]. It is based on the Wheatstone bridge, which allows to observe a mismatch of resistance/impedance by using a difference of electric potential. Historically, galvanometer was used to observe these differences. The De Sauty bridge consists to apply an Alternating Current (AC) signal on a bridge composed by the capacitive sensor, a known reference capacitor and resistors as shown in Figure 8. Then, the difference between the reference capacitor and the capacitive sensor can be found by measuring the unbalancing voltage of the bridge. The advantages of this method are:

- It used a differential measurement, therefore the common noise and external variations which apply on both capacitors shall be cancel.
- This technic can work with a wide capacitance range because it depends on the voltage measurement limitation and the size of the reference capacitor.

But the main drawback is that the precision depends on the precision of:

- the reference capacitor
- the voltage measurement
- the bridge balanced which can be affected by mismatch between resistors or parasitic impedance in the bridge. [26]

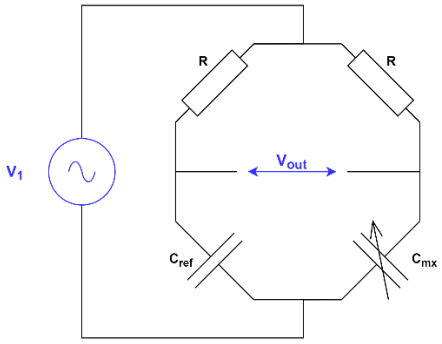

Figure 8: Example of a De Sauty bridge

Nowadays, its principle has been widely reused on more advanced technics, modified De Sauty bridges have been developed to reduce their disadvantages. As example, in [27], Voltage Controlled Resistor (VCR) has been used to balance the bridge. The obtained accuracy is 30fF with a range of 400pF. Or recently, in [28] a capacitive sensor has been set to detect bleeding during intraoperative radiotherapy. De Sauty bridge has been used with Operational amplifier (Op. Amp.) which can have a resolution of 100fF.

1.5.2.2 Charge sensitivity amplifier

Charge Sensitivity Amplifier (CSA) has similarity with the De Sauty bridge, it has a capacitive sensor (C_{mx}) and a reference capacitor (C_{ref}) [29]. A signal (V_1) is applied to the capacitive sensor and an opposite signal ($-V_1$) is applied on the reference capacitor.

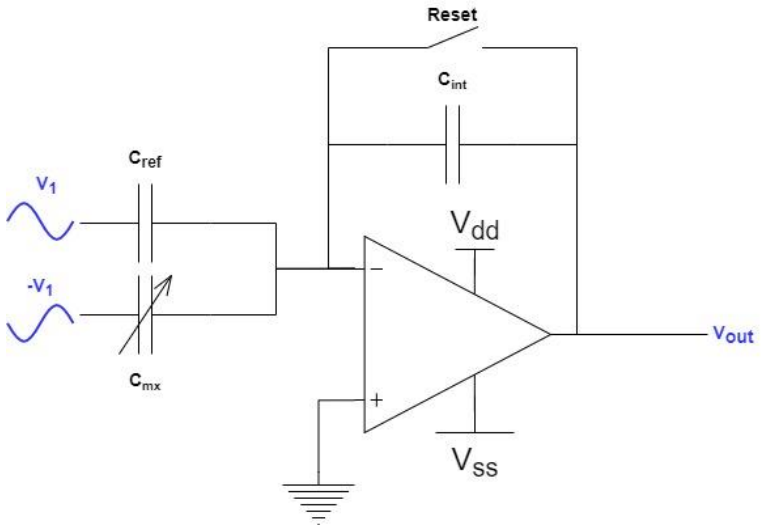

Figure 9 : Charge sensitivity amplifier

According Millman theorem applied at the negative input of the Op. Amp.

$$V^- = \frac{\frac{V_1}{Zc_{mx}} + \frac{-V_1}{Zc_{ref}} + \frac{V_{out}}{Zc_{int}}}{\frac{1}{Zc_{mx}} + \frac{1}{Zc_{ref}} + \frac{1}{Zc_{int}}} = V^+ = 0 \rightarrow V_{out} = V_1 \times \left(\frac{Zc_{int}}{Zc_{ref}} - \frac{Zc_{int}}{Zc_{mx}}\right)$$

With $Zc = \frac{1}{jC\omega}$ the ω is the same for all capacitors. Thus, the equation can be simplified:

$$V_{out} = V_1 \times \left(\frac{C_{ref} - C_{mx}}{C_{int}}\right)$$

Therefore, the output voltage is proportional to the difference between the sensor and the reference capacitors. The integrator function done by (C_{int}) integrates charge between the capacitors (C_{mx}) and (C_{ref}) into voltage. To prevent saturation of the integrator, a reset shall be implemented. Adding switched capacitor to improve the systems is generally done. The main drawbacks are charge injection and parasitic capacitance, especially when switched capacitor is used.

In [30], a differential Charge Sensitive Amplifier has been set for micromechanical capacitive sensor. The differential methods and optimization have been presented to limit the effects of parasitic effects. The authors were able to reach a resolution of 3aF. In the biomedical field, the publication [31] presents a capacitive sensor used to monitor the intracranial pressure. This capacitive sensor is based on a CSA coupled to a Successive Approximation Recursive Analog to Digital Converter (SAR ADC). The resolution reached is 4fF with a measurement range at 9.5pF. Finally, in [32] a submicrowatt implant using a capacitive sensor to monitor biological variable has been presented. The challenge of the implant is the small size and low power requirement. This implant can be powered by near field and the capacitive sensor works in a 4pF to 8pF range with an Effective Number Of Bits (ENOB) between 8 and 9.

1.5.2.3 Lock-in detection

Lock-in detection uses an AC signal (V_1) applied to the capacitive sensor. The frequency of the signal can be above the mega-Hertz range to attenuate the effect of the parasitic resistors compared to the capacitor. This creates a current which is converted into voltage through a Trans-Impedance Amplifier (TIA). Finally, a Lock-In Demodulator (LID) uses AC signal (V_1) and its quadrature ($V_1{}'$) to demodulate the output signal of the TIA (V_{out}) to the Direct Current (DC) domains. Then, tunable low pass filters removes artefact frequency as it is presented in Figure 10. Finally, the phase shift between (V_1) and (V_{out}) can be analyzed to know the value of the capacitive sensors [33, 34]. The main advantage of this technics is its high reliability against the noise due to the LID. It is generally used for the detection of small elements as cells, protein, or particles due to its high precision. The drawback of this technics is its complexity, energy cost and its ability to detect only slow capacitance variations [35, 36, 37, 38, 39].

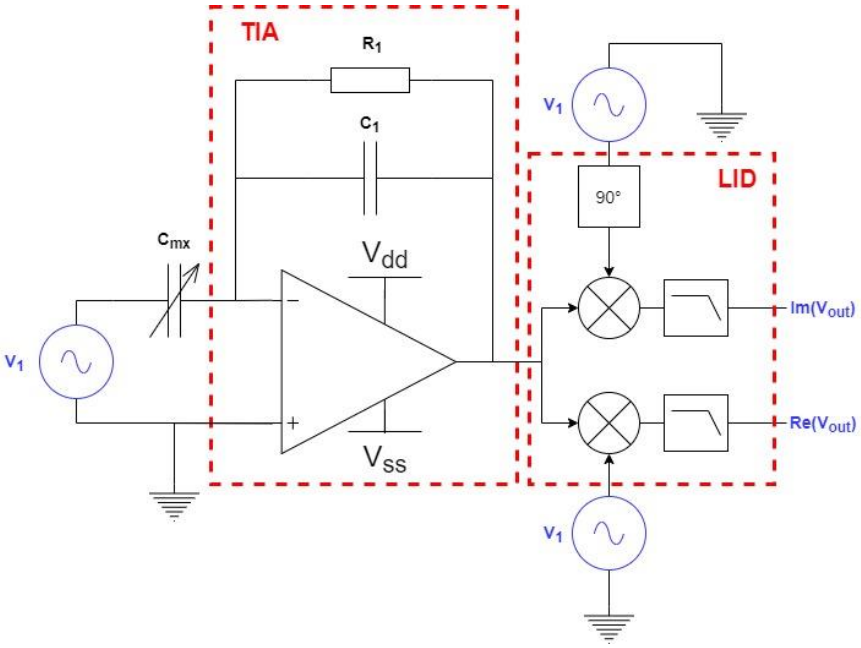

Figure 10 : Lock-in detection schematic

In [40], a capacitive sensor using lock-in detection to detect cells is presented. This article deals with System on Chip (SoC) with co-design on electronic, fluidic and chemistry to improve the detection level and reach ultra-low noise domain. Comparative analysis has been done by presenting some work which reach Zepto-Farad level (10^{-21} F). This is a very specific application which tends to approach the physical limitation. As presented in [35], a device has been developed to detect airborne particulate matter. This SoC can reach a resolution of 65 zF (0.065 aF) by using a differential electrode designed directly on the same subtract than the electronics as presented in Figure 11.

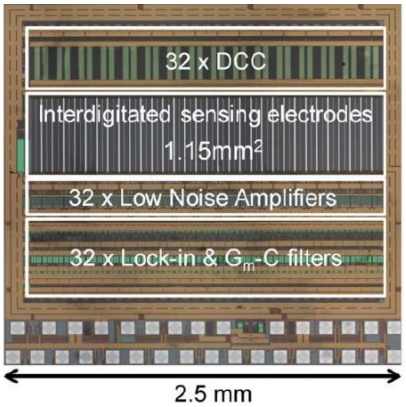

Figure 11: Lock-in SoC designed presented in [29]

1.5.2.4 Charge based capacitance measurement (CBCM)

This technic uses the capacitive sensor and a reference capacitor [41, 42]. As presented in Figure 12, when the Transistors T_3 and T_4 are active, controlled by V_2, the capacitors charges according $C \times \frac{du}{dt}$ with u varying from 0V and trying to reach approximatively Vdd (depending on the Vds of the transistors). At the opposite when transistors T_1 and T_2 are active, controlled by V_1, the capacitors discharge according $C \times \frac{du}{dt}$ with u varying from the present capacitor voltage to 0V. The transistor T_5/T_6, T_7/T_8 and T_9/T_{10} act as currents mirror. Therefore, the output current will depend on the charging and discharging current of both capacitors. is therefore the variation of voltage across the capacitor. When

$$i_{out}(t) = i_{t7}(t) - i_{t9}(t) \; with \begin{cases} i_{t7}(t) = g \times ic_{mx}(t) = g \times C_{mx}\dfrac{du}{dt} \\ i_{t9}(t) = g \times ic_{ref}(t) = g \times C_{ref}\dfrac{du}{dt} \end{cases}$$

$$i_{out}(t) = g\left(C_{mx}\frac{du}{dt} - C_{ref}\frac{du}{dt}\right)$$

Finally, the output voltage is obtained by using a known capacitor as a current integrator. By considering that the capacitors reach the maximum voltage (V_c) at the end of the acquisition periods (T), the current will also depend on (g) which is the gain of current mirrors.

$$\int_0^T i_{out}(t)\,dt = g\int_0^{V_c}\left(C_{mx}\frac{du}{dt} - C_{ref}\frac{du}{dt}\right)dt$$

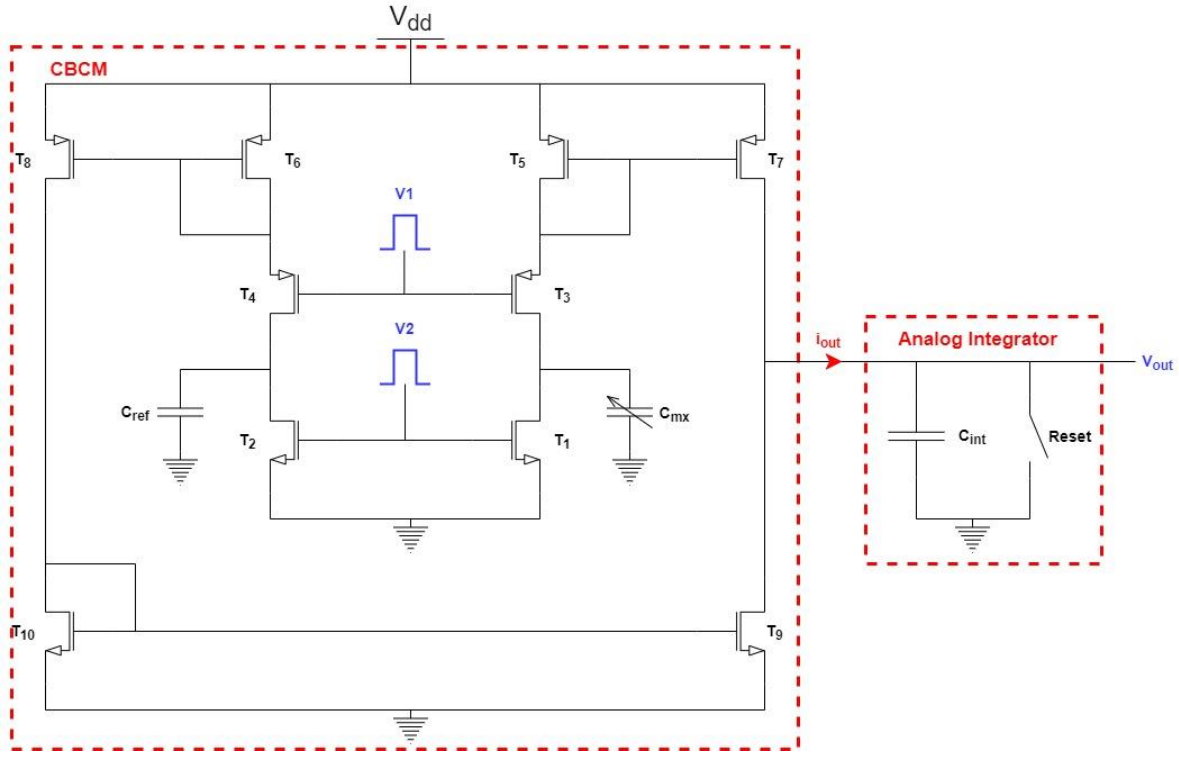

Figure 12: Capacitance to voltage converter - CBCM

This technic has been initially presented in [43], its principle is explained, and the estimated sensitivity is 10 aF. In [44], this technic is applied to life-science domains especially for laboratory on chip applied to protein interaction quantification, cellular monitoring… The device presented in this reference can monitor cellular or molecular activities by using a modified CBCM with current-controlled oscillator and frequency output with a sampling frequency at 100 kHz. This

device can measure a capacitance in the range of 70 fF with a resolution of 10 afF with interpolation and compensation of the distortion.

1.5.3 Capacitance to current (C2I)

This topology allows low power and high-speed operation [45, 46]. A known and controlled current source feeds paralleled capacitive sensor and reference capacitor. Then, a current-differencing block, does a subtraction of these two-branch currents. Switches are placed in parallel of each capacitor to discharge capacitors and avoid charge saturation. When the switches are closed, the currents on each branch are the same, therefore the output current is equal to 0A. When the Switches are opened the currents will depend on the capacitors and parasitic capacitances. The drawback of this methods is its sensitivity to any parasitic capacitance at the input of the system (discharge switch or stray capacitance). A special attention shall be done on the routing.

$$I_{in} = I_{mx} + I_{ref}(+I_{stray}) = \frac{dV}{dt} \times \left(C_{mx} + C_{ref}(+C_{Stray})\right) \rightarrow \frac{dV}{dt} = \frac{I_{in}}{C_{mx} + C_{ref}(+C_{stray})}$$

$$I_{out} = I_{mx} - I_{ref} = \frac{dV}{dt} \times (C_{mx} - C_{ref}) \rightarrow \frac{dV}{dt} = \frac{I_{out}}{C_{mx} - C_{ref}}$$

$$I_{out} = \frac{I_{in}(C_{mx} - C_{ref})}{C_{mx} + C_{ref}(+C_{stray})}$$

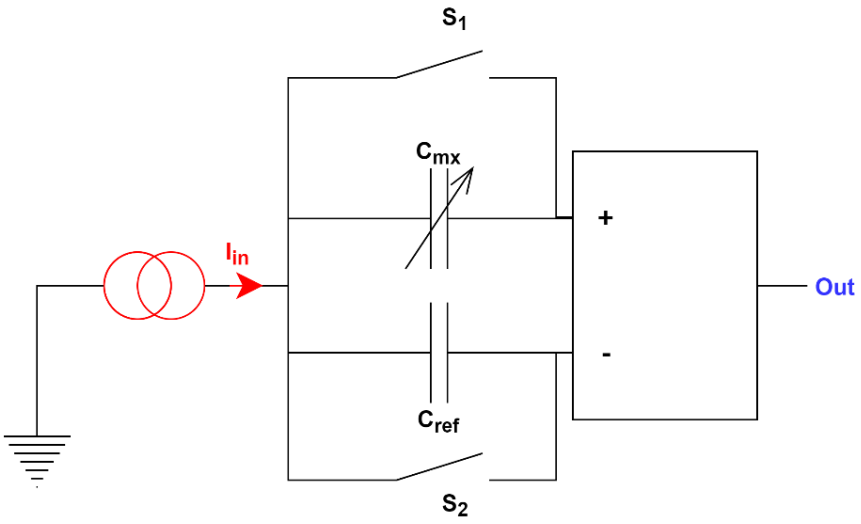

Figure 13: Capacitance to current design

According [47], a SPICE simulation has been done to present a capacitance to current topology. The circuit presented in this reference gives a ratio-metric result directly $x = \frac{C_1 - C_2}{C_1 + C_2}$. This topology allows to have a fast conversion speed and low power consumption due to the low complexity and minimum post-processing needs. In [48], a capacitance to current topology has been presented with a range of 750fF with a resolution of 1.1fF

1.5.4 Capacitance to time (C2T)

Variation of capacitance can impact oscillating signal by adapting the period of a signal, it is called Pulse Frequency Modulation (PFM), or its duty cycles, which is called Pulse Width Modulation (PWM). The main advantage to use capacitance to time conversion is the easy interfacing with MCU by using a counter.

1.5.4.1 Pulse Frequency modulation

Pulse frequency modulation can be based on a relaxation oscillator. The capacitive sensor is connected to an input of a comparator. Charging the capacitor by a known current induces a voltage that will reach the comparator threshold [49, 50, 51]. The output of the comparator changes, which allows a transistor to discharge the capacitor until it reaches the second threshold. By counting the time between two rising or falling edges, it is possible to obtain the value of the capacitive sensors. The main drawback is that the precision will depend on many parameters as: the speed of the counter, the precision of the threshold, the propagation time of the comparator and the precision of the current source. In [52, 53], there are examples to detect capacitance change by using an NE555 in an astable configuration.

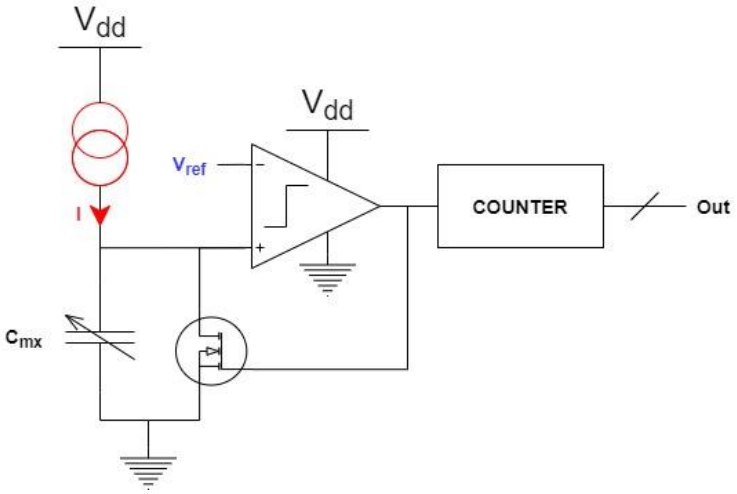

Figure 14: Capacitance to time - Relaxation oscillator

Another configuration using ring oscillators are widely used [54]. By using a capacitive sensor inside a ring oscillator, the capacitor variation will impact the output frequency of the oscillator. The main disadvantage of this topology is the impact of the environment (power supply noise, climatic…) on the structure which can induce bias. To get rid of this effect, a second ring oscillator can be implemented to do differential measurement. The output frequency of this ring oscillator can be converted in digital by using a simple counter. As previously mentioned, the speed and precision of the counter will affect the capacitance accuracy.

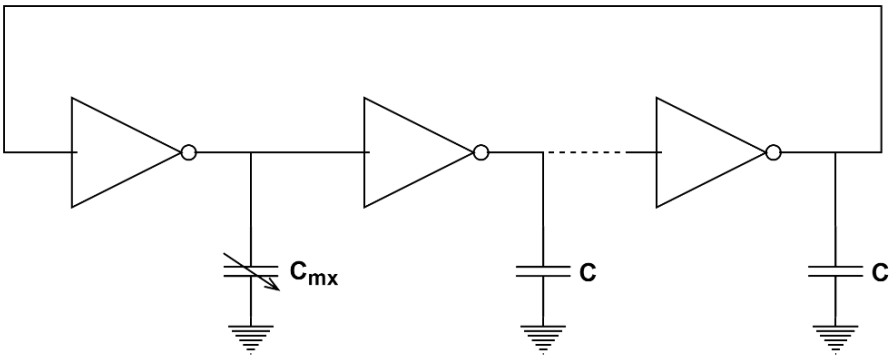

Figure 15: Capacitance to frequency - Ring Oscillator

1.5.4.2 Pulse Width Modulation ratio

In [55, 56, 57, 58], different topologies to convert the capacitance to a variable PWM are presented. This method can be easily converted into voltage using a low pass filter or interface with an MCU or a counter. Detail about a specific design presented in [56, 57] is presented hereafter.

This system is based on a differential measurement using capacitive sensor and reference capacitor. The reference capacitor shall have a close value compare to the capacitive sensor. Triangular signal voltage generated by a ramp generator (RG), synchronous with the system clock, is applied on the common electrode of the capacitive sensor and the reference capacitor. The currents of these capacitors go inside a differential charge amplifier (CA). The output current I_{CA} is therefore dependent on the difference between the two capacitors. Then, the current I_c will depend on current I_{CA} and current sources I_B and I_D. Switches driven by the clock (SA1) and the output (SA2) modify the direction of the current $I_{CA} + I_B$ and I_D respectively. The current I_c is flowing into a capacitor and the voltage across the capacitor is an input of a low hysteretic comparator (CMP). The equation below summarizes the operation on the current

$$I_c = \pm(I_{CA} + I_B) \pm I_D$$

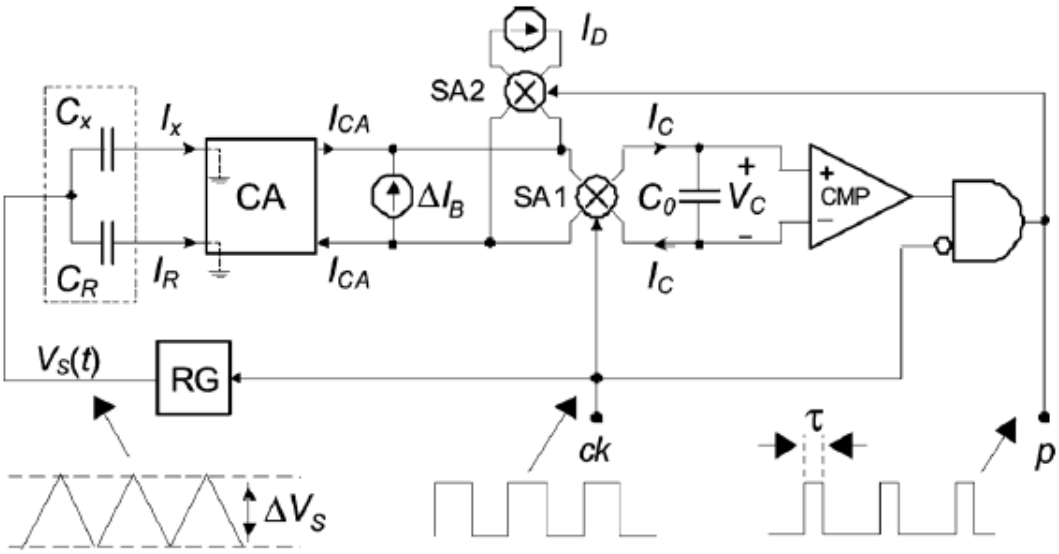

Figure 16: Capacitance to time- PWM [57]

The resolution obtained in the first paper of *P. Bruschi et al* is 0.9fF for a range of 400fF. Then, one year later, *P. Bruschi et al* proposed an updated version where the major improvement is the Figure Of Merit (FOM) decrease from 1851 pJ/step to 10.5 pJ/step

1.5.5 Capacitance to digital (C2D)

To improve integration and power consumption, ADC has been directly integrated after a Capacitance to voltage converter to have the capacitance converted directly in digital and easily interface the chip with an MCU or share on communication bus.

1.5.5.1 Sigma delta

The ΣΔ converter allows to obtain data with low noise due to oversampling. It uses a charge balancer cadenced at a frequency (F_1) to charge and discharge capacitive sensor. Then, charges are integrated, and a feedback loop adapts the reference capacitor according the digitalized/comparator output of the integration. The bit stream can be treated by a decimation filter to give an interfaceable digital output.

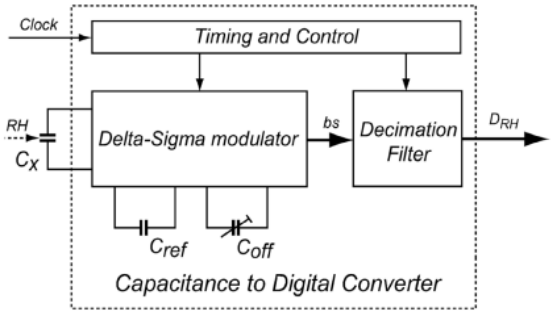

Figure 17: Capacitance to Digital: $\Sigma\Delta$ converter [23]

This technic is well explained in [59], a differential capacitance acquisition using a ΣΔ converter is used to measured humidity on a smart Radio-Frequency IDentification (RFID) sensor. This device has a resolution of 70 aF for a range of 0.54 pF to 1 pF.

1.5.5.2 Successive Approximation Register (SAR)

The SAR topology works in multiple succession of the two steps presented below to approximate the value of the capacitive sensor.

- First step,
  - The Op-Amp is driven as a buffer by switching on T_1 $(V_{L1} = 0)$, therefore the negative input is equal to V_{ref}
  - The logic signal $V_{L2} = 1$ so the programmable reference capacitors are connected to V_{ref} on both sides. Thus, they have no potential difference at their pins
  - The capacitive sensor is connected at the potential reference (0 V) at one side through transistor T_3 $(V_{L1} = 0\ V)$
  - The charges are equal to $Q = C_{mx} \times V_{ref}$
- Second step,
  - The Op-Amp is driven as an integrator by switching off T_1 $(V_{L1} = 1)$, The integration is done by the capacitor C_{int}
  - The logic signal $V_{L2} = 0$so the programmable reference capacitors are connected to potential reference (0 V) in one side and at capacitive sensor and integrator at the other side

- The capacitive sensor is connected at V_{ref} at one side through transistor T_2 $(V_{L1} = 1)$ and at the programmable reference capacitor and the integrator at the opposite side
- The charge stored in C_{mx} will flow in the reference capacitor and the integrator. The output voltage of the integrator will enter in comparator to V_{ref} which will adapt the programmable reference capacitors to approach the value of C_{mx} after some iteration.

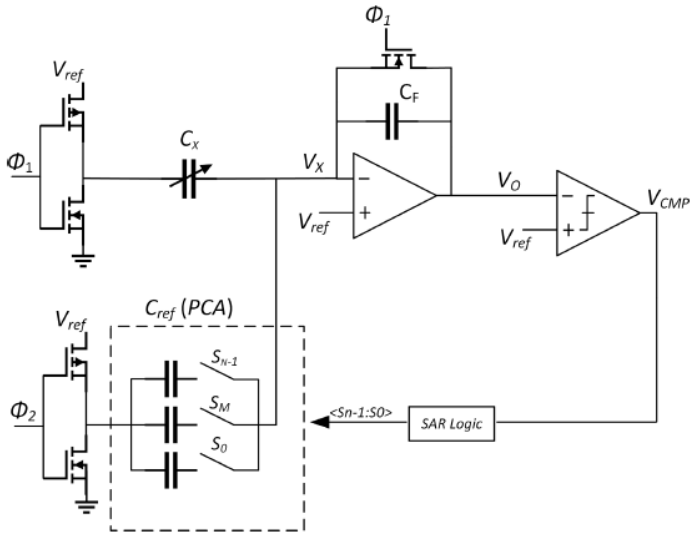

Figure 18: Capacitance to Digital: SAR converter [23]

In [60, 61], capacitance to digital converter based on a SAR converter is presented with design advice and information about non-ideality behavior. According tests with the architecture proposed in [60], a resolution of 2.75 fF is obtained for a capacitance range of 16 pF.

1.5.6 Phase shift (C2Φ)

The last method uses the phase shift between two signals created by a reference oscillator and an oscillator depending on the capacitive sensor. The stability of the oscillators can be impacted by environmental variation. Therefore, the design shall pay attention that the two oscillators depend on the same environmental variation, to remove the external parasite during the phase shift subtraction [62, 63]. The sensing resolution obtain is few aF resolution.

1.5.7 Discussion

The previous topologies have strengths and weaknesses, their main characteristics are presented in the table below. These characteristics are:

- The capacitance resolution,
- The capacitive range,
- The power consumption,
- The Figure Of Merit (FOM), which consists to give the energy used at each conversion steps
- The conversion timing
- The footprint

Table 2: State of the art of capacitance measurement

Name	*Type*	*Sub-type*	*Resolution [fF]*	*Range max [pF]*	*Power [µW]*	*FOM [pJ/Conv-Step]*	*Times [µs]*	*Footprint [mm2]*	*Ref.*
Mantenuto 2014	C2V	Sauty	30	400					[27]
García-Gil 2021	C2V	Sauty	100						[28]
Saukoski 2005	C2V	CSA	3.00E-03						[30]
Ghanbari 2017	C2V	CSA	4.75	9.5	0.13	3.9			[31]
Trung 2015	C2V	CSA	15.6	8	5.5	13.7	640		[32]
Zhong 2018	C2V	CSA	0.054	0.145	350			6	[29]
Manickam 2010	C2V	Lock in	0.0064		84800		80000	4	[38]
Ciccarela 2016	C2V	Lock in	6.50E-05		84000		25000	6	[35]
Gonzzini 2009	C2V	Lock in	1.50E-04		60000		80000	0.5	[36]
Mazhab-Jafari 2012	C2V	Lock in	5.10E-03		1800		100	1.68	[37]
Babay 2020	C2V	Lock in	0.06	0.67					[34]
Chen 1996	C2V	CBCM	0.01						[43]
Forouhi 2018	C2V	CBCM	0.01	0.07	103		1	64.5	[44]
Prakash 2009	C2V	CBCM	0.015	0.05	165				[42]
Couniot 2016	C2V	CBCM	0.45	0.056	30		27000	0.1	[41]
Singh 2009	C2I	N/A	1.13	0.75	725				[48]
Dimitropoulos 2006	C2I	N/A	0.4	0.81	50				[45]
Scotti 2014	C2I	N/A	0.8	1.8	220		2	0.03	[46]
Brushi 2007	C2T	PWM	0.9	0.4	16500	1851	50	0.2	[55]
Brushi 2008	C2T	PWM		0.76	84	10.8	33	0.53	[56]
Nizza 2013	C2T	PWM	0.8	0.256	84		380	0.52	[57]
De Marcellis 2019	C2T	PWM	0.1	197	68000				[58]
Mohammad 2017	C2T	PFM	0.18	1.5					[54]
He 2015	C2T	PFM	0.25	8	14	1.87	210	0.05	[51]
Tan 2012	C2T	PFM	0.2	6.8	211.2	49	7600	0.51	[59]
Heidary 2010	C2T	PFM	0.005	5.8	5000	4700	1E06	3	[50]
Wolffenbuttel 1987	C2ϕ	N/A	0.4	0.28					[63]
Tan 2013	C2D	ΣΔ	0.07	1.06	10.3	1.4	800	0.28	[49]
AD7745	C2D	ΣΔ	0.004	8	2310		1100	22.5	[64]
Gaugaz 2019	C2D	ΣΔ	0.21	1	900		80000		[65]
Omran 2014	C2D	SAR	2.75	16	303	34	650	0.07	[60]
Ha 2014	C2D	SAR	6	75.3	0.16	1.3	4000	1.4	[61]

As it is presented in Figure 19, the topologies presented in the publications have been plotted according their power consumption against the capacitance resolution on logarithmic scale. The first observation done is that a theorical limit seems to appear and it has been represented by the red dotted line on the graph. The second observation is that the most precise measurement is done by using C2V-Lock-in technics, but they are also the techniques which have the higher power consumption, it can reach several milli-watt. At the opposite, the topology which used less energy is C2V-CSA, with an embedded SAR for [61]. But they have the worse resolution, in the order of 0.1fF. The compromise between

power consumption and resolution seems to fit for C2V-CBCM architecture which is in the center of the graphs near the red limit.

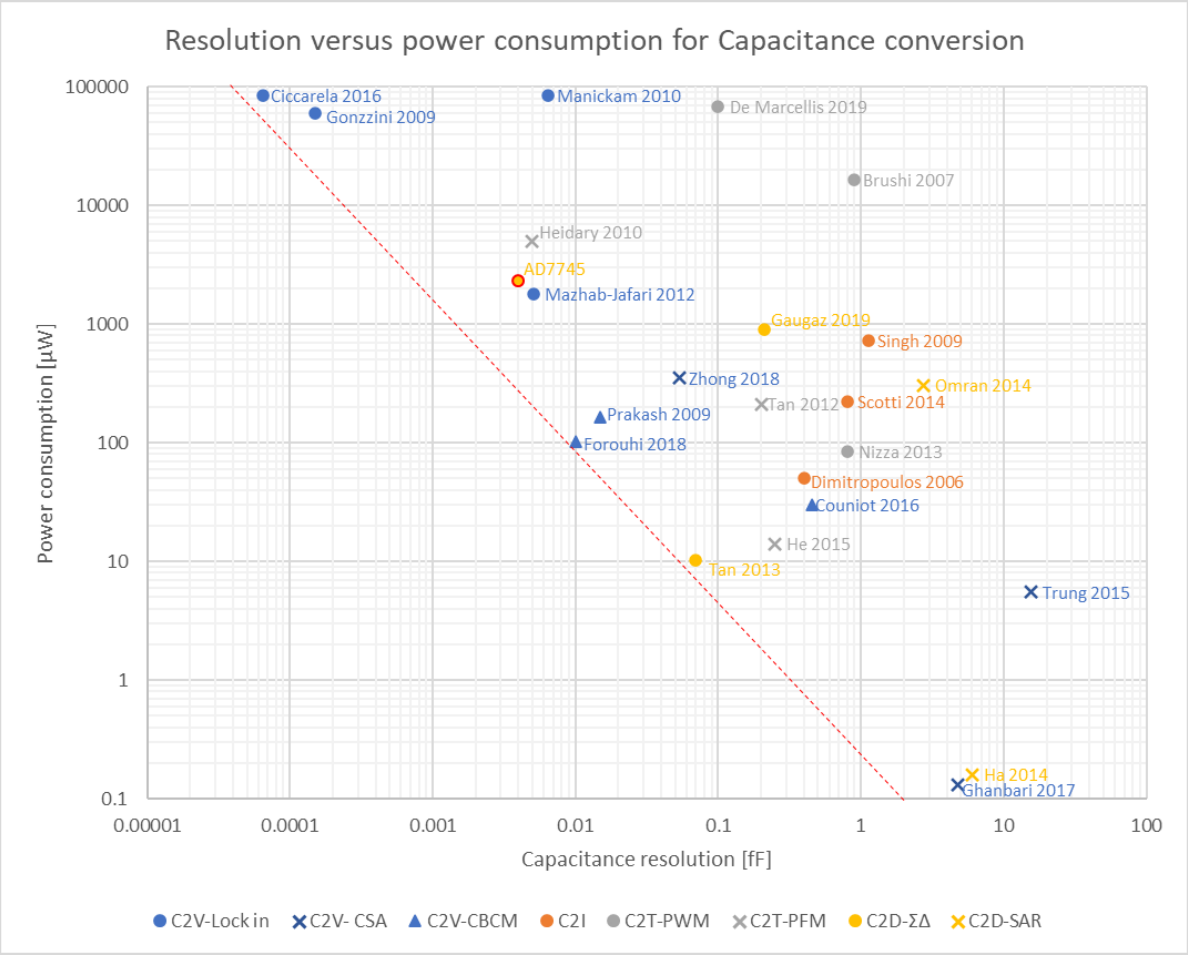

Figure 19: Comparative graph between Power consumption and capacitance resolution for capacitive measurement chip

1.5.8 Conclusion

As seen in the discussion, C2V-CBCM and C2D architectures seem to fit quite well the smart pen cap requirements where the objective is to have a low power consumption device with a resolution below 5 fF. Capacitance to digital converter using ΣΔ topology has been selected due to the simplicity to interface and the availability of such components directly on the market. The AD7745 from Analog device has been selected according its price, its availability for a rapid mass-production and its I^2C interface which facilitates the development and the use of this chip.

In paralleled an Application Specific Integration Circuit (ASIC) has been developed in partnership with an EPFL Teams [65] through a CTI project (grant n°25386.1 PFLS-LS). It is based on a C2D-ΣΔ configuration and fits the need for the smart pen cap, and it can communicate through Serial Peripheral Interface (SPI). This ASIC can be considered for large mass-production and to be not dependent of Analog Device®.

Currently, the AD7745 has been integrated in the Analog PCB of the smart pen cap. Due to the number of electrode and the need to switch them into excitation and measurement pins, switch has been added between the electrode and capacitance to digital converter.

1.6 Switches

1.6.1 Introduction

The smart pen cap has multiple electrodes which improve the drug level accuracy as presented in sections 2.3 and 3.3. A switching component shall connect the electrodes to the capacitance converter selected in the previous section. This switching component shall have close property as the capacitance converter:

- Small footprint to design a discreet device for the patient
- Low power consumption to let a long period to replace batteries
- Low parasitic impedance to not disturb the capacitance measurement
- Allows to connect the 4 electrodes to the excitation and measurement signals independently

The Capacimeter and the electrode are linked through the switch according Figure 20.

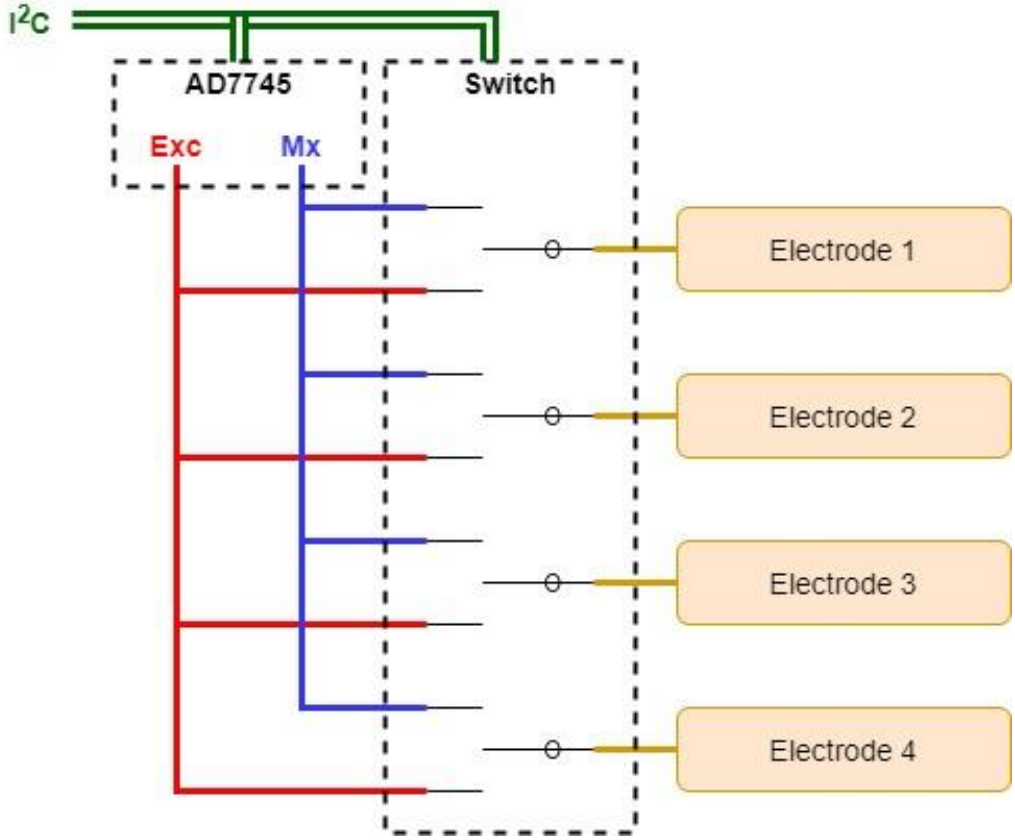

Figure 20: Schematic overview of Capacimeter, switch and electrode

1.6.2 Switch matrix

The first component used was a switching matrix which gives a lot of freedom for interconnection between signals and electrodes and can be easily connected to a MCU by using an I²C bus interface. The component selected was an ADG2128 from Analog Device® [66]. It has been finally abandoned due to its cost, its power consumption, and the possibility to create short circuit in case of wrong driving. They are their main properties:

1. The price: approx. 10 USD
2. The parasitic
    - $C_{off} = 6pF$ and $C_{on} = 9.5pF$
    - Channel to channel CrossTalk: $-62dB$ $(with\ R_L = 75\Omega, C_L = 5pF\ and\ f = 5MHz)$
3. The power consumption $5V \times 0.1mA = 500mW$
4. Possibility to create short circuit if a firmware error occurs

1.6.3 Single Pole, Double Throw (SPDT) Switch

The MAX4571 switch from Maxim [67] is currently used for smart pen cap prototypes, it is less flexible than the switch matrix, but it is still easily interfaceable with an MCU by using I²C bus. The main properties are:

1. The price: approx. 7 USD
2. Lower parasitic
    - $C_{off} = 9pF$ and $C_{on} = 9.5pF$
    - Channel to channel CrossTalk: $-90dB$ $(with\ R_L = 600\Omega\ and\ f = 20kHz)$
3. The power consumption $3V \times 0.01mA = 30mW$

Due to its low price, its availability on the market and low power consumption, this chip has been selected to manufacture the product.

1.6.4 Microswitch

During feasibility, Proof of Concept prototype has been designed using a MicroElectroMechanical Systems (MEMS) micro-switch to reduce parasitic impedance. Two chips ADGM1304 from Analog Device [68] have been placed on the analog PCBA. They have been used due to their extremely good behavior in switching and low parasitic capacitance. But there are extremely expensive, very sensitive to choc and Electro-Static Discharge (ESD), and finally seemed to not improve the signal noise ratio (SNR).

1.7 Basic test of the prototype

1.7.1 Introduction

Multiple iteration of prototypes has been manufactured. Hereafter is presented the results obtain with the last version of the smart pen cap. Capacitance monitoring of the Printed Circuit Board Assembled (PCBA) alone then with electrodes without any pen have been done to observe the basic level of noise for the device.

1.7.2 No electrode

A first test with the PCBA alone has been done to observe the level of noise of this system. By doing a run test of one hour, the capacitance range is 0.289 fF and 99.9% of the points are in ±0.087 fF

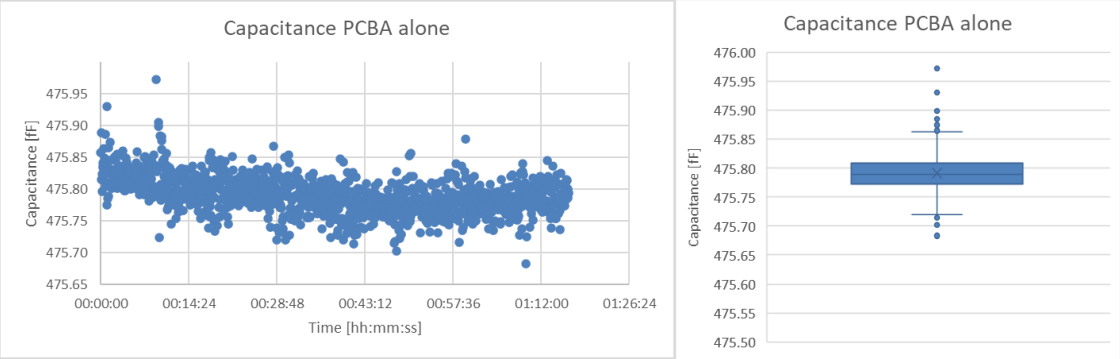

Figure 21 : Capacitance on a PCBA alone

1.7.3 With electrode

Electrode, electrode holder and shielding have been added to the device to observe the noise of the full system. Temperature and relative humidity of the air impacted the measurement. In this case, the relative humidity is neglected and only temperature is measured using a commercial sensor SHT35. The capacitance (blue curve) and temperature (red curve) variations are presented in Figure 22.

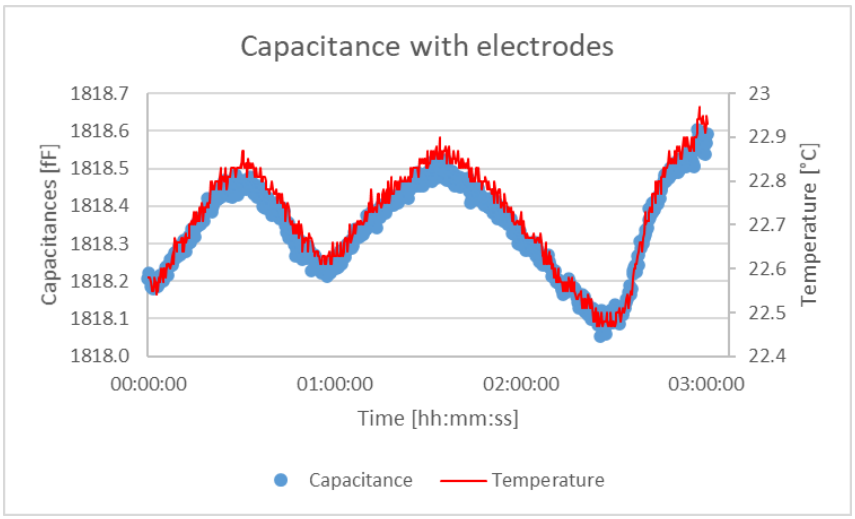

Figure 22: Empty value of full smart pen cap

The curves have a good correlation, it is possible to compensate the capacitive value by the temperature value acquired by the sensor, the Figure 23 is obtained. Therefore, the capacitance range is 0.124 fF and 99.9% of the points are in ±0.059 fF.

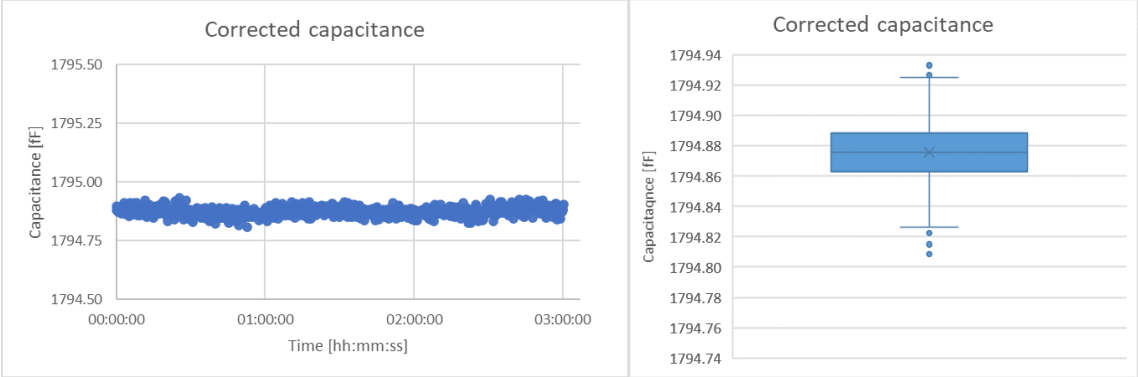

Figure 23 : Empty value of full smart pen cap compensated

The value when the full smart pen cap is assembled is better than the PCBs alone, this effect can be explained by the temperature compensation and the shielding which protects the electrode against external noise.

Due to the nature of this noise, a digital filtering could increase the precision of the device, but the target value is 5fF which is ~40 times larger than the noise range. Therefore, these results are considered as acceptable.

1.8 Chapter conclusion

In this chapter, a description of the injector pen and the smart pen cap have been done. The main requirements have been presented which are the power consumption consideration, the dimension of the device and the measurement technics. To measure the amount of liquid inside the injector pen, the capacitive measurement has been selected compare to other physical techniques due to its contactless property, the independence from the gravity and its precision.

Then a bibliography study has been done by presenting different technics to measure the capacitance. Capacitance to digital converter from the market AD7745 has been selected due to its low power consumption, its resolution below 5 fF, its price and the ease of interfacing to a MCU using I^2C bus. On this bus, a switch to connect electrode to AD7745 and a climatic sensor SHT35 measuring ambient climatic environment have been added.

The link between the electrodes and the capacitive to digital converter goes through a commercial switch MAX4571 which allows to assign electrodes to the measurement or excitation signal. A quick presentation of three switches used during the development has been done.

Finally, measurements have been realized by:

- Firstly, assembling analogic and digital PCBA and sending empty measurement using BLE through the MCU (CyBLE022001). This gives a noise at ±0.087 fF
- Then, the mechanics and electrodes were connected to the electronics, the data show that the capacitance changes according the temperature variation. By compensating the capacitance variation using climatic sensor data, the noise obtained is ±0.059 fF

The systems are therefore able to measure the volume variation of drug inside an injector pen if the capacitance variation is larger than ±0.059 fF. The next chapter will focus on the optimization of the capacitance variation versus the level of drug by changing electrodes to improve electric field in the liquid column.

Chapter 2. Electric field geometry

2.1 Chapter introduction

The geometry of the electric field in the device plays an important role because it will determine the capability of the smart pen cap to measure a variation of capacitance to allow a detection of a 10 µL volume change inside the injector pen. This chapter will start by presenting a bibliography overview of the different electrode configurations used to measure a volume inside a tank. Then, a basic configuration with two opposite paralleled plate capacitive sensor will be detailed as baseline. Finally, two semi-cylindrical electrode model will be presented.

2.1 Bibliography study

The problems concerning measuring a liquid level inside a container is widely studied in the literature and many electrode configurations propositions have been proposed. The constraint of this study is that the container is already defined by injector pen manufacturers. Therefore, it cannot be modified to increase detection performance by modifying geometry of the cartridge. Moreover, the cartridge is contained inside a plastic holder, and some assembly tolerances between the holder and the cartridge exist and due to the concept of a reusable pen cap device, positioning tolerance between the injector pen and the pen cap must be considered as presented in Figure 24. The angular position between the pen cap and the injector pen cannot be fixed. The objective is to have the best liquid level sensitivity with the lowest dependance of the cartridge position inside the electric field.

- The two parallel flat electrode configuration is studied in section 2.2, it is the basic solution to measure a volume and it can be easily manufactured. [69, 70]
- The coplanar electrode configuration described in [53] is a basic assembly which is widely used. In container measurement, this configuration is generally used to detect a threshold or presence of liquid at a defined level. This electrode configuration is quite easy to manufacture but it will be sensible to the distance between the liquid column and the electrode.
- The interdigital electrode configuration is an extension of the coplanar electrode. They are presented in [71, 72]. It allows to measure continuous levels inside a tank. These electrodes are easily manufacturable and parameters as spacing between plates are presented in the aforementioned publication. For the smart pen cap device, the cartridge tolerance will impact the measurement and it will not be possible measuring the remain drug volume precisely.
- The double ring electrode configuration could reduce the problems of the cartridge position. This configuration has been studied in [73] by placing two electrode rings side by side. With this technic, the angular position error is removed, but the radial and axis tilting angle errors still affect the capacitance. Therefore, it is still not possible to precisely measure a volume of water. Moreover, the sensitivity of this configuration is not optimal because the field is stronger between the electrode and weaker at the center, where the cartridge is positioned.
- The two semi-cylindrical electrode configuration is widely used, commonly it is used to observed two phases of liquid in tubular geometry and measure fill levels (Example for oils). This solution has been studied in section 2.3 because it seems to give the best results in sensitivity according to [74, 75]
- Two helicoidal electrode could be a good alternative to the semi-cylindrical electrode. This solution is well represented but it is difficult to manufactured. According [39, 76] , it does not have the largest resolution, but it should cancel the angulare and tilting position problems.

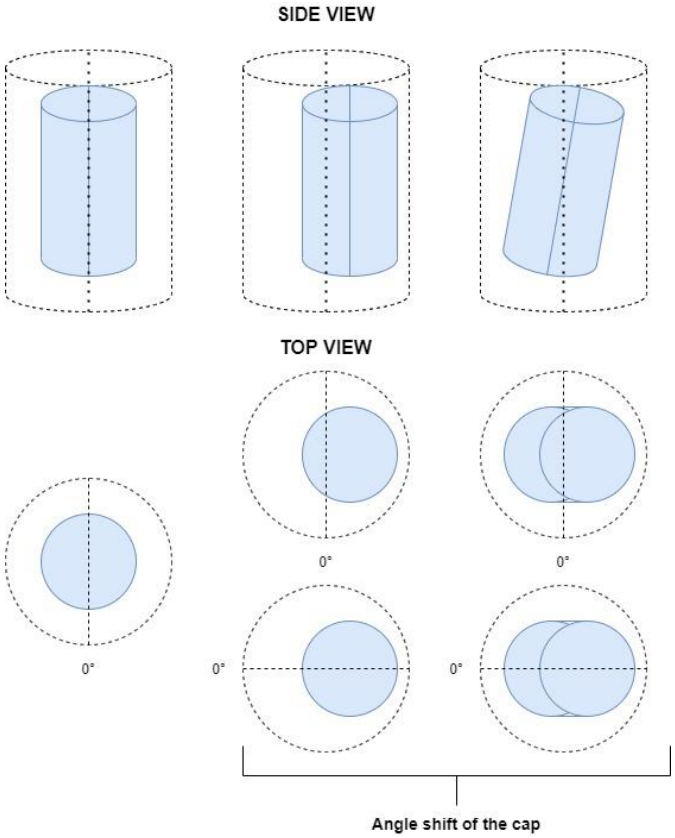

Figure 24 : Cartridge position error (Center, misalignment offset and angle shift, tilting of the cartridge)

2.2 Two parallel electrode

2.2.1 Introduction

The simplest capacitor is the two flat electrode capacitor because the electric field shall be uniform between electrode. In this case, the modification of the electric field by changing materials is only considered between the electrode, thus the electric field which is external to the uniform section is considered constant as a paralleled fixed parasitic capacitance.

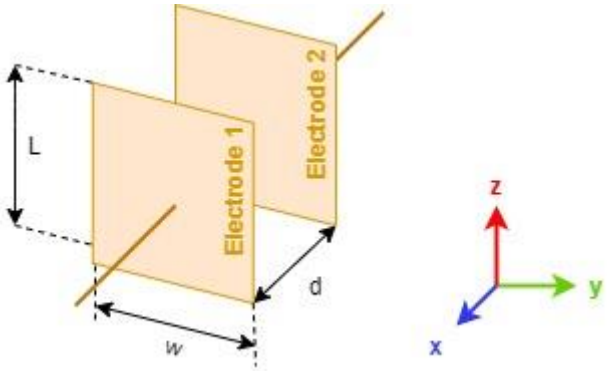

Figure 25 : Measurement and parasitic capacitance

2.2.2 Theory

2.2.2.1 Empty capacitor

Using the Maxwell Gauss equation with ε is the electrical permittivity (relative permittivity times absolute permittivity) and ρ is charge density.

$$\vec{\nabla}.\vec{E} = \frac{\partial E_x}{\partial x} + \frac{\partial E_y}{\partial y} + \frac{\partial E_z}{\partial z} = \frac{\partial E_x}{\partial x} + 0 + 0 = \frac{\rho}{\varepsilon} \rightarrow \partial E_x = \frac{\rho}{\varepsilon}\partial x$$

The voltage is the difference of electric field along the x axis and the charge density is the number of charges by the volume: $\rho = \frac{Q}{A}$

$$\mathrm{U} = \int_0^d dE_x = \int_0^d \frac{\rho}{\varepsilon} dx = \frac{\rho d}{\varepsilon} = \frac{Qd}{\varepsilon A}$$

And finally, the capacitance shall be represented as the number of charges on the Voltage.

$$C = \frac{Q}{U} = \frac{Q\varepsilon A}{Qd} = \frac{\varepsilon A}{d} = \frac{\varepsilon_0 \varepsilon_r A}{d}$$

The capacitor has these values:

- Electrode distance: $d = 15\ mm$
- Electrode area: $A = L \times w = 23 \times 15 = 345\ mm^2$
- Air permittivity (at 25°C): $\varepsilon_r = 1$
- Absolute permittivity: $\varepsilon_0 = 8.8541878128 \times 10^{-12}\ \mathrm{F/m}$

This gives an empty capacitance of:

$$C = \frac{\varepsilon_0 \varepsilon_r A}{d} = \frac{8.8541878128 \times 10^{-12} \times 1 \times 0.000345}{0.015} = \boldsymbol{203.65\ fF}$$

2.2.2.2 Capacitor with a pen

To be able to calculate a capacitance with different materials between plates, a segmentation of plates into infinitesimal flat capacitor is used. This technic will be named “Partial-Capacitance Network” in this document. These capacitors are considered in parallel, therefore it is possible to add them.

$$C_{serie} = \sum \Delta C_{xy} = \sum\sum \frac{\varepsilon \Delta x \Delta y}{d}$$

But, for some of these capacitor sections, a discrete stack of different materials is possible. Therefore, the serial capacitor formula is required.

$$C_{parallele} = \sum\sum \frac{1}{\sum \frac{1}{C_z}} = \sum\sum \frac{1}{\sum \frac{\Delta z}{\varepsilon \Delta x \Delta y}}$$

So, if the discrete paralleled capacitance association is transformed into an integral form, the equation below is obtained.

$$\sum\sum \frac{1}{\sum \frac{\Delta z}{\varepsilon \Delta x \Delta y}} \rightarrow \iint \frac{1}{\sum \frac{\Delta z}{\varepsilon dx dy}}$$

The injector pen and the cartridge are considered centered in the device, therefore the device has two symmetry axes and only a quarter of the model can be considered as presented in Figure 26 and Figure 34. This is representative of the complete capacitance because the equivalent electrical model is $C = \frac{C_A \times C_C}{C_A + C_C} + \frac{C_B \times C_D}{C_D + C_D}$. Due to the symmetry, each quarter of the capacitor is equal to the others $C_A = C_B = C_C = C_D$, therefore: $C = \frac{C_A \times C_A}{2 \times C_A} + \frac{C_A \times C_A}{2 \times C_A} = C_A$

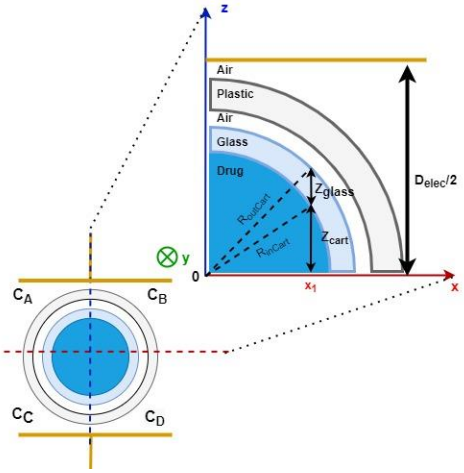

Figure 26: Two flat electrodes with a cartridge

Therefore, the capacitance value can be written as the electrode integral along x and y and series capacitor corresponding to the different materials layer that the electric field will go through.

$$C = \iint_{[0;0]}^{[\frac{W}{2};L]} \frac{dxdy}{\frac{\Delta z_{air1}}{\varepsilon_{air}} + \frac{\Delta z_{Holder}}{\varepsilon_{plastic}} + \frac{\Delta z_{air2}}{\varepsilon_{air}} + \frac{\Delta z_{Cartridge}}{\varepsilon_{glass}} + \frac{\Delta z_{drug}}{\varepsilon_{drug}}}$$

The thickness of the different layer will depend on their radial position. Therefore, by using Pythagoras equations and the radius of the different layers, it is possible to obtain the thickness of materials for all radial positions. When the radial position is larger than a material radius, the square root will give an imaginary result and by selecting the real value, the results will be equal to 0 mm.

$$\begin{cases} \Delta z_{air1} = real\left(\frac{d}{2} - \sqrt[2]{{r_{outHolder}}^2 - x^2}\right) \\ \Delta z_{Holder} = real\left(\sqrt[2]{{r_{outHolder}}^2 - x^2} - \sqrt[2]{{r_{inHolder}}^2 - x^2}\right) \\ \Delta z_{air2} = real\left(\sqrt[2]{{r_{inHolder}}^2 - x^2} - \sqrt[2]{{r_{outCart}}^2 - x^2}\right) \\ \Delta z_{Glass} = real\left(\sqrt[2]{{r_{outCart}}^2 - x^2} - \sqrt[2]{{r_{inCart}}^2 - x^2}\right) \\ \Delta z_{drug} = real\left(\sqrt[2]{{r_{inCart}}^2 - x^2} - 0\right) \end{cases}$$

The y integration is solved easily because no geometries or domain variation occurs along the y axis which is the depth of the device.

$$C = L \times \int_0^{W/2} \frac{dx}{\frac{\Delta z_{air1}}{\varepsilon_{air}} + \frac{\Delta z_{Holder}}{\varepsilon_{plastic}} + \frac{\Delta z_{air2}}{\varepsilon_{air}} + \frac{\Delta z_{Cartridge}}{\varepsilon_{glass}} + \frac{\Delta z_{drug}}{\varepsilon_{drug}}}$$

With this equation, the x integration is a little bit more complex due to the presence of the x factors inside the square roots of the Δz. The results are therefore computed by the mathematical software Octave®. The difference between full and empty pen is done by changing the ε_{drug} into ε_{air}. The values of the model are presented in Table 3.

Table 3: Flat electrode model parameters

Physical		
Electric permittivity	8.85E-12	F/m
Relative Air permittivity	1	-
Relative Water permittivity	80.4	-
Relative Plastic permittivity	2.5	-
Relative Glass permittivity	4	-
Injector pen geometry		
Cartridge inner radius	0.00475	m
Cartridge outer radius	0.00575	m
Holder inner radius	0.00625	m
Holder outer radius	0.00725	m
Drug length	0.023	m
Real drug volume	1630	µL
Theoretical drug volume	1500	µL
Cap geometry		
Electrode distance	**0.015**	**m**
Electrode width	**0.015**	**m**

The results obtained by varying the electrode distance and the electrode width are presented in Figure 27 and Figure 28

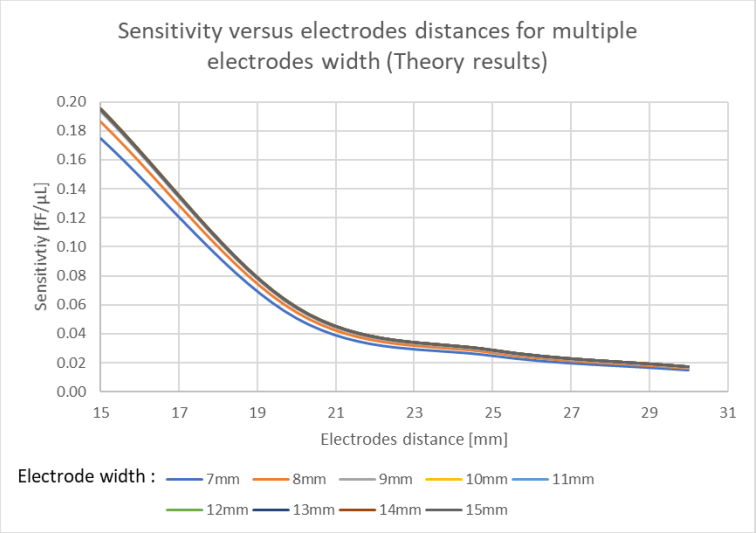

Figure 27: Mathematical model of two flat electrode - electrode distance impact on sensitivity

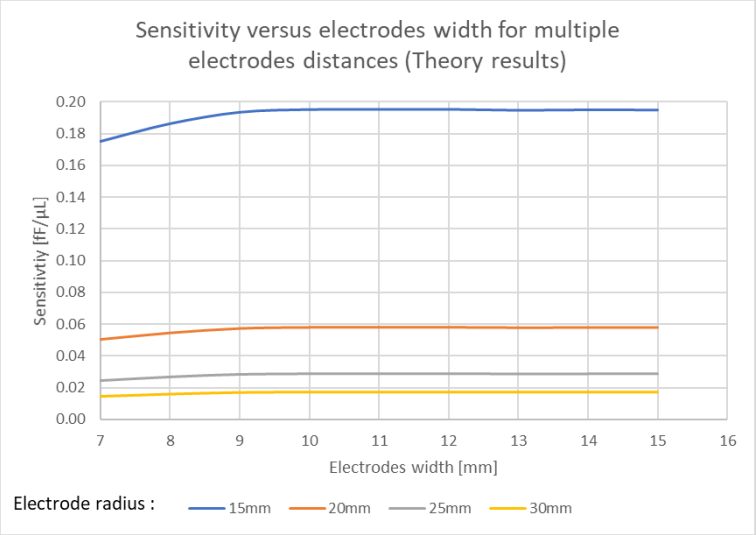

Figure 28: Mathematical model of two flat electrode - Electrode width impact on sensitivity

The electrode distance has a strong impact on the sensitivity. The closer are the electrode from each other, the higher is the sensitivity. The electrode width has as a lower impact on the sensitivity. It can be noticed that the sensitivity increases slightly until the electrode width is larger than the cartridge radius. Afterthat, the sensitivity varies less because almost no variation occurs for the other injector pen material layers between an empty and a full pen.

The results obtained for the value presented in Table 3 is 265.2 fF for an empty pen and 582.8 fF for a full pen. By considering the real drug volume, which is 1630 µL, the sensitivity found is **0.195 fF/µL**, which correspond to 1.95 fF/IU of insulin.

2.2.3 Simulation

2.2.3.1 Empty device

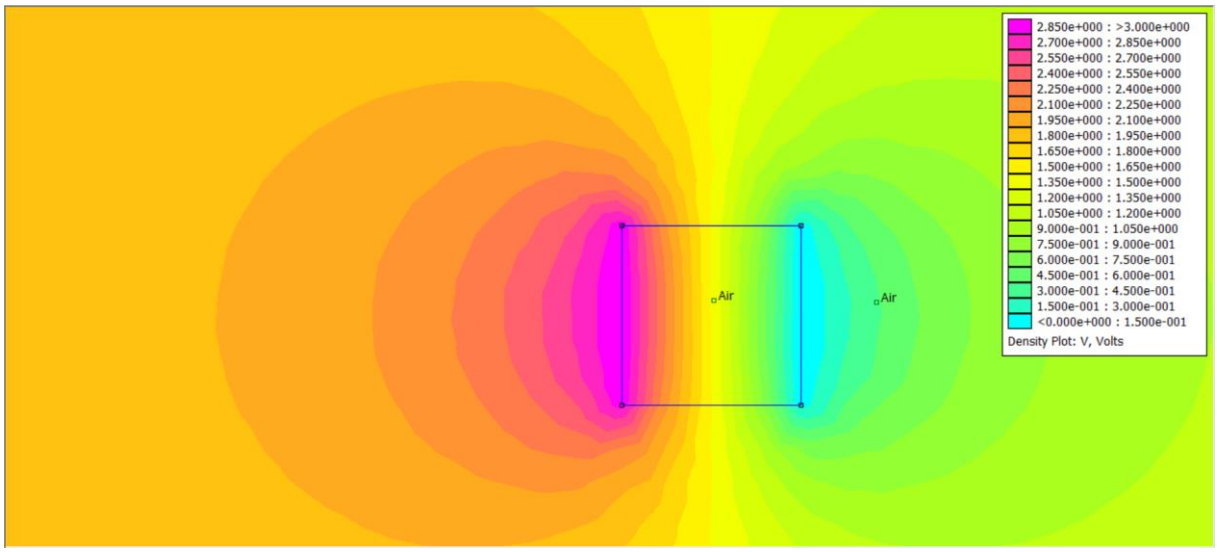

Figure 29: Empty device with two flat electrode

By integrating the charge density in the volume, the simulation software FEMM® can provide the stored energy [W]. From this stored energy, it is possible to obtain the Capacitance using $C = 2\frac{W}{U^2}$ and by knowing the difference of potential between the two plates, which is $U = 3\,V$. For this model, the stored energy inside the electrode area is 0.943 pJ. Then, the capacitance is:

$$C = 2 \times \frac{E_{stored}}{U^2} = 2 \times \frac{0.943E^{-12}}{3^2} = 209.57\,fF$$

Which is close from the theoretical value of $203.65\,fF$ from section 2.2.2.1

2.2.3.2 Device with cartridge

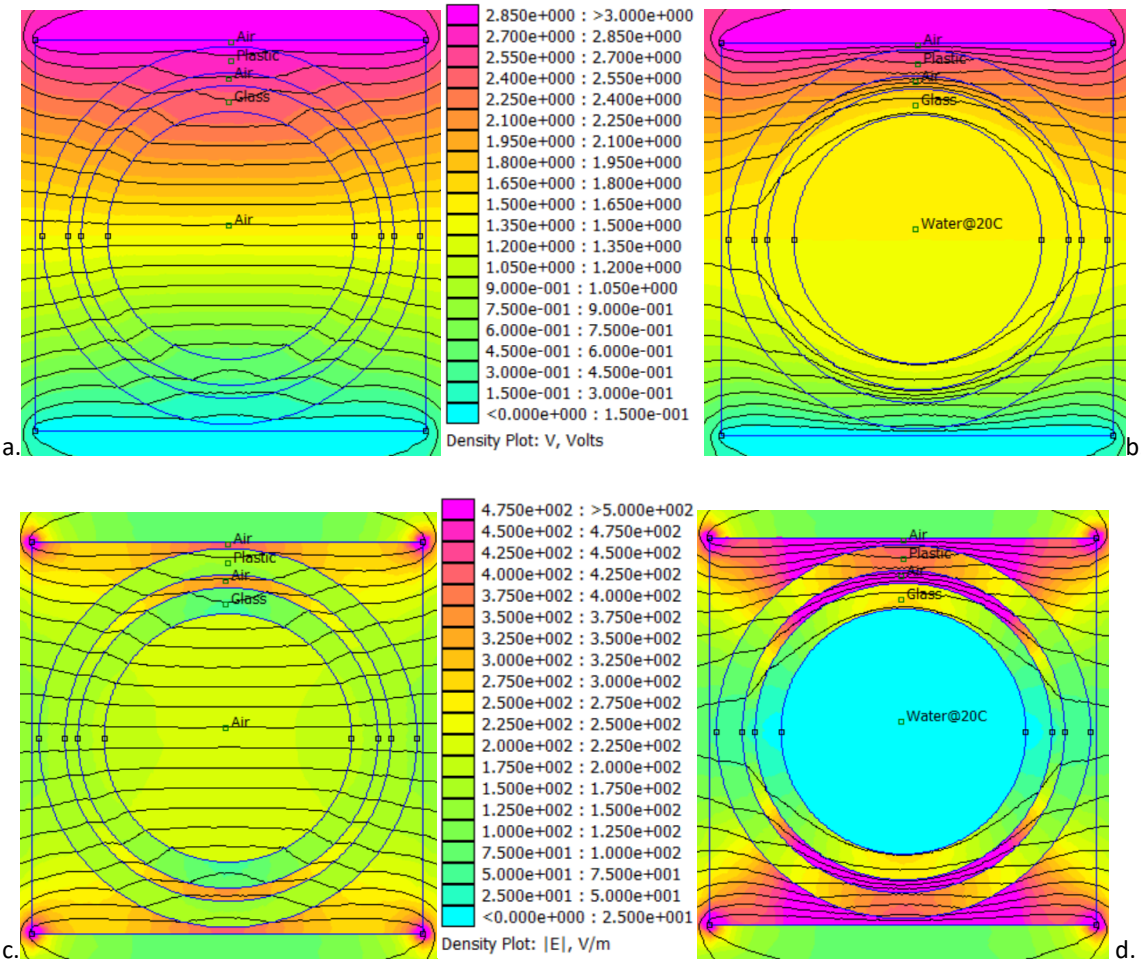

Figure 30 : Two flat electrode with cartridge simulation - **Empty pen** a. Voltage plot, b. Electric field plot – **Full pen** c. Voltage plot, d. Electric field plot

The electric field is stronger outside the water column due to the high relative dielectric permittivity of the water / drug solution (close to 80). Inside the water, the voltage drops over distance is very small. It is graphically visible, in Figure 30, the voltage drop is represented by the number of iso-line (every 0.16 V) in the two-top figure. The figure a. has 12 iso-line in the cartridge filled by air, this corresponds to a voltage drop of ~2 V. Compared to image b, no voltage iso-line are present in the cartridge which indicate that the voltage drop is lower than 0.16 V.

The simulated sensitivity of the device can be computed using the capacitance of the full and the empty pen and the real drug volume which is $1630\ \mu L$. The results obtained are presented hereafter in Figure 31 and Figure 32.

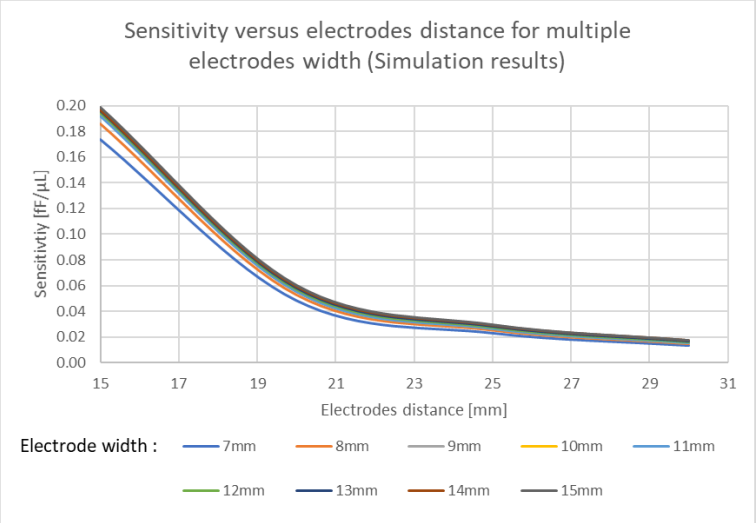

Figure 31: Simulation results of two flat electrode - Electrode distance versus sensitivity

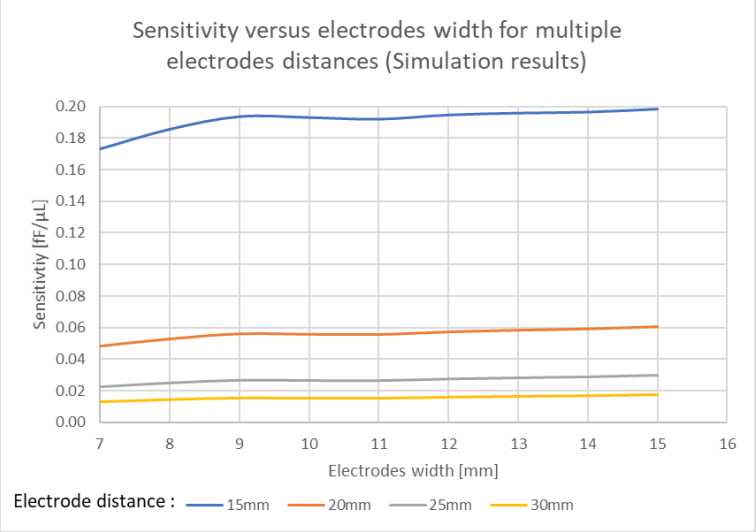

Figure 32: Simulation results of two flat electrode - Electrode width versus sensitivity

The curves seem to have the same behaviors as the mathematical model. The sensitivity is more sensible to the variation of the electrode distance than the electrode width. Thus, the best sensitivity can be reached with the lowest possible electrode distance and the largest electrode width. The capacitance obtained for an empty pen is 313.4 fF and for a full pen 637.1 fF, by considering the real volume of 1630 µL, the simulated sensitivity is ***0.199 fF/µL*** which is close to the theoretical values 0.195 fF/µL.

2.2.4 Discussion

As presented in Figure 33, the results obtain with theory and simulation seem well aligned. The best configuration possible seems to be when the electrode distance is equal to 15 mm and with a width of 15 mm. The theoretical and simulated sensitivity obtained is $\sim \mathbf{0.2}\ \boldsymbol{fF/\mu L}$ which correspond to 2 fF/IU insulin. The difference between simulation and theory comes from the fact that the simulation tools consider the whole electric field while the theory considers only the local electric field. Nevertheless, the difference is small, and the theory can be considered as a good approximation of the capacitance value.

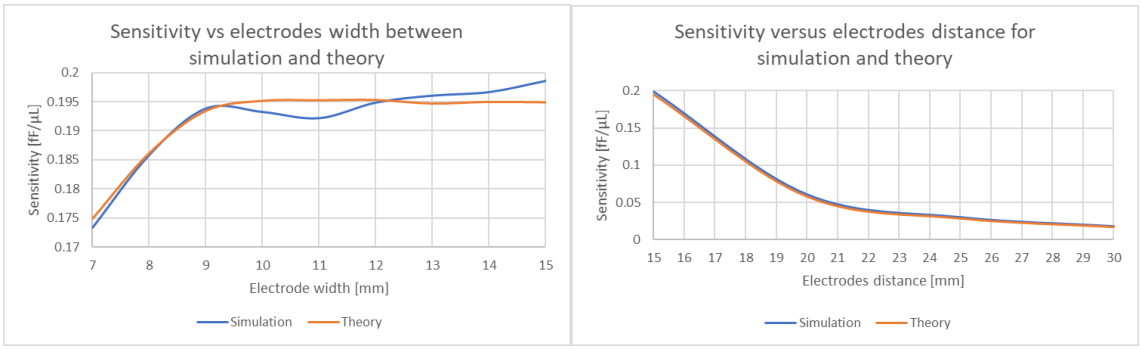

Figure 33 : Comparison between simulation and theory results

2.2.5 Conclusion

In this section, theoretical calculation and finite element simulation have been conducted to find the best possible sensitivity. With a targeted volume detection at 10 µL, the corresponding capacitance variation is approximatively 2 fF which corresponds to the theory and simulation, respectively. This sensitivity is quite low considering the sensitivity obtained with semi-cylindric electrodes presented in section 2.3 and all the vulnerabilities presented in Chapter 3. Moreover, the form factor of the device will be impacted due to the rectangular shape of the electrode, this limits the possibility of reducing the size of the cap into a slim cylindrical shape to meet the user handling requirement. Therefore, this basic measurement method has been rejected for the device development.

2.3 Two semi-cylindrical electrodes

2.3.1 Introduction

To optimize the electric field inside the volume of drug and improve the cap form factor, semi-cylindrical electrodes have been studied. The main difficulty of this configuration is that the electric field is not uniform. Effectively, where the electrodes are closer, the electric field is stronger. This leads to some complication in theoretical mathematical analysis. In the next section two theoretical methods will be presented, then simulation and tests will be performed to consolidate the data.

2.3.2 Theory

2.3.2.1 Partial-Capacitance network methods

In [77, 75, 73, 74], two semi-cylindrical electrode shape capacitor has been studied, and mathematics have been presented to calculate the capacitance using an infinite number of paralleled flat electrode following the curve of the real electrode. This technic is called "Partial-Capacitance Network" in this document. The injector pen and the cartridge are considered centered in the device, therefore the device has two symmetry axes and only a quarter of the model is considered as presented in Figure 34. This is representative of the full capacitance, because the equivalent electrical model is $C = \frac{C_A \times C_C}{C_A + C_C} + \frac{C_B \times C_D}{C_D + C_D}$ and due to the symmetry each quarter is equal to the other $C_A = C_B = C_C = C_D$.

Therefore: $C = \frac{C_A \times C_A}{2 \times C_A} + \frac{C_A \times C_A}{2 \times C_A} = C_A$

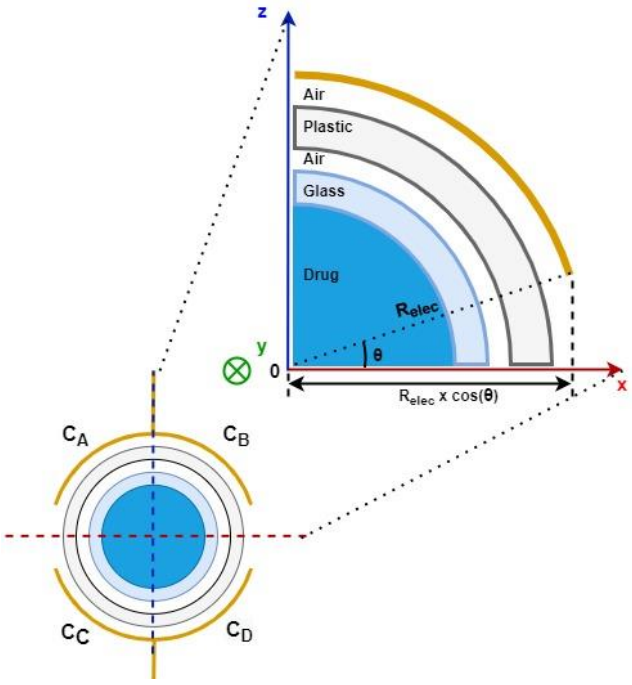

Figure 34 : Semi-cylindrical model

So, by using the equation presented in 2.2.2.2, an infinite number of electrodes is considered. Therefore, the series can be transformed into integral except for Δz, because the distance between the plates will be composed by a discreet number of materials and can be split into a finite series of length

$$C = \sum\sum \frac{1}{\sum \frac{\Delta z}{\varepsilon \Delta x \Delta y}} \rightarrow \iint \frac{1}{\sum \frac{\Delta z}{\varepsilon dx dy}}$$

The limits of the integral will be the origin and the drug length for dy. For dx the limits will be the origin and the projection on x-axis of the starting points of the electrode as it is presented in Figure 34.

$$C = \iint_{[0;0]}^{[R_{elec}\times\cos(\theta);L]} \frac{1}{\frac{\Delta z_{air1}}{\varepsilon_{air}dxdy} + \frac{\Delta z_{Holder}}{\varepsilon_{plastic}dxdy} + \frac{\Delta z_{air2}}{\varepsilon_{air}dxdy} + \frac{\Delta z_{Cartridge}}{\varepsilon_{glass}dxdy} + \frac{\Delta z_{drug}}{\varepsilon_{drug}dxdy}}$$

The $dxdy$ is common to all, therefore it can be moved to the numerator.

$$C = \iint_{[0;0]}^{[R_{elec}\times\cos(\theta);L]} \frac{dxdy}{\left(\frac{\Delta z_{air1}}{\varepsilon_{air}} + \frac{\Delta z_{Holder}}{\varepsilon_{plastic}} + \frac{\Delta z_{air2}}{\varepsilon_{air}} + \frac{\Delta z_{Cartridge}}{\varepsilon_{glass}} + \frac{\Delta z_{drug}}{\varepsilon_{drug}}\right)}$$

The Δz_x can be expressed with the radius of the different interfaces and the position x, by using Pythagoras equations. Only the real parts are considered, because when $x > r_x$, the area is finished, and the results give an imaginary number with a null real part. In Figure 35, an example is given for the glass thickness for a specific x, then the equation for this configuration is given.

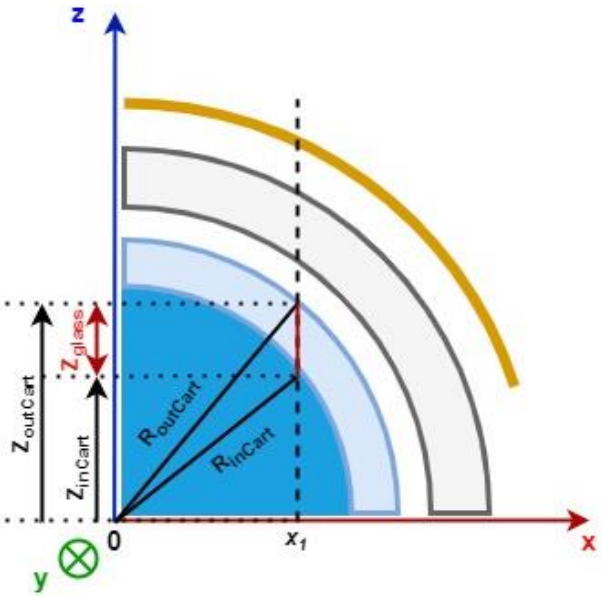

Figure 35: Semi-cylindrical model - Δz example

$$\Delta z_{glass} = z_{outCart} - z_{inCart} = real\left(\sqrt[2]{{r_{outCart}}^2 - {x_1}^2} - \sqrt[2]{{r_{inCart}}^2 - {x_1}^2}\right)$$

So, by applying this method to the other distances

$$\begin{cases} \Delta z_{air1} = real\left(\sqrt[2]{{r_{elec}}^2 - x^2} - \sqrt[2]{{r_{outHolder}}^2 - x^2}\right) \\ \Delta z_{Holder} = real\left(\sqrt[2]{{r_{outHolder}}^2 - x^2} - \sqrt[2]{{r_{inHolder}}^2 - x^2}\right) \\ \Delta z_{air2} = real\left(\sqrt[2]{{r_{inHolder}}^2 - x^2} - \sqrt[2]{{r_{outCart}}^2 - x^2}\right) \\ \Delta z_{Glass} = real\left(\sqrt[2]{{r_{outCart}}^2 - x^2} - \sqrt[2]{{r_{inCart}}^2 - x^2}\right) \\ \Delta z_{drug} = real\left(\sqrt[2]{{r_{inCart}}^2 - x^2} - 0\right) \end{cases}$$

The first integration will be done on dy because no material and geometry change occur along the device center axis.

$$C = \iint_{[0;0]}^{[R_{elec}\times\cos(\theta);L]} \frac{dxdy}{\left(\frac{\Delta z_{air1}}{\varepsilon_{air}} + \frac{\Delta z_{Holder}}{\varepsilon_{plastic}} + \frac{\Delta z_{air2}}{\varepsilon_{air}} + \frac{\Delta z_{Cartridge}}{\varepsilon_{glass}} + \frac{\Delta z_{drug}}{\varepsilon_{drug}}\right)}$$

Which gives the equation hereafter, the x integration is more complex. Therefore, the result of this integral is computed using Octave®.

$$C = L \times \int_{0}^{R_{elec}\times\cos(\theta)} \frac{dx}{\left(\frac{\Delta z_{air1}}{\varepsilon_{air}} + \frac{\Delta z_{Holder}}{\varepsilon_{plastic}} + \frac{\Delta z_{air2}}{\varepsilon_{air}} + \frac{\Delta z_{Cartridge}}{\varepsilon_{glass}} + \frac{\Delta z_{drug}}{\varepsilon_{drug}}\right)}$$

To be able to characterize the theoretical sensitivity of the systems, the cartridge is firstly considered full, then the cartridge is considered empty by replacing $\frac{\Delta z_{drug}}{\varepsilon_{drug}}$ by $\frac{\Delta z_{drug}}{\varepsilon_{air}}$. Hereafter are presented the values considered to compute the capacitance

Table 4 : Semi-cylindrical electrode model parameters

Physical		
Electric permittivity	8.85E-12	F/m
Relative Air permittivity	1	-
Relative Water permittivity	80.4	-
Relative Plastic permittivity	2.5	-
Relative Glass permittivity	4	-
Injector pen geometry		
Cartridge inner radius	0.00475	m
Cartridge outer radius	0.00575	m
Holder inner radius	0.00625	m
Holder outer radius	0.00725	m
Drug length	0.023	m
Real drug volume	1630	µL
Theoretical drug volume	1500	µL
Cap geometry		
Electrode radius	**0.00075**	**m**
Electrode angular width	**160**	**°**

By using Octave®, the impact of some variables can be visualized. The impact on the sensitivity of the *Electrode radius* and the *electrode angular width* has been studied.

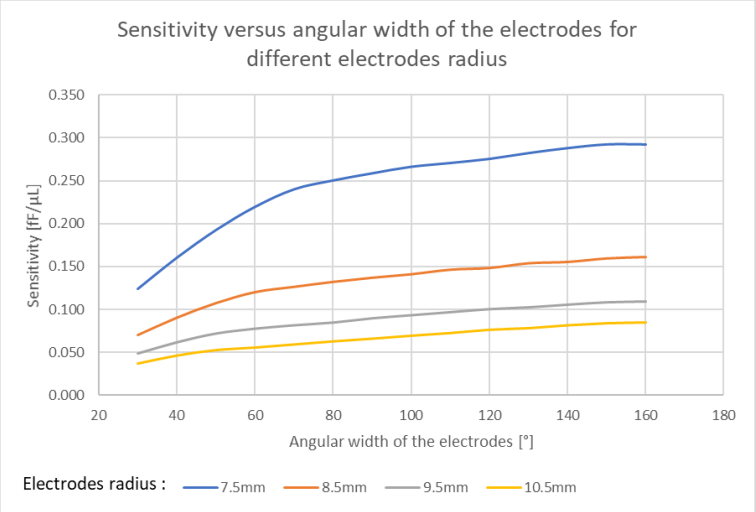

Figure 36 : Mathematical model of semi-cylindrical electrode - Radius impact on sensitivity

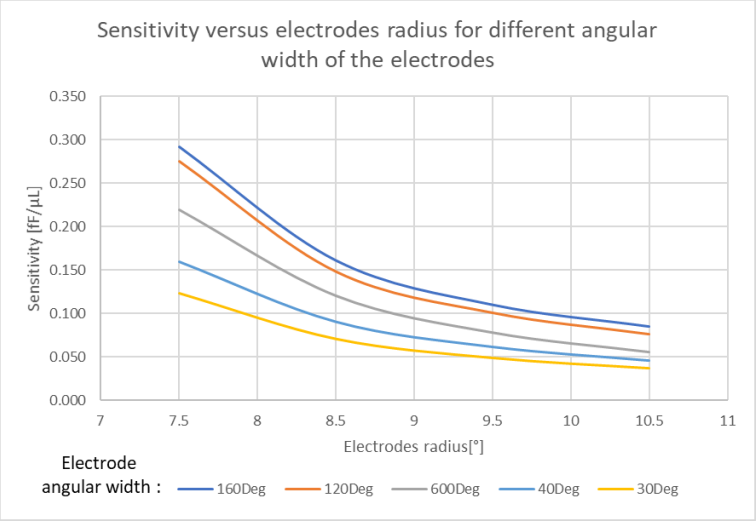

Figure 37 : Mathematical model of semi-cylindrical electrode - Electrode angular width

According Figure 36 and Figure 37, the best sensitivity is obtained with the widest electrode angular width, which is 160°, and the smallest electrode radius, which is 7.5 mm. The cartridge holder has a radius of 7.25 mm, therefore that left 0.25 mm of mechanical clearance around the holder. The results obtained with the value presented in Table 4 are 270.91 fF for an empty pen and 746.8 fF for a full pen. By considering the real drug volume, which is 1630 µL the theoretical sensitivity possible is **0.292 fF/µL** which correspond to 2.92 fF/IU insulin.

2.3.2.2 Conformal mapping

The conformal mapping transforms the geometric domains to facilitate the problem resolution as presented in [78, 79, 80, 81]. The problem can be defined in an imaginary plane $z = x + iy$, each element is considered circular and centered. The electric field is considered inside the electrode circle to respect the 2D Laplace's equation condition $\frac{\partial^2 V}{\partial^2 x} + \frac{\partial^2 V}{\partial^2 y} = 0$. The third dimension is simplified because the depth geometry and materials are constant, therefore the electric field is same at all depth in the interval $[0 : L]$

So, the cercles equation are $z(x, y) = r \times e^{i\theta}$ with

$\theta_{up} \quad = [10° \; 170°] \rightarrow Top\ electrode\ angular\ size$
$\theta_{down} \quad = [190° \; 350°] \rightarrow Bottom\ electrode\ angular\ size$
$\theta \quad = [0° \; 360°] \rightarrow Other\ domains\ are\ full\ cercles$

This gives the model hereafter, the colors are respected until the end of this section

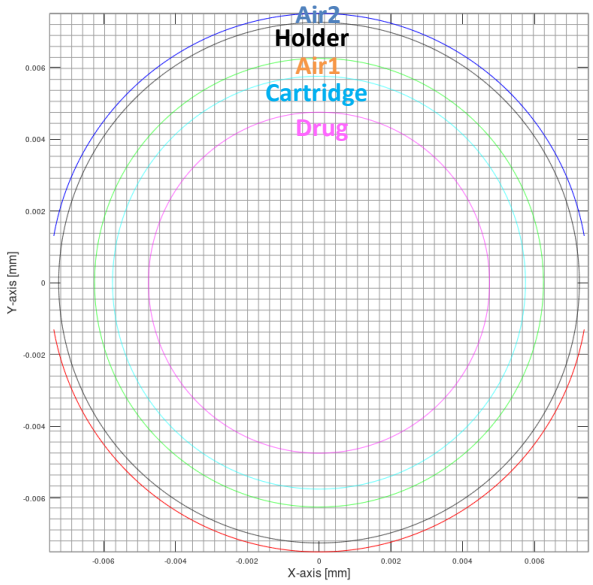

Figure 38 : 2D of the smart pen cap with a pen inside

The first step is to use the Möbius transformation on the electrode circles to project the area of the device into a half infinite planes

$$w(u,v) = \frac{r_{elec} + z}{r_{elec} - z} = \frac{r_{elec} + r \times e^{i\theta}}{r_{elec} - r \times e^{i\theta}}$$

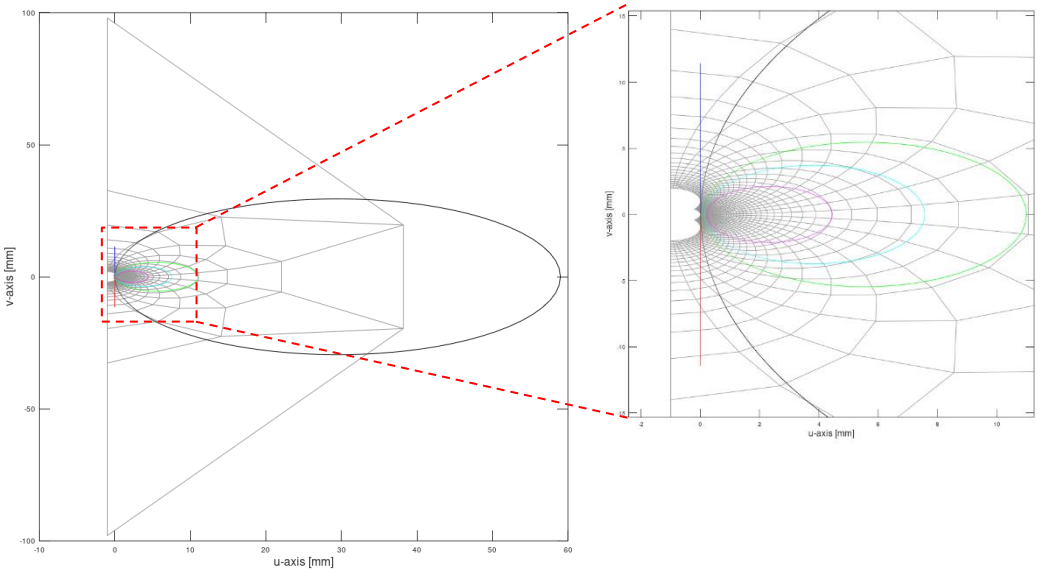

Figure 39: Möbius transformation of the device

Then, the domain is fold back by using a logarithm operator

$$s = \ln w = \ln\left(\frac{r_{elec} + z}{r_{elec} - z}\right) = \ln\left(\frac{r_{elec} + r \times e^{i\theta}}{r_{elec} - r \times e^{i\theta}}\right) = \ln\left(\frac{r_{elec} + r \times e^{i\cos^{-1}\left(\frac{x}{r_{Elec}}\right)}}{r_{elec} - r \times e^{i\cos^{-1}\left(\frac{x}{r_{Elec}}\right)}}\right)$$

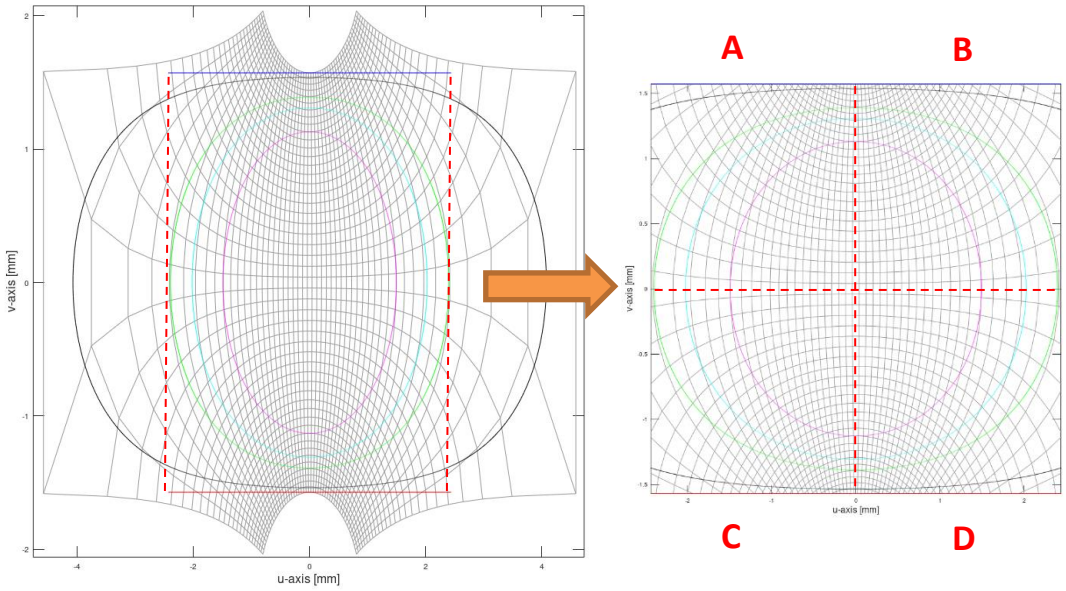

Figure 40 : Fold back of the Möbius transformation of the smart pen cap

In the Figure 40, two symmetries axis appear. There is only a quarter of the model considered as presented in Figure 41.

$$C = \frac{C_A \times C_C}{C_A + C_C} + \frac{C_A \times C_C}{C_A + C_C} \rightarrow C_A = C_B = C_C = C_D \rightarrow C = \frac{C_A \times C_A}{C_A + C_A} + \frac{C_A \times C_A}{C_A + C_A} = C_A$$

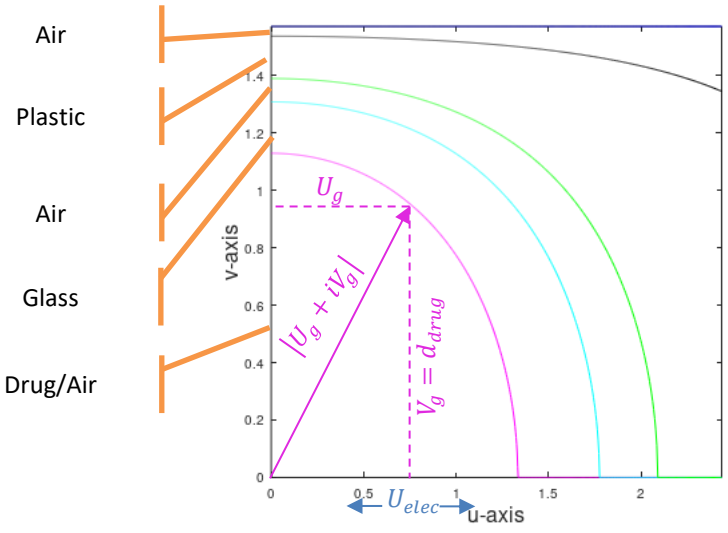

Figure 41 : Quarter of the domain

Then, the capacitance can be expressed according:

$$C = \sum\sum \frac{1}{\sum \frac{\Delta z}{\varepsilon \Delta x \Delta y}} \rightarrow \iint \frac{1}{\sum \frac{\Delta z}{\varepsilon dxdy}} = \iint \frac{dxdy}{\sum \frac{\Delta z}{\varepsilon}} = L \times \int \frac{dx}{\sum \frac{\Delta z}{\varepsilon}}$$

With $\Delta z(x) = d_1(x) - d_2(x)$. The $d_n(x)$ can be obtained using Pythagoras equations which take the square of the modulus of the domain limit of interest. Then, this results is subtracted by the square of the real parts of the electrode size. This subtraction is placed into a square root and only the real parts are considered because it became imaginary when the real variables of the electrode's domain is larger than the modulus of the domain limit of interest. This indicates that the real variable is out the interest area.

$$d_n(x) = Re\sqrt[2]{abs(s_n)^2 - real(S_{elec})^2}$$

$$d_n(x) = Re\sqrt[2]{abs\left(\ln\left(\frac{r_{elec} + r_n \times e^{i\cos^{-1}\left(\frac{x}{r_{elec}}\right)}}{r_{elec} - r_n \times e^{i\cos^{-1}\left(\frac{x}{r_{elec}}\right)}}\right)\right)^2 - real\left(\ln\left(\frac{r_{elec} + r_{elec} \times e^{i\frac{\pi}{2}}}{r_{elec} - r_{elec} \times e^{i\frac{\pi}{2}}}\right)\right)^2}$$

The different distances are obtained by replacing the r_n by the radius of the domain of interest. Then by subtracting each distance, the thickness of each materials is obtained as presented in Figure 42.

$$\begin{cases} \Delta z_{drug} = d_{drug}(x) - 0 \\ \Delta z_{cartridge} = d_{cartridge}(x) - d_{drug}(x) \\ \Delta z_{air1} = d_{inHolder}(x) - d_{cartridge}(x) \\ \Delta z_{holder} = d_{outHolder}(x) - d_{inHolder}(x) \\ \Delta z_{air2} = d_{elec}(x) - d_{outHolder}(x) \end{cases}$$

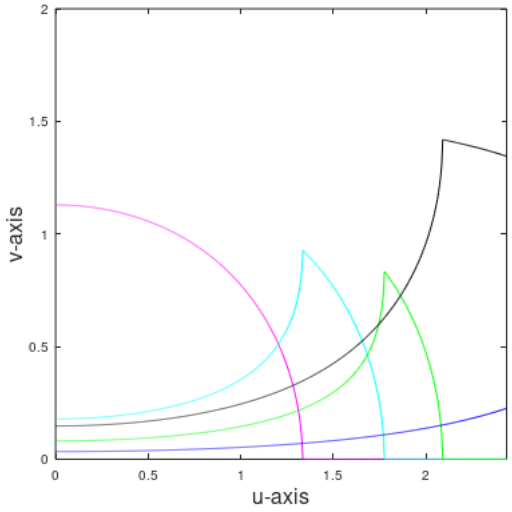

Figure 42: Thickness of each materials along u-axis

Therefore, the $\Delta z(x)$ can be replaced in the equation below with Δu the partial-size of the electrode $\Delta u = \frac{max(real(s_{elec}))}{Samples\ number}$

$$C = L \times \sum \frac{\Delta u}{\frac{\Delta z_{drug}}{\varepsilon_{drug}} + \frac{\Delta z_{cartridge}}{\varepsilon_{glass}} + \frac{\Delta z_{air1}}{\varepsilon_{air}} + \frac{\Delta z_{holder}}{\varepsilon_{plastic}} + \frac{\Delta z_{air2}}{\varepsilon_{air}}}$$

A first approach is using discrete methods and calculate the capacitance for a finite number of samples equals to 1000 using Octave® and the script in "Appendix: Conformal mapping Script". This sample rate is a compromise between 10 000 samples which take too much computing times and 100 samples which is too low to have stable results. The capacitance variation along the u-axis is presented in Figure 43 for a full and an empty pen.

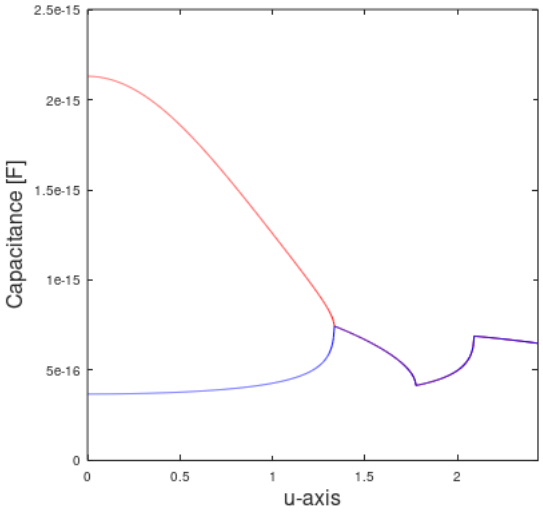

Figure 43: Discrete solving of the conformal mapping for a full and empty pen

By considering the device with an electrode's angular width of 160° and an electrode radius of 7.5 mm, the capacitances obtained are 1428.2 fF for a full pen and 450.5 fF for an empty pen. Therefore, the sensitivity for a volume of 1630 µL is $\mathbf{0.599}\ \boldsymbol{fF/\mu L}$ which corresponds to 5.99 $fF/dose$ of insulin.

Other method using the integral computation on Octave® with the script in "Appendix: Conformal mapping Script", therefore the sum operator can be replaced by the integral form in the equation below.

$$C = L \times \int \frac{dx}{\frac{\Delta z_{drug}}{\varepsilon_{drug}} + \frac{\Delta z_{cartridge}}{\varepsilon_{glass}} + \frac{\Delta z_{air1}}{\varepsilon_{air}} + \frac{\Delta z_{holder}}{\varepsilon_{plastic}} + \frac{\Delta z_{air2}}{\varepsilon_{air}}} \qquad \textit{(Eq 1)}$$

By considering the device as before, with an electrode's angular width of 160° and an electrode radius of 7.5 mm, the capacitances obtained are 947.1 fF for a full pen and 185.4 fF for an empty pen. Therefore, the sensitivity for a volume of 1630µL is $\mathbf{0.467}\ \boldsymbol{fF/\mu L}$ which correspond to $4.67\ fF/dose$ of insulin.

The mathematical methods are compared in Figure 44. For reference, the results obtained in 2.3.2.1 (partial capacitance network) is plotted in grey. First observation is that the curves are aligned in the first part of the graphs. But for large angular electrode, the conformal mapping technic does not have the flat section as the partial capacitance network. Therefore, the sensitivity is almost double for conformal methods compared to the partial capacitance network technics. Then, the two conformal mapping methods have been compared. Even if they have same behaviors, a discrepancy appears for large electrode angular width that could be due to the edge limits and samples number. The simulations results will be compared to these theoretical results.

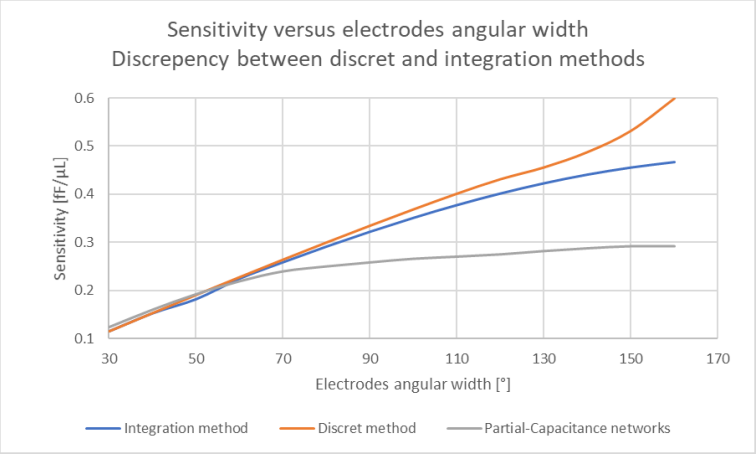

Figure 44: Mathematics methods results for impact of the electrode angular width

2.3.3 Simulation

To corroborate the results obtained with the mathematical models, simulation have been realized with the full model of the smart pen cap and the injector pen. The same variable parameters have been analyzed which are the electrode radius and the angular width of the electrode. The simulation results for a device with an electrode radius at 7.5 mm and electrode angular width of 160° are presented in Figure 45.

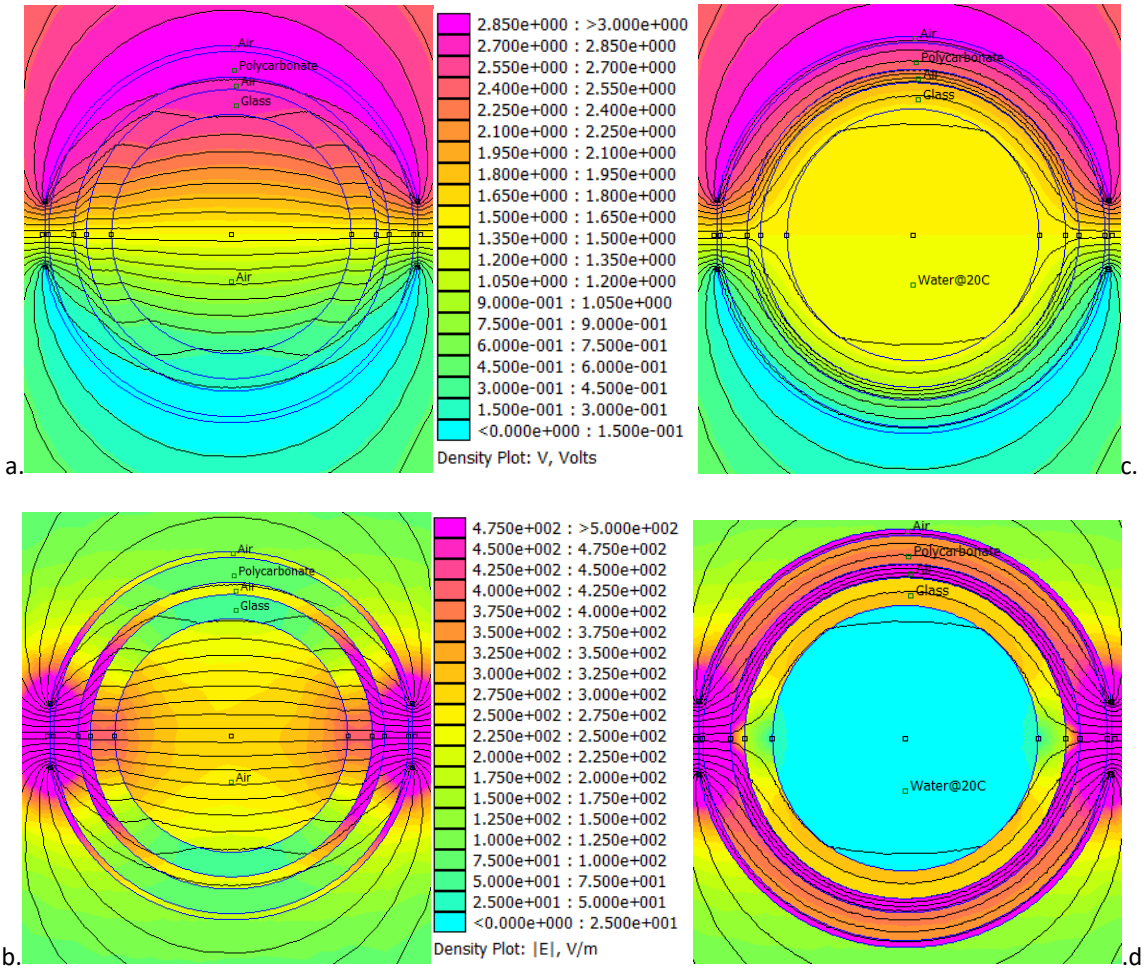

Figure 45: Semi-cylindrical electrode with iso-voltage lines - **Empty pen** a. Voltage plot, b. Electric field plot – **Full pen** c. Voltage plot, d. Electric field plot

Again, the electric field is stronger outside the water column due to the high dielectric permittivity of the water / drug solution. I.e., inside the water, the voltage drops over distance is very small. It is graphically visible that the water column is effectively decreasing the electrode distance, thereby increasing the capacitance.

By integrating the charge density in the volume, the software can provide the stored energy [W]. From this stored energy, it is possible to obtain the Capacitance using $C = 2\frac{W}{U^2}$ and by knowing the difference of potential between the two plates, which is $U = 3\ V$.

The simulated sensitivity of the device can be computed using the Capacitance of the full and the empty pen and the real drugs volume which is $1630\ \mu L$. The results obtained are presented hereafter in Figure 46 and Figure 47.

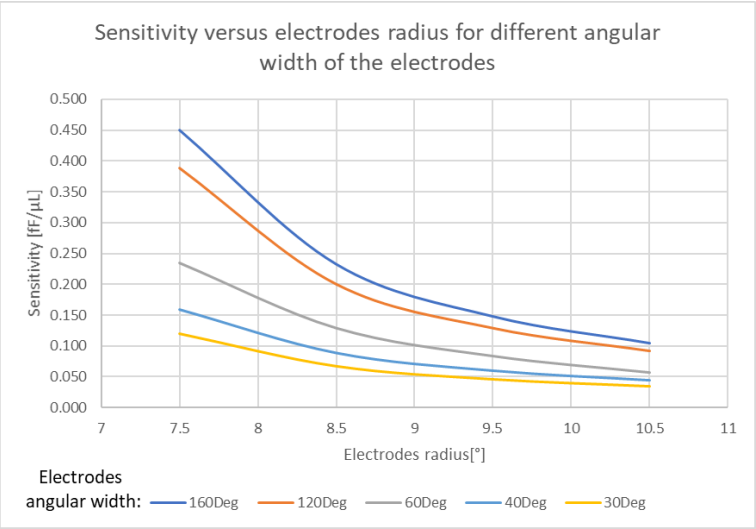

Figure 46: Simulation results of semi-cylindrical electrode - Radius impact on sensitivity

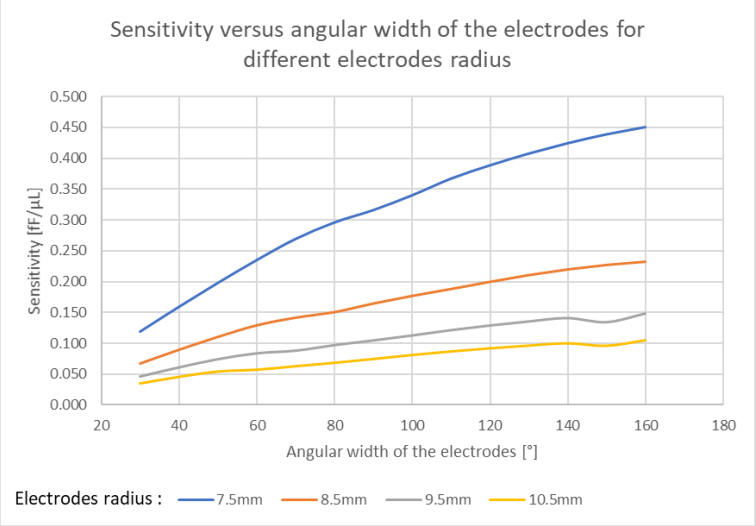

Figure 47: Simulation results of semi-cylindrical electrode - Electrode angular width

The curves seem to have the same behaviors as the mathematical model. The sensitivity is more sensitive to the radius variation than the electrode width. The best sensitivity can be reached with the lowest possible radius and the widest electrode angular width. The best sensitivity possible is ***0.457 fF/µL*** with an electrode radius of 7.5 mm and an electrode angular width of 160°. This is close to the sensitivity obtained with the conformal mapping methods which is $0.467\ \mathrm{fF/\mu L}$

2.3.4 Experiments

Experiments have been conducted to confirm that it is possible to measure the remaining volume of drug inside the injector pen. These devices have been used as proof of concept. In this chapter, the parasitic effects have been reduced as much as possible by fixing the angular position of the pen inside the cap and controlling the climatic variation.

2.3.4.1 Materials and methods

There are materials used to do experiments

- Injection pen
- Precision scale
- Plastic container
- Needles
- 2 x New CR2032 Battery cells
- Computer with a BLE receiver and acquisition software

The experimental protocol is presented in the “Appendix: Protocol Injection” and only the 0° angle between the pen and the cap have been considered to limit the effect of the mechanical tolerance between pen and pen cap.

2.3.4.2 Results

The results obtained during injection have been analyzed, Figure 48 gives examples of pen injections for phase 1 (multiple injection of 120 µL) and phase 2 (multiple injection sequence of 20 µL, 120 µL, 380 µL and 720 µL) injections for one cap

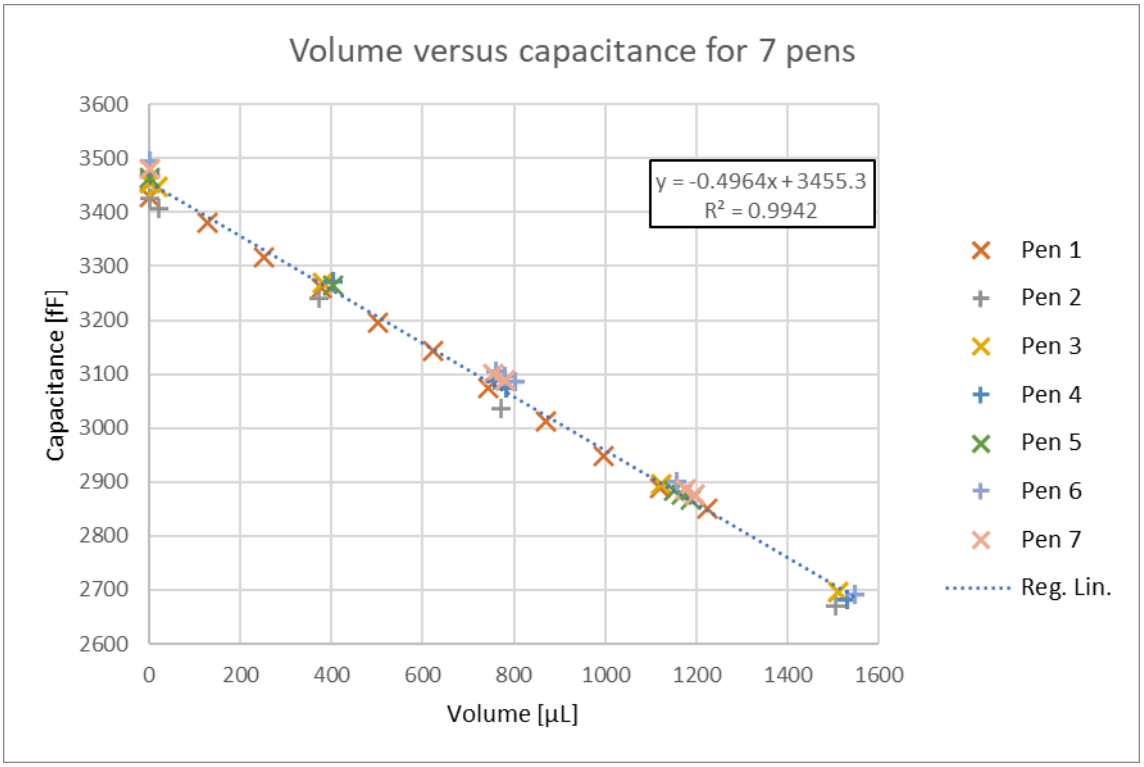

Figure 48: Capacitance versus injection (ejected volume)

The values are converted to µL to compare directly results with weight versus capacitances. A calibration has been done and it follows the protocol presentend in “Appendix: Calibration liquid/capacitance”. This prevents biasing results by auto-calibration effects, i.e., using the acquired data and its regression to convert the capacitance value to volumes.

This calibration of the conversion factor must be done for each different cap. For this smart pen cap, the conversion factor obtained is **0.520fF/µL**

The points obtained seem to be random as it is presented in Figure 49, therefore an analysis considering the points follow a Gaussian repartition have been chosen to represent these data hereafter.

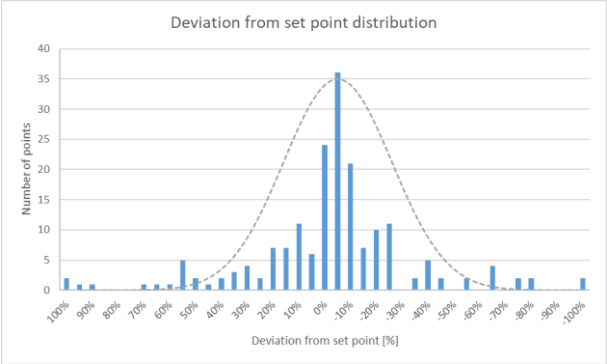

Figure 49: Deviation from set point distribution

The weight injection results are represented in blue in the graphs below and the capacitance injection values are represented in orange. Red dot line represents the set points, and the orange dot points represent limit at ±1 IU which is ±10 µL.

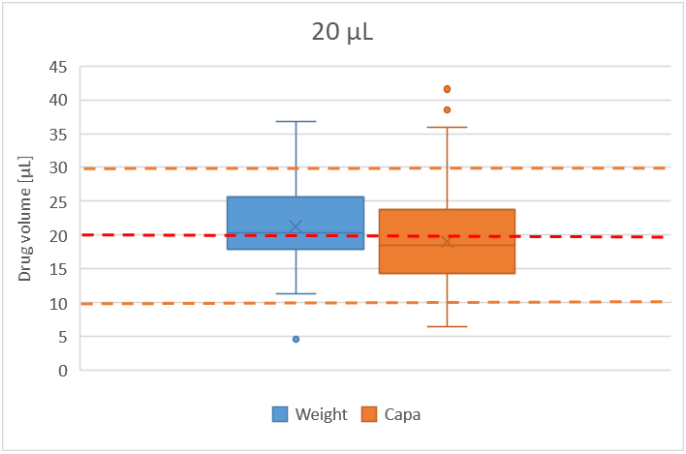

Figure 50: 34 times 20 µL injections

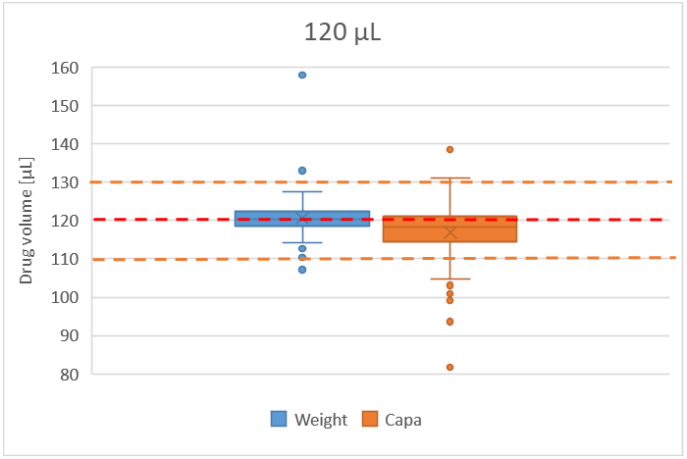

Figure 51: 82 times 120 µL injections

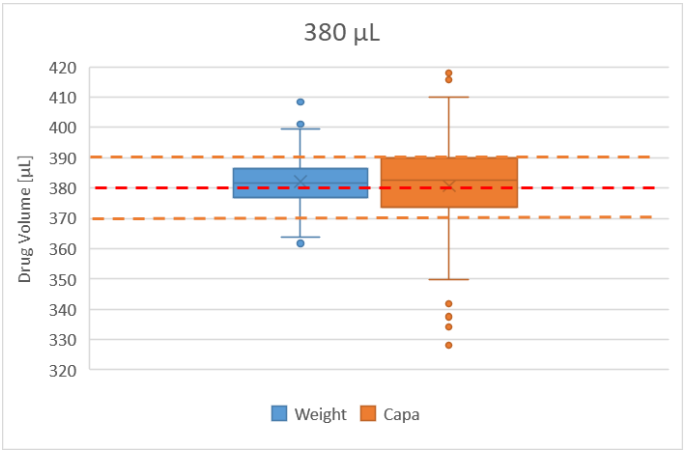

Figure 52: 37 times 380 µL injections

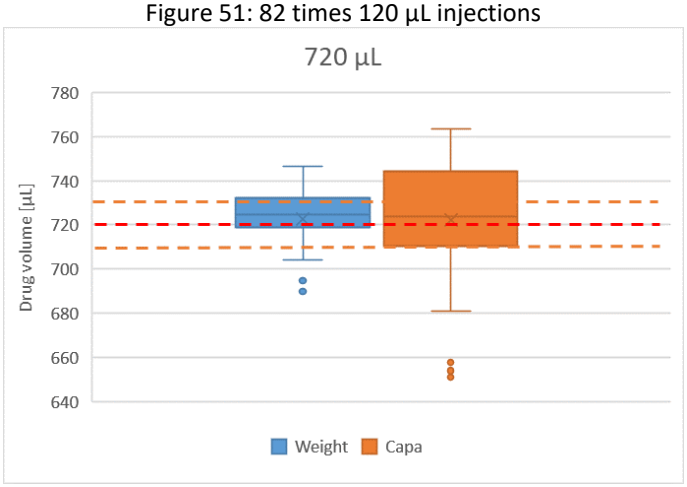

Figure 53: 34 times 720 µL injections

2.3.4.3 Discussion

The first observation is that the conversion factor obtained by calibration **0.520 fF/µL** is quite close to the slope obtained by this data set **0.496 fF/µL** with a good corelation factor R^2 99.5%. The weight data are presented in Table 5, it appears that the weight seems to have a good accuracy and a precision quite close to ± 1 IU (±10 µL) compared to the set points. The accuracy is always negative which tends to proves that the volume is in average under-estimated that correspond to a systematic error.

Table 5 : Weight accuracy and precision for injections

Set points [µL]	*Accuracy*	*Precision [2 STD]*
20	-1.57	13.87
120	-0.66	11.55
380	-2.51	20.58
720	-2.7	28.54

The capacitance values are represented in Table 6, the accuracy deviation from the set points and the precision increase when the injected dose increase. For large doses the precision is larger than 2 IU of insulin which represent 20 µL.

Table 6 : Capacitance accuracy and precision for injections

Set points [µL]	*Accuracy*	*Precision [2 STD]*
20	0.34	16
120	2.84	16.63
380	-2.87	30.58
720	-4.16	50.19

In Figure 54 and Table 7, each capacitance values are compared to the injected volume and the error between these two items have been analyzed. The precision and the accuracy deviation from the ejected weight increase when the injected dose increase. However, the precision is better when the capacitance is compared to the weight (Table 7) than the set points (Table 6) except for the 120 µL injection.

Figure 54: Weight minus capacitance error for different volume injections with fixed angle between pen and pen cap

Table 7: Weight minus capacitance errors for one angle

Set points [µL]	*Accuracy*	*Precision [2 STD]*
20	1.91	12.39
120	3.5	19.8
380	0.02	29.28
720	-1.46	39.65

The ISO11608-1 [82], standard has been created to specify requirements and test methods for needle-based injection systems. This standard is used as reference to compare and qualify injector pens. According to that standard, the injector

pen used corresponds to C categories: multi-dose, and non-replaceable container. So, by applying the two-side dose accuracy limit given in the section 7.4.2.1 of this standard

$$with \begin{cases} DR = 10\ \mu L \rightarrow Minimum\ dialing\ resolution \\ \alpha = DR = 10\ \mu L \rightarrow V_{set} \leq TP \\ \beta = 5\% \end{cases}$$

The transition points between relative error and absolute error is given by:

$$TP = \frac{100 \times \alpha}{\beta} = \frac{100 \times 10}{5} \cong 200\ \mu L$$

Therefore, to find the upper limit (U) and lower limit (L) the values below are considered

$$\text{When} \begin{cases} V_{set} \leq TP \rightarrow \begin{cases} U = V_{set} + \alpha \\ L = V_{set} - \alpha \end{cases} \\ V_{set} > TP \rightarrow \begin{cases} U = V_{set} + \frac{\beta \times V_{set}}{100} \\ L = V_{set} - \frac{\beta \times V_{set}}{100} \end{cases} \end{cases}$$

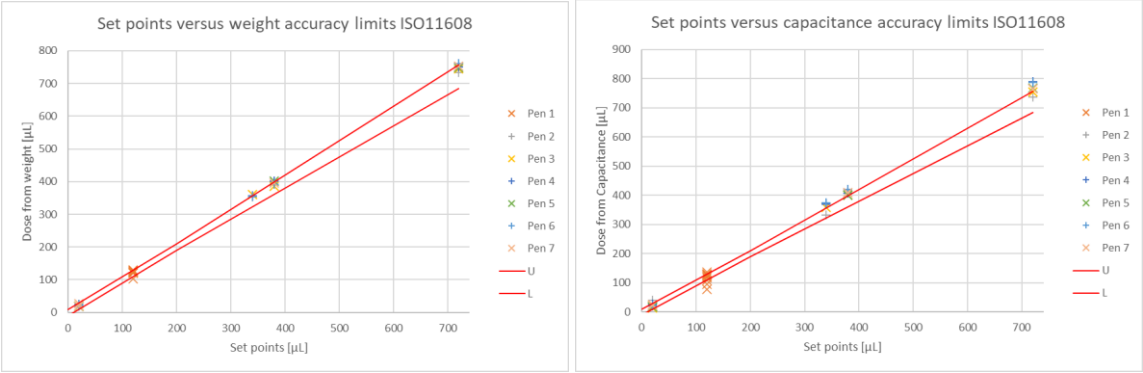

Figure 55 : Injection versus ISO11608 limits

As presented in Figure 55, the points are close to the upper limit of the ISO11608 for weight derived doses. For the capacitances results, it appears that the points are a bit above the upper limits, especially for large injection steps.

2.3.4.4 Conclusion

An under-estimation of the volume has been observed for ejected weight versus the set-points. Therefore, some discrepancy can exist between the injected and remaining volume due to loss in different elements as it is presented in section 3.6 (volume inside needle, lost droplet, bubbles…).

For the capacitance values, the injected volume variation will add error to the sensor errors. An effect appears in Table 6, the precision errors increase with the amount of injected drug, this can be linked to the error between remaining and ejected volume, if the loss volume increase with the injection volume therefore the errors will increase for large dose.

The last analysis tries to remove injection variation by directly comparing the capacitance values to the ejected weight. The capacitance precision is improved except for 120 µL injection. The error due to loss volume is still present because the capacitance values are not compared against the remaining volume.

Finally, results are computed according the ISO11608-1, it appears that the results for capacitance are straddling the upper limits of this standards.

2.3.5 Section Conclusion

In Figure 56, the partial capacitance networks and conformal mapping (discret and integration) are compared to the results obtained with the simulation. It appears that the conformal mapping with the integration methods is closed to the curve obtained with the simulation tools.

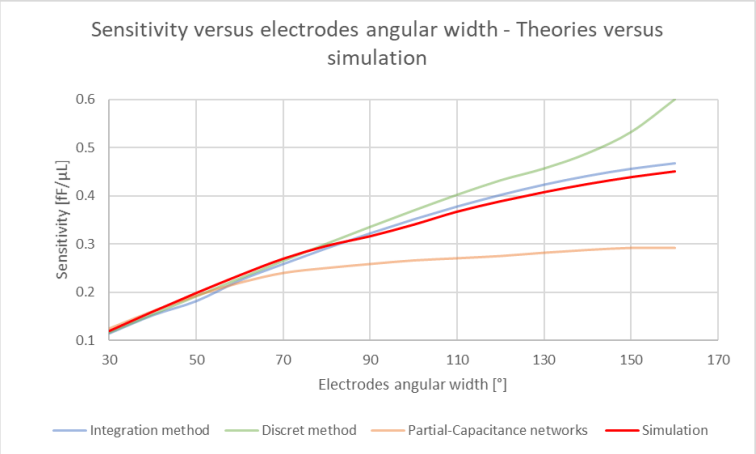

Figure 56 : Impact of the electrode's angular width on the sensitivity - Theories versus Simulation

The sensitivity found with the conformal mapping integration is $\mathbf{0.467}\ \boldsymbol{fF}/\mu\boldsymbol{L}$ which corresponds to the value obtained by simulation, ***0.457 fF/µL.*** Experiments with 160° electrode angular width and 7.5mm electrode radius have been conducted and the theoretical and simulated sensitivity have been confirmed by the experiments which have a conversion slope of **0.496 fF/µL**. Therefore, the sensitivity obtained by dose of insulin (= 10 µL) is **4.96 fF/IU**. By using 0.520 fF/µL to convert the capacitance into volume in section 2.3.4, the errors of the systems have been shown. To avoid the error accumulation between set dose versus injected weight and injected weight capacitance, the error is considered between injected weight and capacitance because it represents the reality of the injection. The errors increase with the amount of injected drug. For the largest injection, the error is equals to $\pm 40\ \mu L$ which represents $\pm$4 IU which correspond to a ~10% error. By considering the error of the other injection values, it is possible to detect $2^{\pm 1}$ IU, $12^{\pm 2}$ IU, $38^{\pm 3}$ IU and $72^{\pm 4}$ IU.

2.4 Chapter conclusion

The partial-capacitance networks theory, which is considering an infinite amount of paralleled capacitor, works well for flat capacitor and results have been confirmed by simulation. But, by applying the partial-capacitance networks to semi-cylindric capacitor, as presented in different publications, the results obtained seem aligned with simulation until a certain limit which is correlated to the cartridge size. Unfortunately, the results start to diverge from simulation and tests results after this limit. By using the more advanced technics of Conformal mapping, the results correspond to simulation and test as presented in Figure 57.

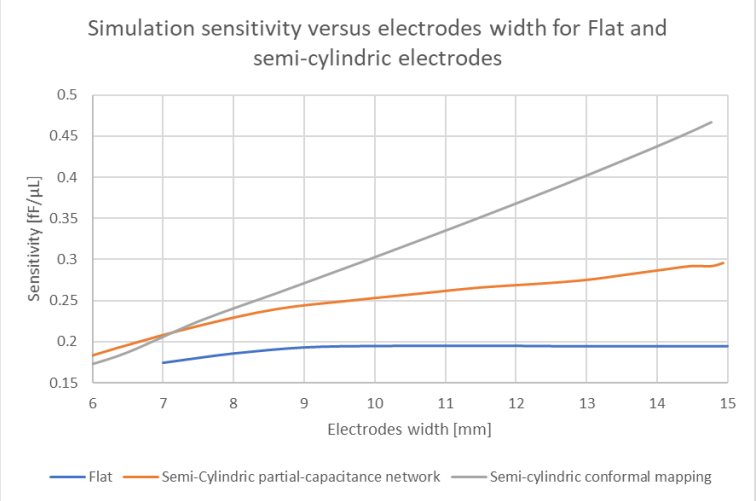

Figure 57: Sensitivity versus electrode width results for different electrode shape and theory

This phenomenon can be explained by the bend of the electric field which is considered with conformal mapping as presented in Figure 58.

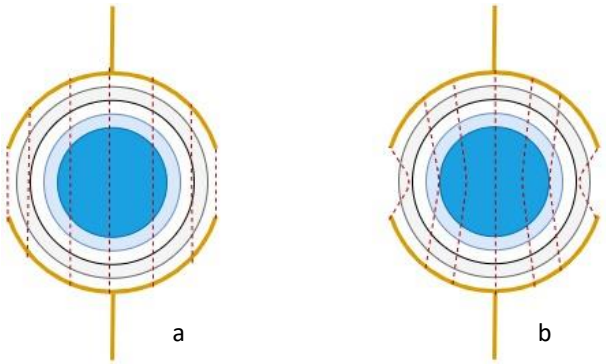

Figure 58: schema of electric field in the injector pen. a: Partial-capacitance network representation, b: Conformal mapping

This section proves that it is possible to detect the injection drug volume with an error close to the standard ISO11608-1 limits [82]. The cylindric shape electrode configuration has been selected for the development of the smart pen cap due to the promising result and the small footprint capability. But the conditions of used inside this section have been considered ideal. Other parameters will impact the measurement error and therefore decrease the signal error ratio. These parameters are: climatic variation, position of the injector pen and cartridge inside the device, ejected versus remaining volume discrepancy… These parameters will be presented in the next section.

Chapter 3. Parasitic effects

3.1 Chapter Introduction

Many parasitic effects can disturb the drug volume measurement inside the injector pen due to the physic of the sensor. Different solutions have been imagined to compensated or limited the impact of these effects on the accuracy of the sensor. In the next sections, firstly, the effect of the perturbation of external electric fields will be presented. Secondly the error due to the electric field geometry and position of the cartridge have been analyzed. Next section will discuss about the impact of the air bubbles inside the cartridge. Then, the climatic variation impact on the measurement will be presented. After that, the discrepancy between the measurand which is the remaining volume inside the cartridge, and the volume of interest, which is the ejected volume, have been observed. To finish the cap-to-cap variability due to manufacturing tolerance have been shown. All these parasitic effects will give an overview of the errors that impact and limit the accuracy of the system.

3.2 External electric field perturbation

3.2.1 Section Introduction

The perturbation of the external electric field impacts the capacitance measurement by adding a parallel impedance to the measurement area. This can happen when the user takes in his hand the device for examples. To prevent this perturbation, a copper shielding connected to the reference of the device has been added [83]. This shielding will contain the electric field generated by the AD7746 inside the device. Therefore, any variations outside this area will have low impact on the inner electric field as presented in Figure 59. Another requirement for this device is that it shall be able to communicate using Bluetooth® protocol. Therefore, Bluetooth® Radio Frequency (RF) waves shall be impacted as less as possible by this shielding. By using a copper cylinder shield covering the electrode area and let the Bluetooth emitter above this area. This will authorize the Bluetooth communication operating and protect the electric field of the interest area from external perturbation. For manufacturing purpose, a cylinder of copper has been designed and it has been connected to the PCBA voltage references.

3.2.2 Simulation and discussion

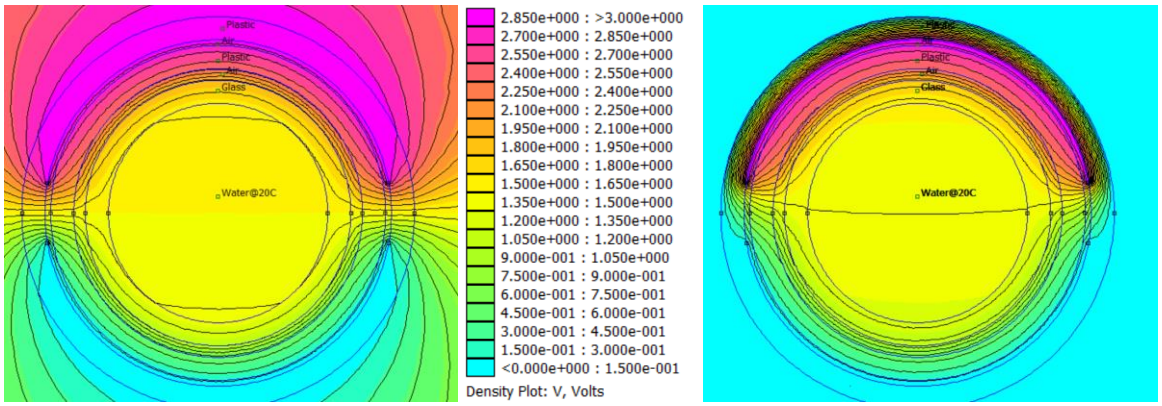

Figure 59: Simulation with and without shielding

By adding the shielding, the capacitance will change slightly. According simulation, an offset of 90 fF appears for empty and full cartridge capacitance. This offset does not impact the drug level acquisition because the electric field between

electrode and shield is determined by the pen cap thickness of the plastic and the use of the differential measurement methods subtract this offset as it is presented in Table 8.

Table 8 : Shielding impact on capacitances

	Capacitance without shielding [FF]	Capacitance with shielding [FF]
Full cartridge	696.9	787.3
Empty cartridge	1432.3	1522.5
Full – empty cartridge	**735.4**	**735.2**

3.2.3 Conclusion

To conclude this section, adding a shielding allow to suppress external perturbation by restricting the electric field inside the smart pen cap as presented in Figure 59, right image. The shielding does not impact the measurement due to the differential measurement. This shielding can be easily manufactured due its simple geometry.

3.3 Pen position inside the smart pen cap

3.3.1 Introduction

Tolerance between the center of the cartridge and the center of the electric field can be impacted by the tolerances between the injector pen and the pen cap, but also, between the cartridge and the cartridge holder because the cartridge is not fully maintained according the design of the selected injector pen. So, due to the non-linearity of the electric field, the capacitance will change for a same cartridge depending on its position inside the electric field. By moving the cartridge and/or the pen following a circular path along the electrode. The capacitance will have a sinusoidal shape because the cartridge and/or pen will go through high and low electric fields concentration area. The electric field will depend on the distance between the electrode which is not constant. Any discrepancy between the circle trajectory's center of the cartridge and/or pen and the center of electric field will impact the sinusoidal shape. These effects presented in Figure 60 will be detailed in next subsections.

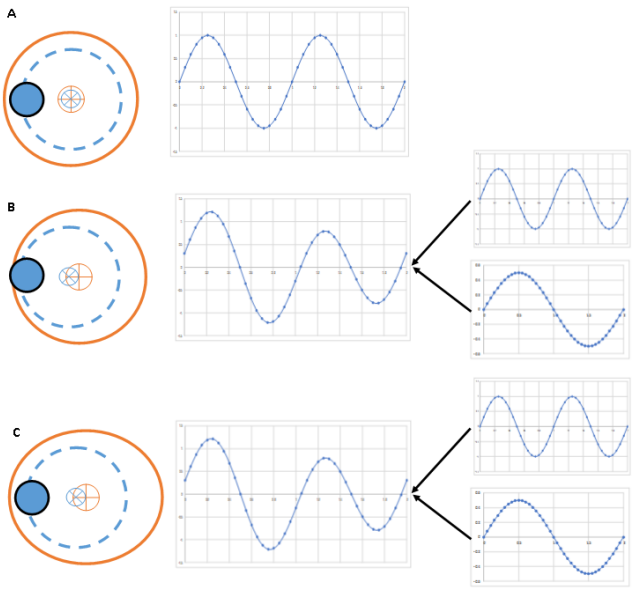

Figure 60 : Cartridge trajectory and its center in blue and electric field limit and center in orange. Graphs on the right represents capacitances. A – Center trajectory and electric field, B – Uncenter trajectory and electric field, C – Deformed electric field

3.3.2 Semi-cylindrical electrode

3.3.2.1 Sub-section introduction

Considering the two semi-cylindrical electrode, the movement of the pen and the cartridge can be analyzed using the conformal mapping technics presented in section 2.3.2.2. Therefore, the position of the cartridge inside the smart pen cap can be defined by:

- Movement of the injector pen inside the smart pen cap, the pen center axis is considered parallel with the smart pen cap and the maximum deviation measured is 0.25 mm, as presented in Figure 61a.
- Movement of the cartridge is a little bit more complex because it is hold at the injection side of the pen. The cartridge can move with an angular tilt between the center axis of the pen and the center axis of the cartridge. At the plunger side, the maximum deviation is 0.5 mm as illustrated in Figure 61b.

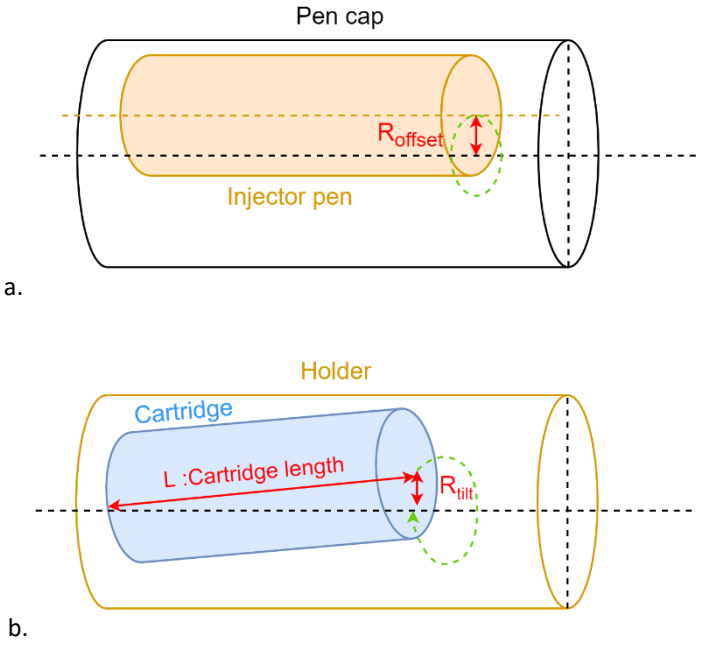

Figure 61 : Pen and cartridge movements schematic

3.3.2.2 Theory

The equation *Eq 1* given in section 2.3.2.2, shall be updated because the model is not anymore symmetric due to the shift of the cartridge and/or the pen inside the pen cap. Therefore, the full capacitance model will be considered.

- Firstly, the pen center offset is added to the all the pen domains definition by using this equation, where ***n*** shall be replaced by the domain of interest:

$$Offset = r_{offset} \times e^{i\theta_{offset}} \rightarrow \boldsymbol{Z_n = Offset + R_n \times e^{i\theta_n}}$$

- Secondly, the cartridge tilting impacts the drug and glass areas of the pen. This tilting offset will depend on the tilting angle θ_{tilt} and distance dL from the injection side. It will be added at the previous equation. Here, **n** can be replaced uniquely by glass and drug domains.

$$Tilt = dL \times \sin\left(\frac{r_{tilt}}{L}\right) \times e^{i\theta_{tilt}} \rightarrow \boldsymbol{Z_n = Offset + Tilt + R_n \times e^{i\theta_n}}$$

Finally, the integral has been modified to consider the whole system

$$C = L \times \int \frac{dx}{\frac{\Delta z_{drug_{Up}} + \Delta z_{drug_{Down}}}{\varepsilon_{drug}} + \cdots + \frac{\Delta z_{air2_{up}} + \Delta z_{air2_{down}}}{\varepsilon_{air}}}$$

By computing this equation using Octave® and changing the position of the cartridge, the results in Figure 62 are obtained.

a 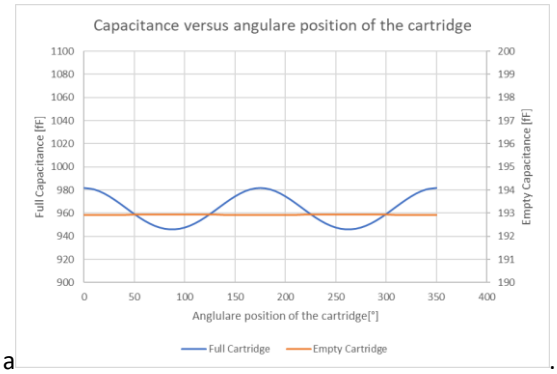

. b. 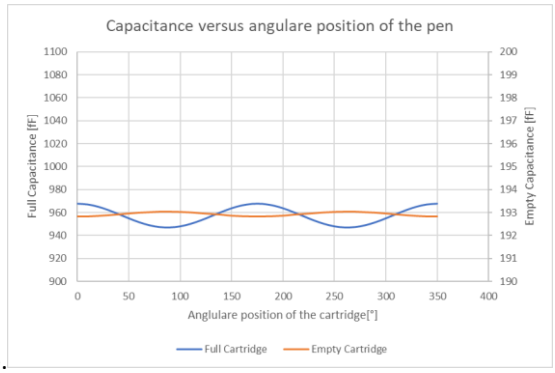

c. 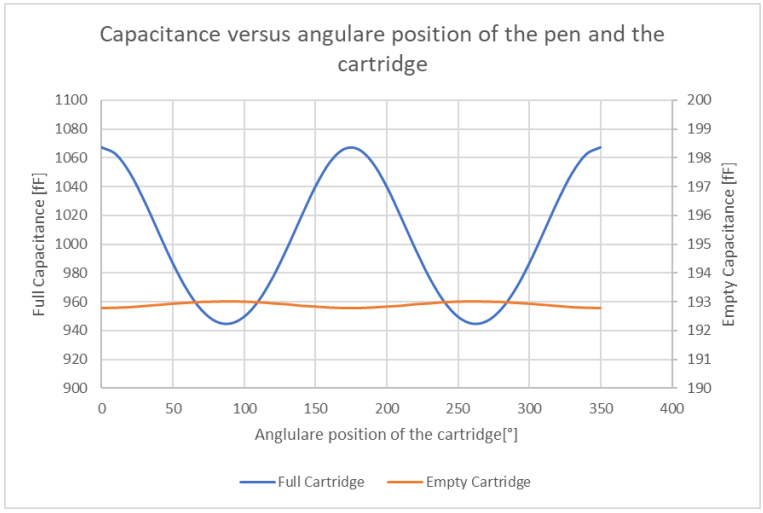

Figure 62 : Conformal mapping - Tilting

The capacitance has a sinusoidal shape which indicates that the cartridge and/or pen goes through high and low electric field concentration as it has been shown in section 2.3.3. Each movement will be observed separately, then the combined displacement of the cartridge and the pen at their maximum position have been done.

- The maximum capacitance variation depending the cartridge position is 35.45 fF (±35.45 µL) for a full pen and no variation for an empty pen as presented in Figure 62a.
- The maximum capacitance variation depending on the position of the pen is 20.85 fF (±20.85 µL) for a full pen and 0.2 fF for an empty pen as presented in Figure 62b.
- By considering the pen and the cartridge in the maximum radial position, the capacitance variation is 122.4 fF for a full pen and 0.2 fF for an empty pen as presented in Figure 62c. This variation will induce an error of ±122.4 µL and that corresponds to an error of ±12.2 IU. The variation for an empty pen is lower because all domains of empty pen have electric permittivity close to air permittivity. Therefore, the variation of empty pen is considered negligeable.

The errors due to the cartridge and the pen offsets do not sum directly, because the electric field is not linearly increasing/decreasing from the radial distance. Thus, when the pen and the cartridge are at the maximum radial position, the

drug is closer from electrode. Therefore, the difference between high and low concentration electric field along the electrode is larger.

3.3.2.3 Discussion

The angular width of the electrode has an impact on the error due to the position of the cartridge. As presented in Figure 63, the error decreases when the angular width decreases, which unfortunately equally correspond to a decreasing of the sensitivity. Adapting angular width to find the best compromise between accuracy and rotations errors can be done, but it is not an optimal solution. Therefore, a second idea presented in section 3.3.3 has been investigated.

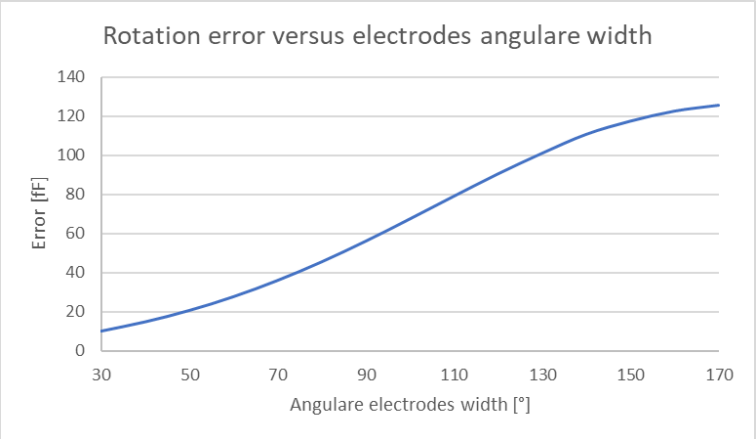

Figure 63: Rotation error versus angular electrode width for 2 semi-cylindric electrode

Perfect sinusoid has been considered in the beginning of this sub-section. But this is an ideal case to present the electric field variation problem. Obtaining these results by experiments are difficult because:

- The pen can be imperfectly centered inside the cap and the cartridge can have a certain tilting angle. A theoretical analysis has been conducted considering that the pen was shift by $d = \binom{0.25\ mm}{0.5\ mm}$ with an angle of by $\theta = \binom{30°}{60°}$, as presented in Figure 64,. Then, the cartridge is tilted at its maximum position inside the injector pen and turns along the electrode. The smart pen cap should have two same electric field concentration maximums. But, due to the pen shift, the cartridge will go through a larger maximal then a lower maximal.

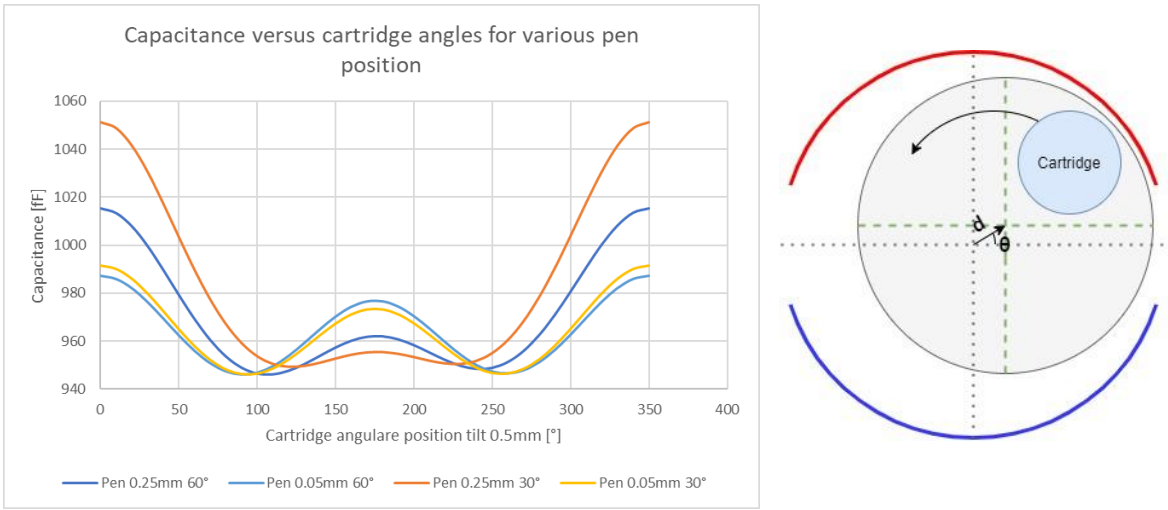

Figure 64 : Tilting cartridge inside a not centered pen

- Tolerances in electrode placement can impact the electric field. For examples if an electrode is shifting a little bit at one side. The electric field will become unbalanced. One side will be stronger than the other one. As it is shown on Figure 65, a variation of 2° to 6° can induce a peak-to-peak error of 2.6 fF to 10.5 fF. This corresponds to a placement tolerance about ±0.25 mm to ±0.75 mm.

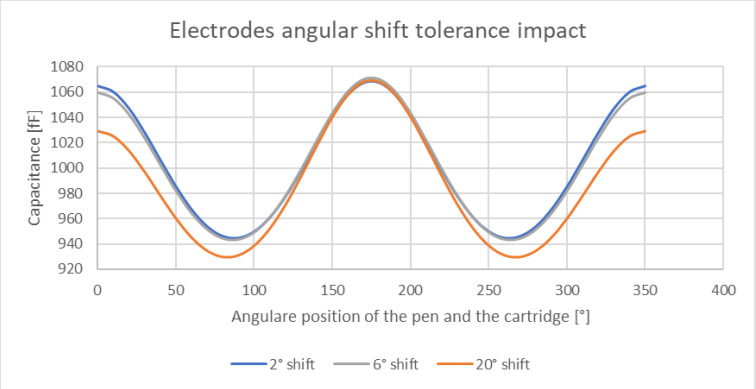

Figure 65 : Electrode angular shift tolerance impact

- And other geometric deformation can be imagined as ovalization of the cap, radial positions of the electrode...

3.3.2.4 Experiment

Experiments have been done to confirm the theoretical results. A cartridge has been glued at its maximum tilted position and the pen is turned by 30° step inside the smart pen cap. The figure hereafter has been obtained. A deformed sinusoid shapes appears where the behavior seems to correspond to the theory. The maximum peak-to-peak error is almost $15\ fF$ which could be due to a not centered pen and/or electrode angular positioning error. The capacitance variation obtained for the sinusoid is $\sim 21.5\ fF$ which is conform with the range obtained in theory.

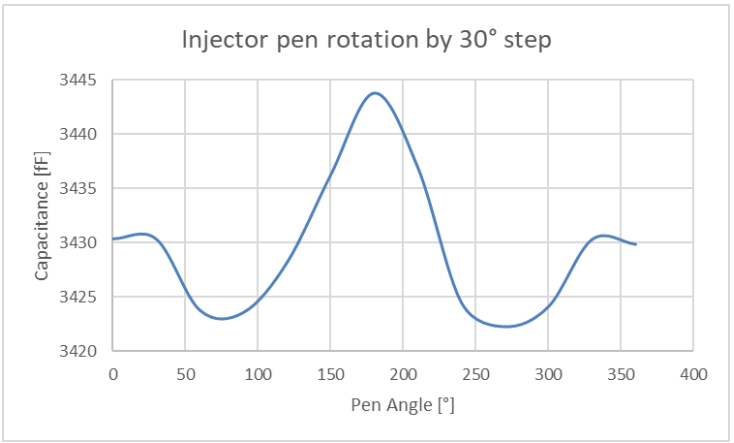

3.3.2.5 Sub-section conclusion

Therefore, for a same level of drugs inside the cartridge the capacitance can change according the radial angle and the tilting angle of the cartridge and the injector pen. So, one variable will depend on five parameters, and therefore it is impossible to solves the error with the current configuration.

$$C \rightarrow \begin{Bmatrix} Drug\ level \\ Cartridge\ position \begin{bmatrix} Angulare \\ tilting\ angle \end{bmatrix} \\ Pen\ position \begin{bmatrix} Angulare \\ Radial \end{bmatrix} \end{Bmatrix}$$

3.3.3 Quarter-cylindrical electrode

3.3.3.1 Sub-Section introduction

As presented in the previous section, the movement of the cartridge and the pen can induce not negligeable bias in the measurement. Trying to limit this error, a four-electrode device has been created. The sensor configuration will use two excitations electrode versus two measurement electrode. Then the electric field is shifted by 90° by shifting by one electrode excitation and measurement signals. Therefore, if the cartridge is placed in an area with low electric field, the next measurement it will be in a high electric field. In [84], the effect of high and low electric field density is well represented. Reconstruction of element in the electric field using switching electrode inside a cylinder is discussed in [85].

3.3.3.2 Theory

By using the previous conformal mapping methods and shifting the electric field by 90°, Figure 66 is obtained. The two capacitances obtain have been averaged and the theoretical error has been drastically reduced from 122.5 fF to 11.64 fF.

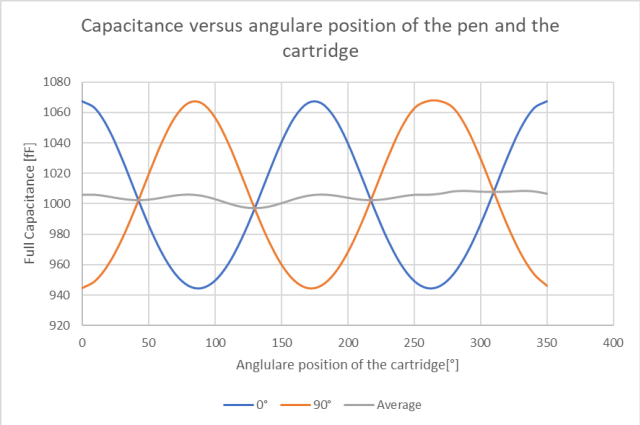

Figure 66: 2 orthogonal electric field with center eccentric offset of the cartridge

3.3.3.3 Discussion

These theoretical results have been obtained with centered pen and perfectly symmetric device. The positioning and manufacturing errors presented in the previous section will impact the results. By shifting an electrode of 4° and uncenter the pen by 0.25mm at 60° the results are given hereafter

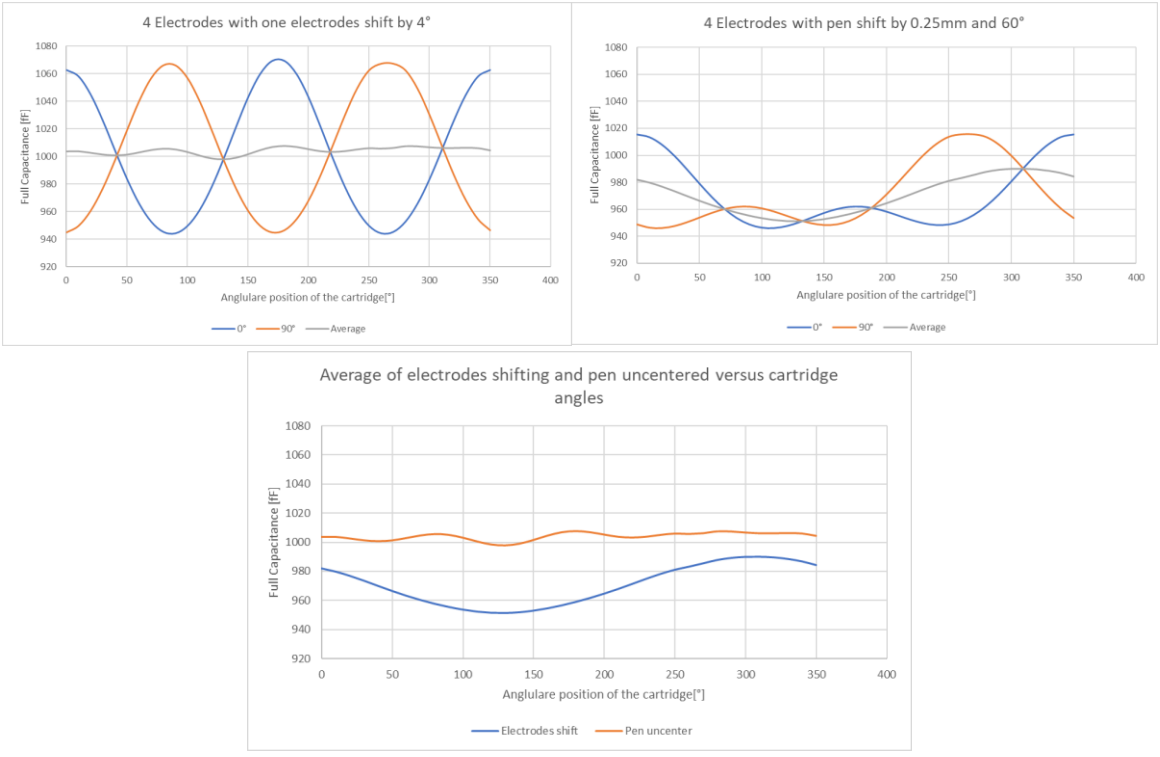

Figure 67: Error due to electrode shift and uncenter pen on a 4-electrode device

As presented before, the error due to electrode shift is 10 fF which is a little bit less than results presented at the end of 3.3.2. For the uncentered pen, the errors increase from 11.64 fF to 38.91 fF, the two capacitances obtained by shifting the electric field do not compensate directly as presented at the beginning of this section. This can be explained by the fact that the electric field concentrations are not equal to the opposite when the electric field switch due to the shift of the cartridge. This pen center error is the main contributor to the global error due to geometric problems.

3.3.3.4 Experiments

Tests have been realized to observe the comportment of the capacitance when a pen with a tilted cartridge is turned by 30° steps. The results are presented hereafter. Two sinusoids phase shift by almost 90° are visible.

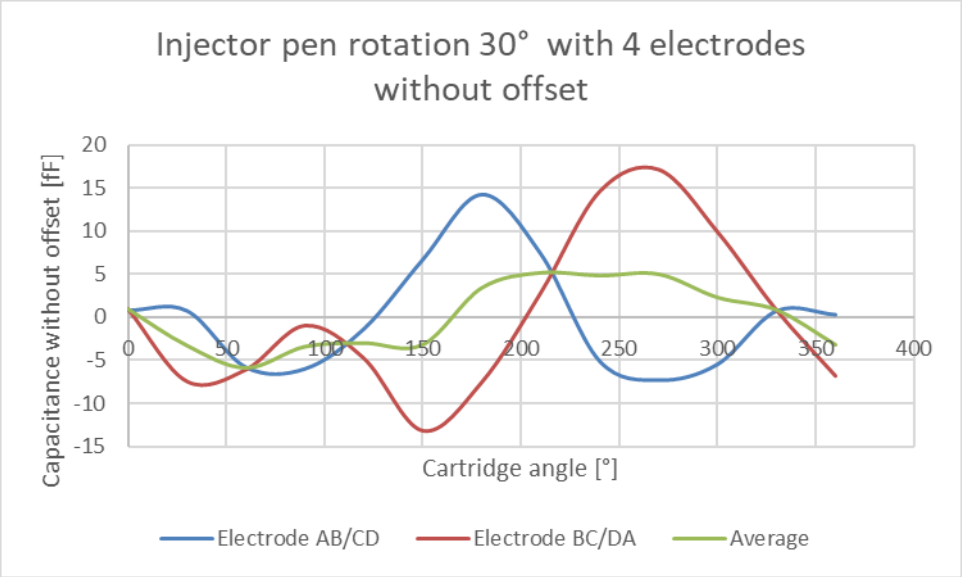

Figure 68 : Rotation test with 4 electrode pen cap

The errors range depending on the cartridge and pen angular position is 21.5 fF for AB/CD electrode configuration and 30.3 fF for BC/DA electrode configuration angles. By averaging the two capacitances configuration the errors decrease to 11 fF which correspond to ±11 µL corresponding approximatively to ±1 IU of insulin. These results are in the theoretical interval discuss in the previous subsection.

3.3.3.5 Sub-Section conclusion

Using four electrode and averaging the two orthogonal electric field reduce the capacitance variation due to the cartridge position inside the smart pen cap. An error persists and the possibility to use more electrode to correct the remaining errors have been considered. By imagining an 8-electrode device, the electric field can be shift by 45° and the capacitance can be averaged on a larger number of different angles acquisition. But, by analyzing theoretically this method, the error reduces only from 11 fF to 8.1 fF. This is a low reduction compare to the increasing of the manufacturing and the electronic design complexity by doubling the number of electrode.

3.3.4 Three-electrode

3.3.4.1 Sub-section introduction

To have a compromise between the sensitivity and the rotation error, three-electrode configuration has been imagined. By using 110° electrode placed every 120° inside the cap. Due to assymetric equivalent electrode width (110° as excitation and $2 \times 110°$ as measurement), the electric field is stronger at one point and weaker at the opposite. With this configuration, by displacing the cartridge along the electrode, a single sinusoid shape appears. This is different from the 4-electrode model which have a double sinusoid shape. Moreover, the 4-electrode device can have four position of the electric field, but due to the symmetry the opposite configuration (switch the measurement and the excitation electrode) give the same results and do not contribute to add more information. With the 3-electrode device, the capacitance can be acquired with three different electric fields oriented at 120° each.

3.3.4.2 Theory

By using the previous conformal mapping methods and considering 110° and 220° electrode then computing the three capacitance by turning the electric field each 120° the Figure 69 is obtained. The three capacitances obtained have been averaged and the theoretical error has been drastically reduced from 178 fF to 5 fF.

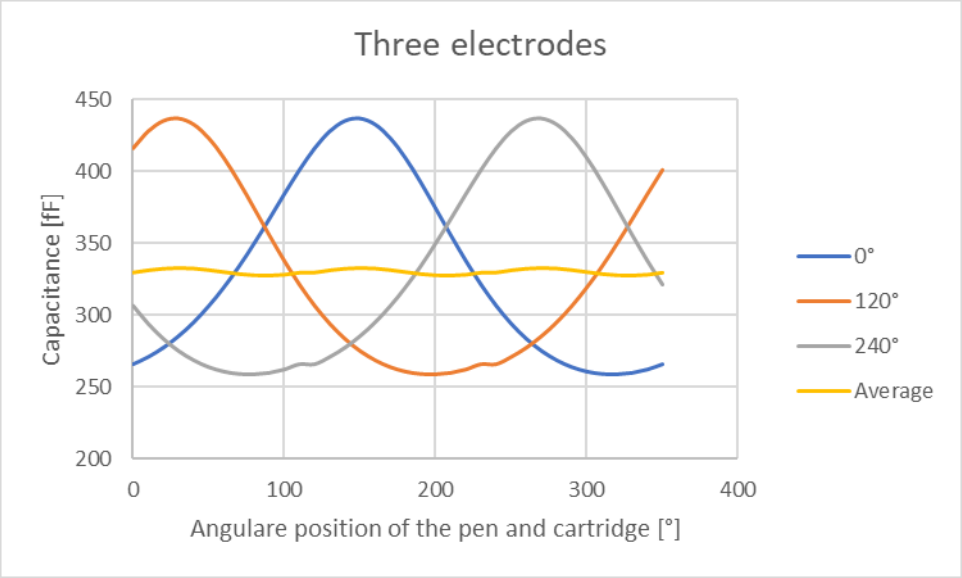

Figure 69: Error due to electrode shift and uncentered pen on a 3-electrode device

The error range for the average capacitance at 5 fF is two times better than four-electrode configuration. But the sensitivity of this three-electrode configuration is only 0.152 fF/µL which is 3 times less than the 4-electrode device. Therefore, this solution cannot replace four-electrode technic.

3.3.4.3 Sub-section conclusion

Despite the three-electrode technic is not very efficient, it can be used with four-electrode device by switching one electrode in excitation and the three other electrode in measurement (85° excitation and 255° measurement). This will help to know the position of the pen inside the smart pen cap by applying a specific algorithm using the ratio between each electrode's capacitance. This algorithm will not be presented in this document for intellectual properties purpose.

3.4 Bubbles

3.4.1 Introduction

While the function of both needle and pen is supposed to be checked before each shot by ejecting and observing a small dose into the air to remove bubbles in the cartridge, this step is frequently skipped by many patients [86]. In one study only 16 % of patients primed their pens correctly [87]. This can lead to massive malfunctions of the pen and underdosing due to the compressibility of the air during an injection. These bubbles can be created when the patient let the needle on the injector pen during a long period. Due to temperature variation, insulin is dribbling out and eventually replaced by air [88]

Figure 70: Bubble inside an injector pen

As presented in the previous section, the position of the cartridge inside the smart pen cap impacts the measured capacitance. By extension, the presence of bubbles and their position can impact the acquired values. To easily simulate the effect of the bubbles, they are considered with a cylinder shape due to use of $2D^{1/2}$ simulation tools which considers only extrusion on z-axis.

3.4.2 Simulation

Bubbles with a diameter of 0.5 mm and 1 mm have been simulated. 1 mm is generally the maximum size observed inside the cartridge. The pen and the cartridge are considered centered to only observe bubbles position impact on the capacitance. These bubbles are displaced along the limit of the cartridge with 30° steps. Results obtained are shown in Figure 71

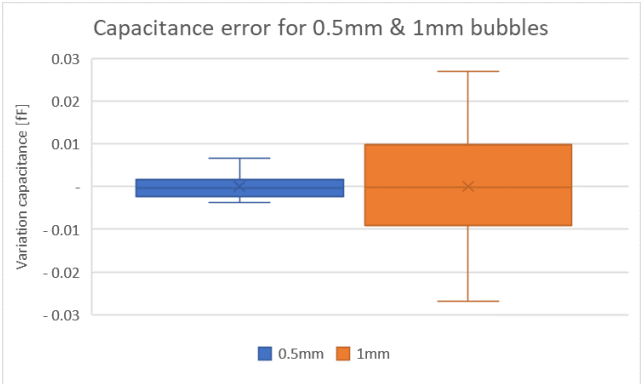

Figure 71: Bubble effects

3.4.3 Discussion

According the side figure, the variation is larger with larger air volume. By displacing the bubbles along the cartridge limits the capacitance variation is maximally ±0.03 fF for a 1 mm diameter bubbles.

3.4.4 Conclusion

As shown previously, bubbles have low impact on capacitance and can be neglected compared to other parasitic effects. But, due to the compressibility of air compared to incompressibility of drug, these bubbles will have an important impact on the ejected versus remaining volumes error.

3.5 Climatic

3.5.1 Introduction

This section aims to present the results of climatic tests and the methodology to compensate the capacitance measurements for temperature and relative humidity variation. The capacitance variation due to climatic effect is widely studied in literature as shown in [89, 90]. The measured capacitance depends on the electric permittivity ε of the sample (mainly the drug volume inside the injection pen, but also the plastic of the pen as well as the air inside), which are themselves sensitive to variation in temperature and relative humidity. The climatic conditions influence thus the estimation of the ejected drug and need to be compensated for. To study the climatic effect on the smart pen and establish a compensation methodology, tests have been realized and are presented hereafter. Five device configurations have been studied:

- PCBA of the smart pen cap alone
- Encapsulated PCBA of the smart pen cap alone
- Smart pen cap
- Smart pen cap with references electrode
- Smart pen cap with reference electrode and analog PCBA encapsulated

3.5.2 Materials and methods

Hereafter the list of material used to perform climatic tests

- Climatic Chamber Vötsch® 4018
- Smart Pen Cap
- PCBAs of the smart pen cap alone
- Injection pen (1.5mL)
- Bluetooth Low Energy (BLE) Receiver
- Computer

Two climatic conditions were programmed with a duration of 3 h each:

- 23°C – 30%
- 32°C – 30%

The reference electrode has been dimensioned to have a capacitance close to the value of the capacitive sensors. There are based on two face-to-face flat plates of approximatively 5 x 10 mm with a space of approximatively 1 mm which give: $C_{ref} = \frac{\varepsilon \times L \times W}{d} \cong 443\ fF$

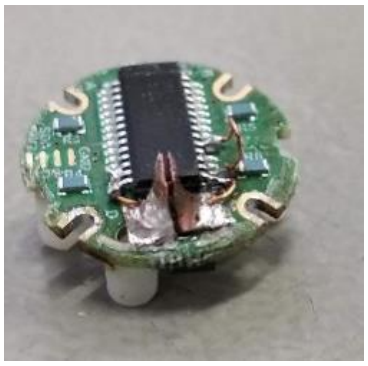

Figure 72: Analog PCBA with reference electrodes

3.5.3 Results

3.5.3.1 PCBAs of the smart pen cap alone

In Figure 73, the capacitive sensor (blue) and the PCBA tracks capacitance (red) are plotted. These measurements show that the two capacitances have the same behavior.

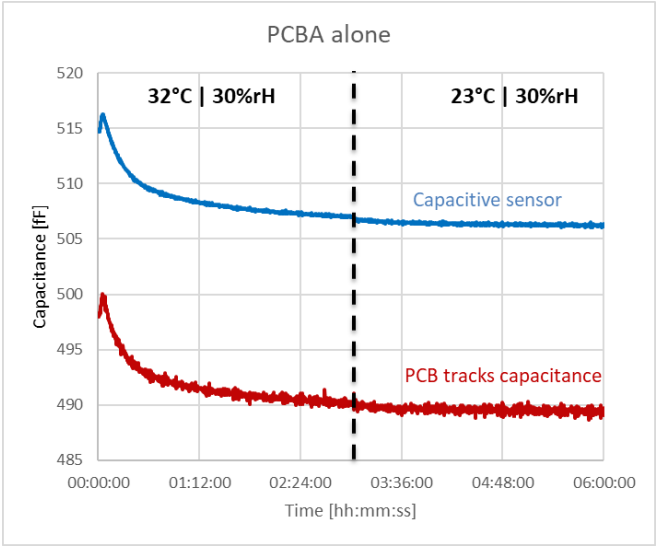

Figure 73 : PCBA alone at 23°C and 32°C

3.5.3.2 PCBAs of the smart pen cap alone encapsulated

Figure 73 shows a long-term drift of the values of the two capacitances. This should be due to water absorption of the Smart Pen cap materials as FR-4 and plastic. Therefore, the PCBA has been encapsulated with UV light curable resin (Loctite 3211-LC) to reduce the long-term drift. Figure 74 proves that this encapsulation is very useful to limit this drift. This resin induces an increase of PCBA tracks capacitance (red) and capacitive sensor (blue).

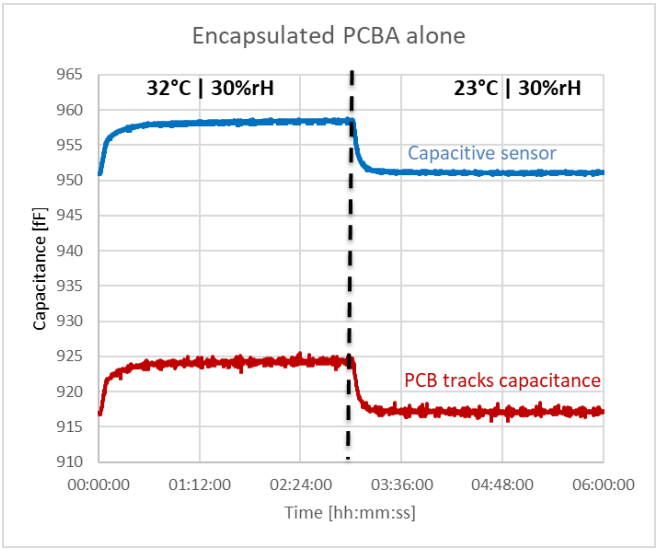

Figure 74: Encapsulated Analog PCBA at 23°C and 32°C

3.5.3.3 Smart Pen cap

Figure 75 represents the effect of the temperature and relative humidity variation on the value of the capacitive sensor and PCBA tracks capacitance for a full assembled smart pen cap with a full injection pen inside. This full injection pen induces an offset on the capacitive sensor. The capacitance of the PCBA tracks is equivalent to section 3.5.3.1 because it has no encapsulation.

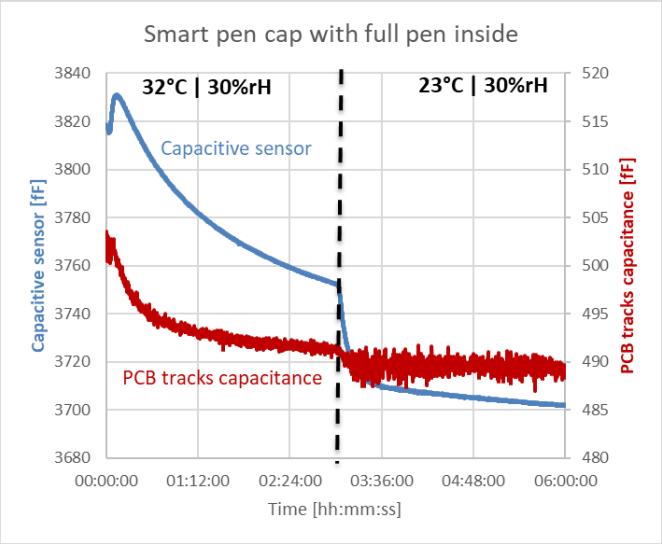

Figure 75: Smart pen cap with a full pen inside at 23°C and 32°C

3.5.3.4 Smart Pen cap with reference electrode

Two copper plates have been soldered on the Analog PCBA and are used as reference capacitor (Figure 72). This reference capacitor is measured through the AD7745 as a stand-alone capacitor and the compensation is done by using capacitive difference in post processing [91, 92]. This is a cheap solution and suitable for industrial design. Then, the PCBA has been assembled in a smart pen cap device. The reference capacitor (red) follows the capacitive sensor (blue) as plotted in Figure 76. The PCBA is not encapsulated with UV resin.

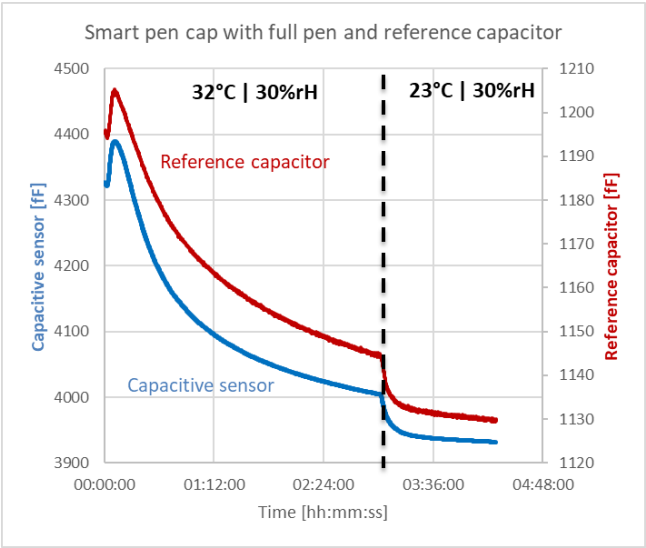

Figure 76: Pen cap with reference capacitor at 23°C and 32°C

3.5.3.5 Smart pen cap with reference electrode and encapsulated PCB

The final test presented in Figure 77 used two reference electrode and an encapsulated PCBA, to have the best possible correlation between reference capacitor and capacitive sensor in order to do differential measurement.

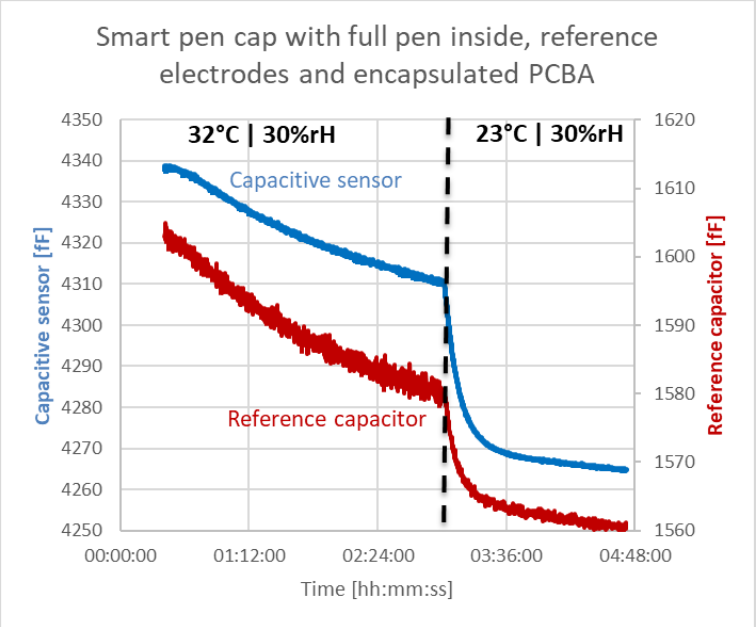

Figure 77 : Pen Cap with reference electrode and encapsulated analog PCBA at 23°C and 32°C

3.5.4 Discussion

According to the environment sensors in the climatic chamber, the PCBAs alone and smart pen cap devices can reach the stabilization after 30 minutes which corresponds to the stabilization time of the climatic chamber. The capacitance has long term drift which is not correlated to climatic variation as it is presented in sections 3.5.3.1 and 3.5.3.3. These long-term drifts could be due to water absorption of materials. Two main ways have been developed to solve this issue:

- Encapsulate the Analog PCBA to reduce the water absorption effect
- Use reference electrode to compensate measurement variation by a same nature variation.

In section 3.5.3.2, the encapsulation seems to solve the long-term drift for the PCBAs. A relation appears in Figure 78 between capacitive sensor and PCBA tracks capacitor with a linear correlation factor R^2: 99.5%. This good correlation factor can be explained by the fact that PCBA tracks for reference and measurement capacitance are quite similar. Comparing the measurement electrode with the reference PCBA tracks a poor correlation is shown in section 3.5.3.3 because these two capacitors do not measure anymore the same environment.

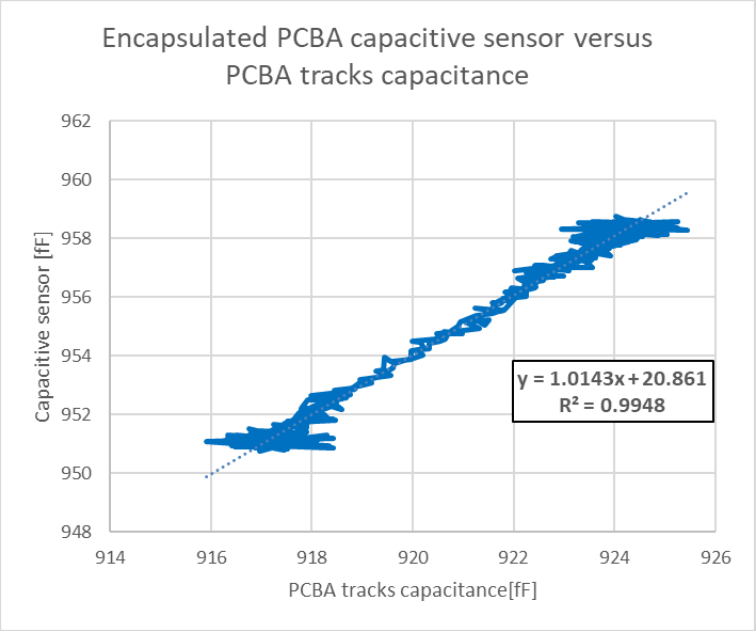

Figure 78: Encapsulated PCBA, capacitive sensor versus PCBA tracks capacitance

To solve the difference between the capacitance of PCBA tracks and the capacitive sensor as shown in Figure 75, reference electrode have been placed in section 3.5.3.4. For the same climatic change, the reference capacitor shows a variation of 70 fF, versus 10 fF for the PCBA tracks capacitor. Therefore, the reference capacitor is more sensitive to temperature variation and it becomes possible to do a differential measurement to reduce the unwanted effects of temperature and relative humidity. A correlation appears in Figure 79 between reference and measurement electrode with a R^2: 98.6%.

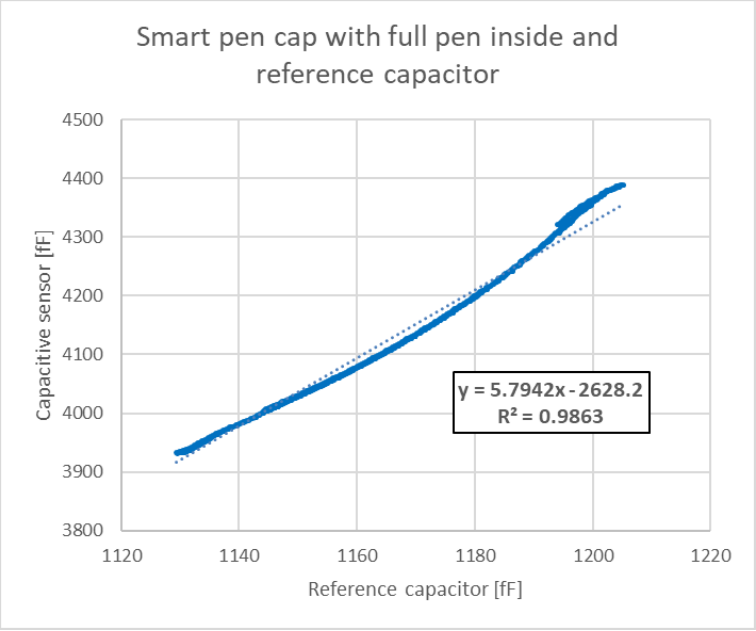

Figure 79: Capacitive sensor versus reference capacitor for a smart pen cap with a full pen inside

In the last section of results 3.5.3.5, the reference electrode and encapsulation are combined. A correlation appears in Figure 80 between capacitive sensor and reference capacitor with the PCBA encapsulated. The correlation factor R^2 is 98.9% with a variation of 80 fF for reference capacitor.

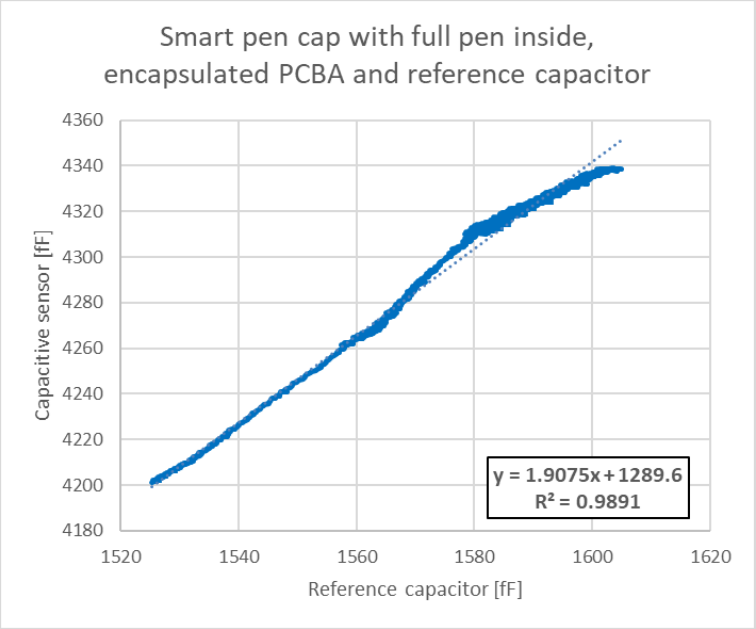

Figure 80 : Smart pen Cap with reference capacitor and encapsulated PCBA

3.5.5 Conclusion

To correct the climatic variation due to the temperature and relative humidity, it has been shown that the unwanted climatic effects can be reduced when

1. adding two reference electrode on the PCBA to realize an additional capacitor
2. encapsulating the PCBA to cancel the effect of water absorption.

By this way, it is possible to compensate the variation on the capacitive sensor by performing a differential measurement as it is shown in Figure 81 when the temperature drops from 32°C to 23 °C.

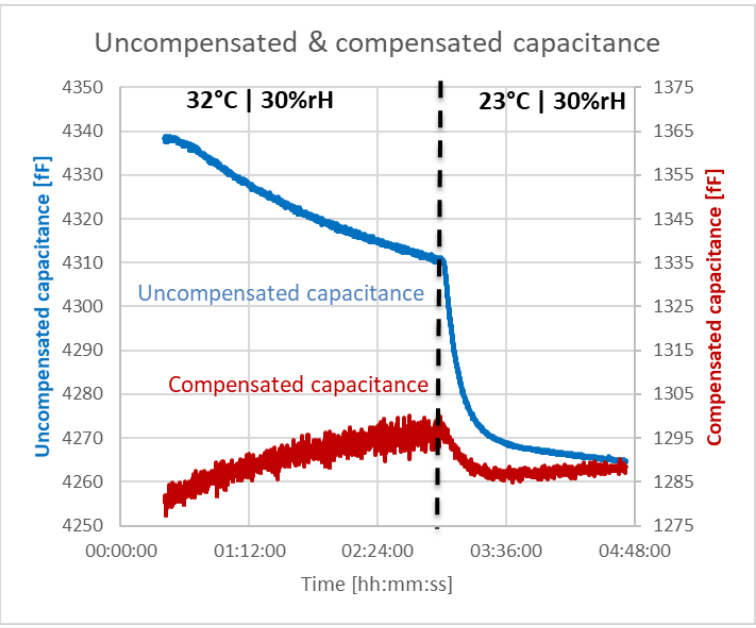

Figure 81: Uncompensated capacitance (blue) and compensated capacitances (red)

According to the results, the uncompensated variation due to climatic is about 72 fF. By using the reference electrode with differential measurement, the compensation of the measurement variation due to climatic is less than 22 fF. This is a 70% improvement of the error. The capacitance value is converted in volume by calibrating the smart pen cap with five pens to obtain the conversion factor which is 0.55 fF/µL This improvement allows to reduce the error from 130 µL (13 IU of insulin) to 40 µL (4 IU of insulin). This is a significant improvement and implementation of reference electrode on a new prototype iteration will be studied.

3.5.6 Compensation factors discussion

According previous sub-section, the climatic effect has been compensated using a conversion factors which is the slope between capacitive sensor and reference capacitor. Only one device has been designed with reference electrode. Other device used climatic sensor (SHT35) to compensate temperature variation. A compensation has been done on 10 pens which gives encouraging results with drastically reduction of the capacitance variation due to temperature (Blue versus red bar in Figure 82). But each cap has been compensated with its own compensation factors which induce problematic industrialization process:

- Do a test to find individual compensation factors, if it will be a climatic test in production, this will take a lot of manufacturing times and increase the price of the device
- Write individual compensation factor during manufacturing

To avoid this manufacturing issue, a global factor has been considered to compensate all smart pen cap. According Figure 82, the global compensation factor gives worse results than individual compensation factor, but the variation is still considerably reduced compared to raw capacitance. A deeper analysis on reference electrode and materials shall be done to improve these results. This work has not been realized during thesis duration.

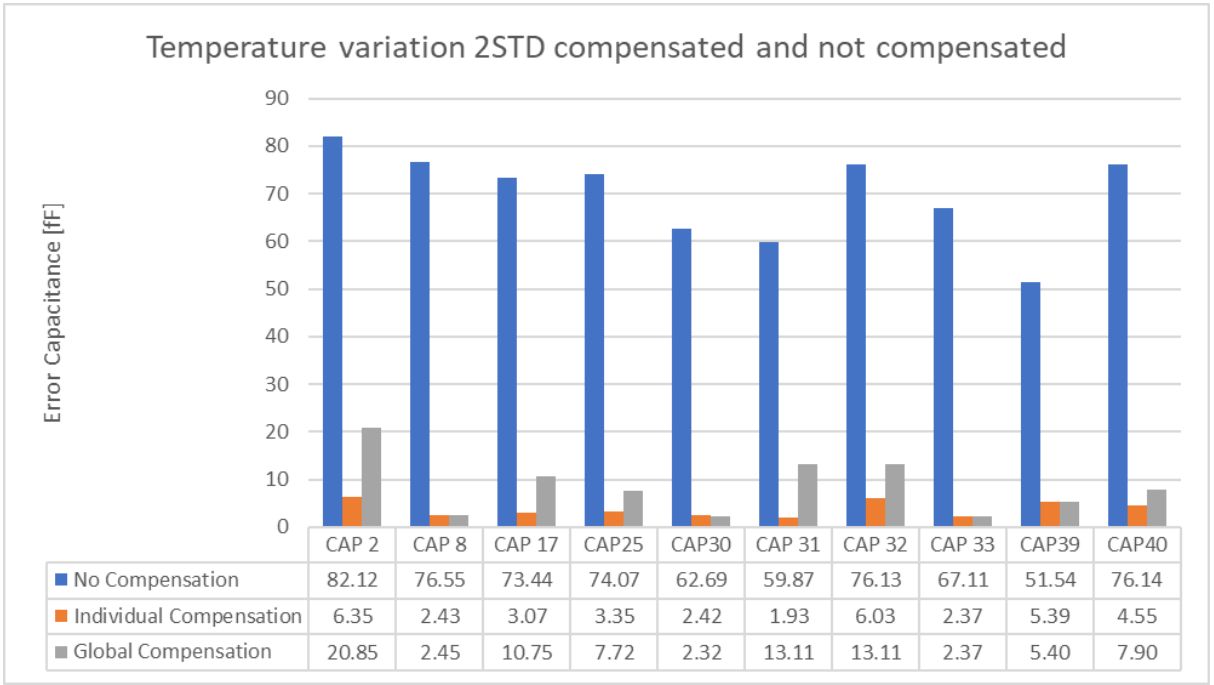

	CAP 2	CAP 8	CAP 17	CAP25	CAP30	CAP 31	CAP 32	CAP 33	CAP39	CAP40
No Compensation	82.12	76.55	73.44	74.07	62.69	59.87	76.13	67.11	51.54	76.14
Individual Compensation	6.35	2.43	3.07	3.35	2.42	1.93	6.03	2.37	5.39	4.55
Global Compensation	20.85	2.45	10.75	7.72	2.32	13.11	13.11	2.37	5.40	7.90

Figure 82: Compensations factors variation

3.6 Ejected and remaining volumes

3.6.1 Introduction

A bias exists due to the technics of measurement. The pharmaceutical industry focus on what is injected in the patient. By design, the capacitive sensor measures the volume inside the injector pen. Therefore, discrepancy exist between ejected volume and the difference of remaining volume between two injections. This can be due to lost droplet, needle loss volume, clogged needle, and bubble compressibility. As presented in [93], 36.9% of user report insulin leakage during the use of the injector pen.

Let the needle on the injector pen or reuse the same needle is currently done by patients for an easier handling of theinjector pen outside home. By not considering the risks of body contamination and degrading the drug. This habit can have a huge impact on the dynamics of the injection as clogged needle, dribbling and creation of air bubbles. [88]

3.6.2 Test methods

Injection tests have been done on three pens with twelve injections of 125 µL. A priming has been done on each pen to limit as much as possible the bubbles inside the cartridge. The drug is ejected into a lab beaker and weight directly to limit the evaporation effect. The scale is tared each time to limit any derived effect. Finally, the ejected weight versus the difference of remaining weight have been compared.

3.6.3 Results

The ejected and delta remaining weight for N=36 are displayed in Figure 83. On the left, a blue box plot representing the difference of remaining weight and on the right, an orange box plot representing the ejected weight.

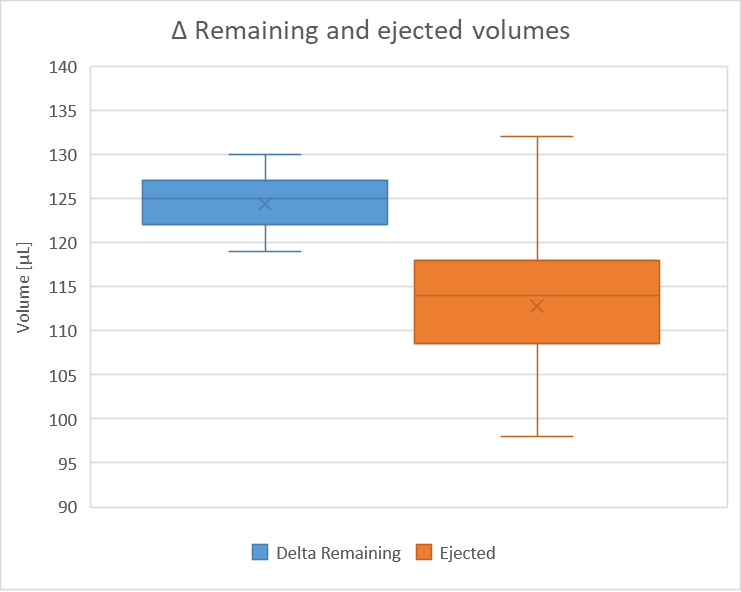

Figure 83 : Δ remaining versus ejected dose error

3.6.4 Discussion

Firstly, the delta-remaining weight is larger than the ejected weight which is normal by considering the delta-remaining weight contains ejected weight and lost weights (needles, drop). Secondly, two effects can be observed and separately treated. The first one is the accuracy problem between ejected and remaining weights which is 11.6 µL (approximatively 1 IU). This accuracy can be corrected by considering the capacitance conversion factor of the smart pen cap versus the ejected weight. The second effect is a precision problem. By considering two standard deviation (95% of the points inside the interval) correspond ±48 µL, approximatively ±5 IU of drugs.

3.6.5 Conclusion

According the previous section, an unerasable error exists due to the discrepancies between the measurand, which is the difference of remaining weight inside the injector pen, and the variable of interest, which is the ejected weight. That ejected weight corresponds to the real amount of drug that the patient will inject himself. This discrepancy has different sources

- the lost droplet which appears when the needle is inserted through the septum. This needle insertion releases drug pressure by ejecting a small amount of drug.
- Bubbles inside the cartridge can also have an impact. Due to the compressibility of air, it absorbs a part of the plunger movement.
- The volume of drugs remaining inside the needle after the injection is not considered by measuring the weight of drugs inside the beaker.

All these errors impact the measurement and correspond to an average deviation of 1 IU and a precision error of ±5 IU.

3.7 Cap-to-cap variability

Due to manufacturing process incertitude, some variation will exist from one smart pen cap to another. The question is that: each smart pen cap will need a calibration, or a batch calibration is sufficient. To answer this question, five caps have been tested to determine their conversion slopes. For each cap five pens have been emptied by 120 µL injection steps to observe the variability of the slope pen by pen, then cap by cap. The slopes obtained have been compiled inside box plot presented in Figure 84.

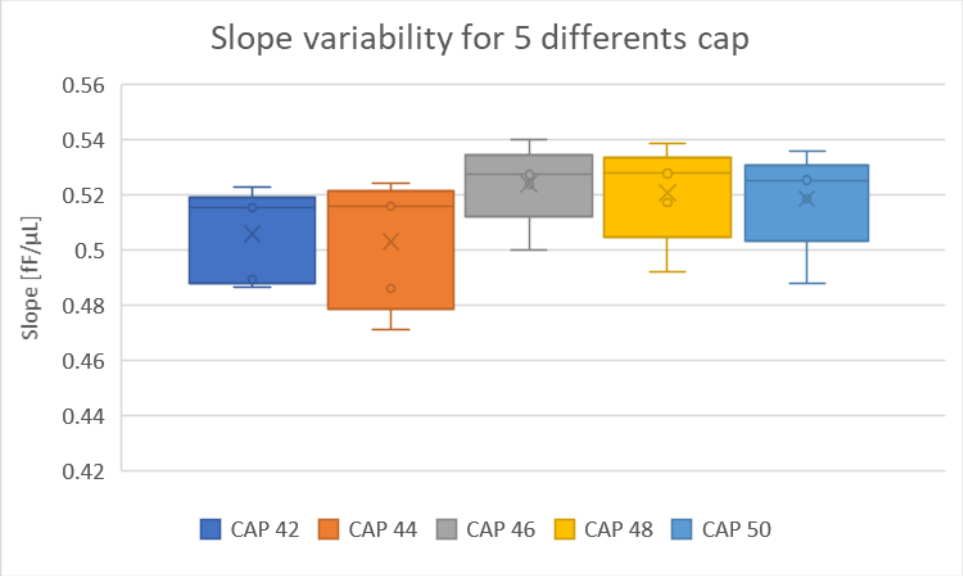

Figure 84 : Cap to cap variability

First observation, the variability seems more pen dependents than pen cap dependents. The cap with the larger slope variability is the cap #44. It has a slope variation from 0.47 fF/µL to 0.53 fF/µL, this creates a full-scall error of ~43 fF. By considering an average slope at 0.5 fF/µL, the Full-Scale error can be ±43 µL. This error can be due to the position of the cartridge inside the cap which has not be defined.

For the Cap-to-cap variation, by considering the average slopes, the variation goes from 0.51 fF/µL to 0.53 fF/µL, this creates a full-scall error of ~14.5 fF. By considering an average slope at 0.5 fF/µL, the Full-Scale error can be ±14.5 µL. The main hypothesis about the fact that the cap-to-cap variability is less pronounced that the pen-to-pen is that it could be due to the average of the five pen slopes. The main errors observe seem more linked to the pen and the cartridge position.

An experiment where the cartridge position is more defined, or by increasing the number of pens shall be done to confirm this hypothesis.

3.8 Chapter conclusion

In this chapter, various perturbations have been studied. These errors will considerably impact the sensitivity of the capacitive sensor. Therefore, some countermeasures to limit and compensate these effects have been done.

- For electromagnetic noise, the device has been shielded to prevent the capacitance variation due to external action.
- The geometric error has been reduced by using 4-electrode devices and averaging two perpendicular electric fields. Then the error was reduced by using an estimation of the position of the cartridge using 2vs2 and 1vs3 electrode configuration algorithm. Then, capacitance was compensated by the estimated position of the cartridge.
- The error due to bubbles has low impact on the measurement but have an impact on the ejected versus remaining error.
- The climatic variation has been compensated by using differential measurements with reference electrode or climatic sensor.
- The ejected versus remaining error is unfortunately built-in error and is due to the difference between the injected volume and the remaining volume inside the cartridge which is measured. Therefore, the system cannot see the loss volumes (needle loss drops, bubble compressibility…) .
- Finally, the manufacturing tolerance induces some errors which can be different from cap to cap and it could impact the calibration strategy (global, by batch, or for each cap). Moreover, the calibration seems to depend on the pen-to-pen variation which can be due to its position inside the smart pen cap.

All these errors have been summarized in Table 9, according these results the main contributors are the ejected/remaining errors which is unavoidable, then the geometric and the climatic (by considering a 10°C change) errors. These two errors can be reduced.

Table 9: Summarize table of all errors

Item	**Mean error**	**Max error**
Electronic noise [µL]	0.376	0.578
Geometric [µL]	23.28	77.82
Climatic [µL/°C]	4.4	4.4
Ejected/remaining [µL]	23.2	96
Manufacturing cap to cap [µL]	0.73 (1 IU)	53.27 (72 IU)
Bubble [µL]	0.01	0.01
Results [µL]	52	232
Results [IU]	±2.6	±11.6

Conclusion

This work has presented a system which allows to measure the level of drug inside an injector pen dedicated for patients who suffer from diabetes. The system overview has been presented in Chapter 1. The system shall be able to communicate with a smartphone to provide information to the user as: the drug level, the history of injections, the storage condition (temperature and relative humidity). A bibliographic study has been conducted where the different technics to measure capacitance have been detailed. It appears that a capacitance to digital topology using ΣΔ converter fit to the need, due to its resolution below 5fF, its low power consumption and the availability of a commercial chip proposed by Analog device for mass production. To allow different electric field configuration, a switch MAX4571 is used to connect the electrodes to the capacitance-to-digital-converter. Finally, a stand-alone test is conducted with PCBA alone and empty device. The noise floor is equal to ±0.087fF and ±0.059fF respectively. This is approximatively 80 times lower than the 5fF limits. Therefore, this architecture has been validated.

Chapter 2 did focus on the shape of the electric field. The objective was to maximize the capacitance variation according to the level of drug. Two different configurations have been studied using theory, simulation, and tests. The first one is the two flat electrode configuration. It is the easiest configuration theory and simulation gives coherent results with a slope of 0.2fF/µL, but due to the shape of the electrode, the casing will be too bulky, and this solution has been abandoned. The second configuration is based on two semi-cylindrical electrode. Two theories were used to analyze this configuration. The first one is based on the infinite number of two parallel flat electrode, but the major drawback of this technic is that it considers the electric field as linear which is not corresponding to the reality. The second method used conformal mapping to take into account the deformation of electric field according the curvature of the electrode. This second method fits to the simulation and the tests. The semi-cylindrical electrode seem to give better results with a slope of 0.5fF/µL and allows for a good form factor of the smart pen cap. For the test, an analysis of the injection which compared results obtained by weight and capacitance seemed to show some discrepancy which can be due to different parasitic effects.

The final chapter deals with parasitic effects. Firstly, the impact of external disturbance of the electric field has been discussed, and the necessity to use a shielding to contain the electric field inside the smart pen cap has been demonstrated. Secondly, due to mechanical tolerances between the injector pen and the smart pen cap and also the conception of the injector pen and the cartridge, the drug can have different positions relative to the electrode. Due to the semi-cylindrical shape of the electrode, the electric field is not uniform, and some high and low electric field areas exist. Therefore, depending on where the cartridge is located, the capacitance can be impacted with an error of approximatively 122.5fF. A proposal has been made to use four electrodes and turning the electric field by 90° in order to average the electric field and attenuate the effect of the cartridge position. The error drastically decreases to 11fF. By increasing the number of electrode above 4, this does not reduce significantly the error compared to the increase of the complexity. A three electrodes device has been also studied and gives good results for compensating the position of the cartridge. But the conversion slope / sensitivity was worse than with the 4 electrodes device. A good compromise was to change the configuration with an excitation electrode against three measurement electrodes in the measuring sequence to have an asymmetric electric field.

Other effects can impact the accuracy of the injector pen and the smart pen cap. Bubbles can appear if the patient does not respect priming instructions or leaves the needle on the pen during a long period of time. These bubbles can impact the ejected volume of drug due to the compressibility of the air. Due to the non-uniform electric field, the bubble

position can have an impact on the measurement. As shown in subsection 3.4, the error due to a bubble is negligeable on the electric field but will have a great impact on the injector pen mechanism, therefore the volume injected will be underdosed. The smart pen cap shall be able to detect these events by comparing the exact amount of drug expelled and the expected injection.

The next subsection was about climatic variation which impacts the measurement due to the humidity absorption and the change of the electric permittivity according the temperature. Encapsulation and reference electrode have been investigated to compensate the climatic variation by impeaching the water absorption and susbtracting the ambient variation respectively. Then, the difference between ejected and remaining volume has been shown, this error cannot be compensated due to the nature of the measurement which focus on the remaining volume. Finally, the cap-to-cap variability due to manufacturing has been shown.

In conclusion, the present study describes the realization of a smart pen cap device. The device is able to measure the drug level inside the injector pen with a precision of 52µL. Since patients undergoing multiple daily injection therapy are currently working in the blind, this is already a considerable improvement. Major deviations from the prescribed or intended dose can be detected by the device and the patient or caretaker alerted, thus improving safety of the therapy and therapeutic outcome. It is especially important that the device may be able to detect severe malfunctions like a clogged injection needle preventing the delivery of the intended dose. The chosen capacitive technique is insensitive to dust, scratches and insertion positioning of the pen into the smart cap. The Bluetooth connectivity can already provide for a good follow up/history of the use of the injector pen to the patient and the medical staff.

However, the current status of the device does not yet allow to resolve the minimal dosing step of the typical insulin pen, i.e. 1 IU. Further improvements of precision are required in order to allow for a precise dose control using the smart pen cap. The biggest remaining challenge lies in reducing parasitic effects of climatic changes and of position inaccuracies of the cartridge in the electric field. Further development work will be required to improve precision and immunity of the measurements to those parasitic effects.

References

[1] World Health Organization, Global report on Diabetes, Geneva: World Health Organization, 2016.

[2] R. Williams, S. Colagiuri, R. Almutairi, P. A. Montoya et et al, IDF Diabetes Atlas 2019, International Diabetes Federation, 2019.

[3] World Health Organization, Definition, diagnosis and classification of Diabetes mellitus and its complications, Geneva: World Health Organization, 1999.

[4] P. P. Brahmkshatriya, A. A. Mehta, B. D. Saboo et R. K. Goyal, «Characteristics and Prevalence of Latent Autoimmune Diabetes in Adults (LADA),» *International Scholarly Research Network Pharmacology,* 2012.

[5] P. Pozzilli et S. Pieralice, «Latent Autoimmune Diabetes in Adults: Current Status and New Horizons,» *Endocrinology and metabolism,* vol. 33, pp. 147-159, 2018.

[6] B. J. Anderson et M. J. Redondo, «What can we learn from patient-reported outcomes of insulin pen device,» *Journal of diabetes science and technology,* vol. 5, n° %16, pp. 1563-1571, 2011.

[7] National Institute for Health and Care Excellence, «Type 2 diabetes in adults: management,» NICE guideline, 16 December 2020. [En ligne]. Available: https://www.nice.org.uk/guidance/ng28/chapter/Recommendations. [Accès le 10 March 2021].

[8] M. Peyrot, A. H. Barnett, L. F. Meneghini et P. -M. Schumm-Draeger, «Insulin adherence behaviours and barriers in the multinational Global Attitudes of Patients and Physicians in Insulin Therapy study,» *Diabetic medecin,* vol. 29, n° %15, pp. 682-689, 2012.

[9] K. Ellis, H. Mulnier et A. Forbes, «Perceptions of insulin use in type 2 diabetes in primary care: a thematic synthesis,» *BMC Fam Pract,* vol. 19, n° %170, 2018.

[10] M. J. Abrahamson et A. Peters, «Intensification of insulin therapy in patients with type 2 diabetes mellitus: An algorithm for basal-bolus therapy,» *Annals of Medecine,* vol. 44, n° %18, pp. 836-846, 2012.

[11] A. H. Frid, G. Kreugel, G. Grassi, S. Halimi, D. Hicks, L. J. Hirsch, M. J. Smith, R. Wellhoener, B. W. Bode, I. B. Hirsch, S. Kalra, L. Ji et K. W. Strauss, «New Insulin Delivery Recommendations,» *Mayo Clinic Proceedings,* vol. 91, n° %19, pp. 1231-1255, 2016.

[12] A. I. Geller, N. Shehab, M. C. Lovegrove, S. R. Kegler, K. N. Weidenbach, G. J. Ryan et D. S. Budnitz, «National estimates of insulin-related hypoglycemia and errors leading to emergency department visits and hospitalizations,» *JAMA Intern Med,* vol. 175, n° %15, pp. 678-686, 2014.

[13] A. Lepple-Wienhues, «Device for attachment to a portable liquid injection device». Switzerland Brevet US Patent US20170224922A1, European Patent EP 2 987 518 B1, August 2017.

[14] Ypsomed, «The intuitive dial & dose reusable pen.,» Ypsomed AG, Burgdorf.

[15] Emperra GmbH, «ESYSTA,» 2017. [En ligne]. Available: https://www.emperra.com/en/. [Accès le 03 06 2021].

[16] MedicalExpo, «Pen Injectors,» 2021. [En ligne]. Available: https://www.medicalexpo.com/medical-manufacturer/pen-injector-13883.html. [Accès le 03 06 2021].

[17] B. Staiger, «Converting Units Of Insulin To Milligrams And Milliliters,» Wälrus, 28 10 2019. [En ligne]. Available: https://walrus.com/questions/converting-units-of-insulin-to-milligrams. [Accès le 17 06 2021].

[18] C. Burns, T. Morris, B. Jones, W. Koch, M. Borer, U. Riber et A. Bristow, «Proposal to initiate a project to evaluate a candidate International Standard,» World Health Organization, Geneva, 2010.

[19] B. Heller, Écrivain, *PenMate Insulin Pen.* [Performance]. 2008.

[20] M. Altmann, Écrivain, *Side by side comparison of a 4mm pen needle with a 12.7mm pen needle.* [Performance]. BD Medical, 2010.

[21] Académie des sciences, Institut de France, «A brief history of hydrometry,» Encyclopedia of the Environment, [En ligne]. Available: https://www.encyclopedie-environnement.org/en/zoom/a-brief-history-of-hydrometry/. [Accès le 2021].

[22] K. Bull, «METHODS OF ACCURATELY MEASURING CAPACITIVE RH SENSORS,» chez *5th International Symposium on Humidity and Moisture*, Rio de Janeiro, 2006.

[23] U. Ferlito, A. D. Grasso, S. Pennisi, M. Vaiana et G. Bruno, «Sub-Femto-Farad Resolution Electronic Interfaces for Integrated Capacitive Sensors: A Review,» *IEEE Access,* vol. 8, pp. 153969-153980, 2020.

[24] J. P. Sanjurjo, E. Prefasi, C. Buffa et R. Gaggl, «A Capacitance-To-Digital Converter for MEMS,» *Sensors,* vol. 17, n° %16, pp. 1312-1329, 2017.

[25] P. G. Edwards et H. W. HERRINGTON, «Sensitivity Characteristics of a Low- Frequency Bridge Network for Locating Opens in Telephone Circuits,» chez *AIEE*, Pittsfield, 1927.

[26] L. K. Baxter, «Circuit Basics,» chez *Capacitive sensors : Design and applications*, IEEE, 1997, pp. 48-60.

[27] P. Mantenuto, A. De Marcellis et G. Ferri, «Novel Modified De-Sauty Autobalancing Bridge-Based Analog Interfaces for Wide-Range Capacitive Sensor Applications,» *IEEE SENSORS JOURNAL,* vol. 14, n° %15, pp. 1664-1672, 2014.

[28] R. García-Gil, S. Casans Berga, E. Sanchis-Sánchez, I. Pérez-Calatayud, J. Pérez-Calatayud et E. Sanchis Peris, «Electronic Design for a Bleeding Detector to be Used in Intraoperative Radiotherapy Applications,» *IEEE SENSORS JOURNAL,* vol. 21, n° %14, pp. 4786-4792, 2021.

[29] L. Zhong, X. Lai et D. Xu, «Oversampling Successive Approximation Technique for MEMS Differential Capacitive Sensor,» *IEEE JOURNAL OF SOLID-STATE CIRCUITS,* vol. 53, n° %18, pp. 2240-2251, 2018.

[30] M. Saukoski, L. Aaltonen, K. Halonen et T. Salo, «Fully Integrated Charge Sensitive Amplifier for Readout of Micromechanical Capacitive Sensors,» chez *IEEE International Symposium on Circuits and Systems*, 2005.

[31] M. M. Ghanbari,, J. M. Tsai, A. Nirmalathas, R. Muller et S. Gambini, «An Energy-Efficient Miniaturized Intracranial Pressure Monitoring System,» *IEEE JOURNAL OF SOLID-STATE CIRCUITS,* vol. 52, n° %13, pp. 720-734, 2017.

[32] N. T. Trung et P. Häfliger, «A Submicrowatt Implantable Capacitive Sensor System for Biomedical Applications,» *IEEE Transactions on circuits and systems—II: Express briefs,* vol. 62, n° %12, pp. 209-213, 2015.

[33] Zurich Instruments, «Principles of lock-in detection,» Zurich Instruments, Zurich, 2016.

[34] M. Babay, C. Hallepee, C. Dalmay, B. Barelaud, E. C. Durmaz, C. B. Kaynak, M. Kaynak, D. Cordeau et A. Pothier, «Highly Sensitive Capacitive Sensor Based on Injection Locked Oscillators with ppm Sensing Resolution,» chez *International Microwave Symposium*, Los Angeles, 2020.

[35] P. Ciccarella, M. Carminati, M. Sampietro et G. Ferrari, «Multichannel 65 zF rms Resolution CMOS Monolithic Capacitive Sensor for Counting Single Micrometer-Sized Airborne Particles on Chip,» *IEEE JOURNAL OF SOLID-STATE CIRCUITS,* vol. 51, n° %111, pp. 2545-2553, 2016.

[36] F. Gozzini, G. Ferrari et M. Sampietro, «An Instrument-on-Chip for Impedance Measurements on Nanobiosensors with attoFarad Resolution,» chez *IEEE International Solid-State Circuits Conference*, 2009.

[37] H. Mazhab-Jafari, L. Soleymani et R. Genov, «16-Channel CMOS Impedance Spectroscopy DNA Analyzer With Dual-Slope Multiplying ADCs,» *IEEE TRANSACTIONS ON BIOMEDICAL CIRCUITS AND SYSTEMS,* vol. 6, n° %15, p. 468, 2012.

[38] A. Manickam, A. Chevalier, M. McDermot, A. D. Ellington et A. Hassibi, «A CMOS Electrochemical Impedance Spectroscopy Biosensor Array for Label-Free Biomolecular Detection,» chez *IEEE International Solid-State Circuits Conference*, 2010.

[39] A. Jaworek et A. Krupa, «Gas/liquid ratio measurements by rf resonance capacitance sensor,» *Sensors and Actuators,* vol. A, n° %1113, p. 133–139, 2004.

[40] M. Carminati, «Advances in High-Resolution Microscale Impedance Sensors,» *Journal of Sensors,* 2017.

[41] N. Couniot, L. A. Francis et D. Flandre, «A 16 16 CMOS Capacitive Biosensor Array Towards Detection of Single Bacterial Cell,» *IEEE TRANSACTIONS ON BIOMEDICAL CIRCUITS AND SYSTEMS,* vol. 10, n° %12, pp. 364-374, 2016.

[42] S. B. Prakash et P. Abshire, «A Fully Differential Rail-to-Rail CMOS Capacitance Sensor With Floating-Gate Trimming for Mismatch Compensation,» *IEEE TRANSACTIONS ON CIRCUITS AND SYSTEMS—I: REGULAR PAPERS,* vol. 56, n° %15, pp. 975-986, 2009.

[43] J. C. Chen, B. W. McGaughy, D. Sylvester et C. Hu, «An On-Chip, Attofarad Interconnect Charge-Based Capacitance Measurement,» chez *International Electron Devices Meeting. Technical Digest*, 1996.

[44] S. Forouhi, R. Dehghani et E. Ghafar-Zadeh, «Toward High Throughput Core-CBCM CMOS Capacitive Sensors for Life Science Applications: A Novel Current-Mode for High Dynamic Range Circuitry,» *Sensors,* vol. 18, n° %110, p. 3370, 2018.

[45] P. D. Dimitropoulos, D. P. Karampatzakis, G. D. Panagopoulos et G. I. Stamoulis, «A Low-Power/Low-Noise Readout Circuit for Integrated Capacitive Sensors,» *IEEE SENSORS JOURNAL,* vol. 6, n° %13, pp. 755-768, 2006.

[46] G. Scotti, S. Pennisi, P. Monsurrò et A. Trifiletti, «88-uA 1-MHz Stray-Insensitive CMOS,» *IEEE TRANSACTIONS ON CIRCUITS AND SYSTEMS—I: REGULAR PAPERS,* vol. 61, n° %17, pp. 1905-1916, 2014.

[47] S. Pennisi, «High-Performance and Simple CMOS Interface Circuit for Differential Capacitive Sensors,» *IEEE TRANSACTIONS ON CIRCUITS AND SYSTEMS—II: EXPRESS BRIEFS,* vol. 52, n° %16, pp. 327-330, 2005.

[48] T. Singh, T. Sæther et T. Ytterdal, «Current-Mode Capacitive Sensor Interface Circuit With Single-Ended to Differential Output Capability,» *IEEE TRANSACTIONS ON INSTRUMENTATION AND MEASUREMENT,* vol. 58, n° %111, pp. 3914-3920, 2009.

[49] Z. Tan, S. H. Shalmany, G. C. M. Meijer et M. A. P. Pertijs, «An Energy-Efficient 15-Bit Capacitive-Sensor Interface Based on Period Modulation,» *IEEE JOURNAL OF SOLID-STATE CIRCUITS,* vol. 47, n° %17, pp. 1703-1711, 2012.

[50] A. Heidary, S. Heidary et G. Meijer, «A Flexible Low-Power High-Resolution Integrated Interface for Capacitive Sensors,» chez *IEEE International Symposium on Industrial Electronics*, 2010.

[51] Y. He, Z. Chang, L. Pakula, S. H. Shalmany et M. Pertijs, «A 0.05mm2 1V Capacitance-to-Digital Converter,» chez *IEEE International Solid-State Circuits Conference*, 2015.

[52] M. Tomasz, «Use Analog Techniques To Measure Capacitance In Capacitive Sensors,» Electronic Design, 12 NOV 2012. [En ligne]. Available: https://www.electronicdesign.com/technologies/analog/article/21796004/use-analog-techniques-to-measure-capacitance-in-capacitive-sensors. [Accès le 2021 MAR 23].

[53] S. Babu et D. H. Somesh, «Design of Self- Compensated Non Contact Capacitive Sensors and Proficient Signal Conditioning Circuit for Multi Threshold Liquid Level Control -A Novel Approach,» chez *IEEE International Conference on Industrial Technology*, Mumbai, 2006.

[54] K. Mohammad et D. J. Thomson, «Differential Ring Oscillator Based Capacitance Sensor for Microfluidic Applications,» *IEEE TRANSACTIONS ON BIOMEDICAL CIRCUITS AND SYSTEMS,* vol. 11, n° %12, pp. 392-399, 2017.

[55] P. Bruschi, N. Nizza et M. Piotto, «A Current-Mode, Dual Slope, Integrated Capacitance-to-Pulse Duration Converter,» *IEEE JOURNAL OF SOLID-STATE CIRCUITS,* vol. 42, n° %19, pp. 1884-1891, 2007.

[56] P. Bruschi, N. Nizza et M. Dei, «A low-power capacitance to pulse width converter for MEMS interfacing,» chez *ESSCIRC 2008 - 34th European Solid-State Circuits Conference*, 2008.

[57] N. Nizza, M. Dei, F. Butti et P. Bruschi, «A Low-Power Interface for Capacitive Sensors With PWM Output and Intrinsic Low Pass Characteristic,» *IEEE TRANSACTIONS ON CIRCUITS AND SYSTEMS—I: REGULAR PAPERS,,* vol. 60, n° %16, pp. 1419-1431, 2013.

[58] A. De Marcellis, C. Reig et M. D. Cubells-Beltrán, «A Capacitance-to-Time Converter-Based Electronic Interface for Differential Capacitive Sensors,» *Electronics,* vol. 8, n° %180, 2019.

[59] Z. Tan, R. Daamen, A. Humbert, Y. V. Ponomarev, Y. Chae et M. A. P. Pertijs, «A 1.2-V 8.3-nJ CMOS Humidity Sensor for,» *IEEE JOURNAL OF SOLID-STATE CIRCUITS,* vol. 48, n° %110, pp. 2469-2477, 2013.

[60] H. Omran, M. Arsalan et K. N. Salama, «An integrated energy-efficient capacitive sensor digital interface circuit,» *Sensors and Actuators A: Physical,* vol. 216, pp. 43-51, 2014.

[61] H. Ha, D. Sylvester, D. Blaauw et J.-Y. Sim, «A 160nW 63.9fJ/conversion-step Capacitance-to-Digital Converter for Ultra-Low-Power Wireless Sensor Nodes,» chez *IEEE International Solid-State Circuits Conference*, 2014.

[62] H. Zhang, L. Zhai, C. Yang, H. Wang et N. Jin, «Capacitive Phase Shift Detection for Measuring Water Holdup in Horizontal Oil–Water Two-Phase Flow,» *Sensors,* vol. 18, n° %17, p. 2234, 2018.

[63] R. F. Wolffenbuttel et P. P. L. Regtien, «Capacitance-to-Phase Angle Conversion for the Detection of Extremely Small Capacities,» *IEEE TRANSACTIONS ON INSTRUMENTATION AND MEASUREMENT,* Vols. %1 sur %2IM-36, n° %14, pp. 868-872, 1987.

[64] Analog Devices, «24-Bit Capacitance-to-Digital Converter with Temperature Sensor - AD7745/AD7746,» Analog Devices, Inc, Norwood, 2005.

[65] F. Gaugaz, F. Krummenacher, F. Gaugaz, M. Kayal, S. Joly, A. Lepple-Wienhues et J. B. Orhan, «A high sensitivity low-power capacitive front-end for insulin injection pens,» *Microelectronics Journal,* vol. 85, pp. 129-134, 2019.

[66] Analog Device, «I2C® CMOS 8 × 12 Unbuffered Analog Switch Array With Dual/Single Supplies: ADG2128,» Norwood, 2012.

[67] Maxim, «Serially Controlled, Clickless Audio/Video Switches: MAX4571,» Sunnyvale, 1999.

[68] Analog Device, «0 Hz/dc to 14 GHz, Single-Pole, Four-Throw MEMS Switch with Integrated Driver: ADGM1304,» Norwood, 2021.

[69] R. T. Bento, R. W. Silva, L. A. Dias, A. F. Filho et A. J. Pitta, «Design, development and application of a real-time capacitive sensor for automatically measuring liquid level,» *Springer Nature Applied Sciences,* vol. 1, n° %1734, 2019.

[70] D. Conchouso, A. Arevalo, D. Castro, M. Kavaldzhiev et I. G. Foulds, «Capacitive Sensor for Continuous Monitoring of High-Volume Droplet Microfluidic Generation,» chez *Conference on Nano/Micro Engineered and Molecular Systems (NEMS)*, Matsushima Bay and Sendai MEMS City, 2016.

[71] A. Pietrikova, S. Zuk et I. Vehec, «Coplanar Capacitive Liquid Level Sensor,» chez *42nd International Spring Seminar on Electronics Technology*, Wroclaw, 2019.

[72] T. Islam et O. P. Maurya, «Design and fabrication of non-contact fringing field capacitive sensor for liquid level measurement,» chez *16th India Council International Conference (INDICON)*, Rajkot, 2019.

[73] S. M. Salehi et A. A. Dastranj, «A Capacitance Sensor for Gas/Oil Two-Phase Flow Measurement: Exciting Frequency Analysis and Static Experiment,» *IEEE SENSORS JOURNAL,* vol. 17, n° %13, pp. 679-686, 2017.

[74] S. Pal et R. Barik, «Design, Development and Testing of a Semi Cylindrical Capacitive Sensor for Liquid Level Measurement,» *Sensors & Transducers Journal,* vol. 116, n° %15, pp. 13-20, 2010.

[75] C.-T. Chiang et Y.-C. Huang, «A Semicylindrical Capacitive Sensor With Interface Circuit Used for Flow Rate Measurement,» *IEEE SENSORS JOURNAL,* vol. 6, n° %16, pp. 1564-1570, 2006.

[76] G. L. Lim, T. B. Tang, N. H. Hamid et W. K. Pao, «Sinusoid Based Calibration for Holdup Measurement in Two-Phase Flow Using Helical Capacitance Sensor,» chez *6th International Conference on Intelligent and Advanced Systems*, Kuala Lumpur, 2016.

[77] S. Das, T. S. Sarkar et B. Chakraborty, «A Semi-Cylindrical Capacitive Sensor Used for Soil Moisture Measurement,» *International Journal of Electrical, Computer, Energetic, Electronic and Communication Engineering,* vol. 8, n° %11, pp. 160-165, 2014.

[78] M. N. Manaf et K. Triyana, «Analytical solutions for capacitance of a semi-cylindrical capacitive sensor,» chez *AIP Conference*, 2016.

[79] C. Fong, «Analytical Methods for Squaring the Disc (Addendum of "Elliptification of Rectangular Imagery"),» chez *ICM*, Seoul, 2014.

[80] S. B. Cahn et B. E. Nadgorny, A Guide to Physics Problems: Part 1: Mechanics, Relativity, and Electrodynamics, Boston: Springer, 1994, pp. 240-243.

[81] J. Mosig, «Static Green's Functions with Conformal Mapping and MATLAB,» *IEEEAntennas andPmpagation Magazine,* vol. 45, n° %15, pp. 123-135, 2003.

[82] «Needle-based injection systems for medical use — Requirements and test methods — Part 1: Needle-based injection systems,» International Standard Organisation (ISO), 2014.

[83] D. Wang, «Capacitive Sensing: Ins and Outs of Active Shielding,» Texas Instruments, Dallas, 2015.

[84] L. G. Lim et T. B. Tang, «Design of Concave Capacitance Sensor for Void Fraction Measurement in Gas-Liquid Flow,» chez *8th International Conference on Information Technology and Electrical Engineering (ICITEE),*, Yogyakarta, 2016.

[85] A. Martinez Olmos, M. A. Carvajal, D. P. Morales, A. Garcia et A. J. Palma, «Development of an Electrical Capacitance Tomography system using four rotating electrodes,» *Sensors and Actuators A: Physical,* vol. A, n° %1148, pp. 366-375, 2008.

[86] S. J. Ogyaadu, D. W. Lam, L. Norlander, J. Robic, C. M. Levister, S. Anderson, S. Loebner, S. E. Loebner, L. Ekhlaspour et M. Breton, «Trends in Insulin Pen Priming,» chez *Am Diabetes Assoc*, 2018.

[87] P. M. Trief, D. Cibula, E. Rodriguez, B. Akel et R. S. Weinstock, «Incorrect Insulin Administration: A Problem That Warrants Attention,» *Clin Diabetes,* vol. 34, n° %11, pp. 25-33, 2016.

[88] A. H. Frid, L. J. Hirsch, A. R. Menchior, D. R. Morel et K. W. Strauss, «Worldwide Injection Technique Questionnaire Study: Injecting Complications and the Role of the Professional,» *Mayo Clinic Proceedings,* vol. 91, n° %19, pp. 1224-1230, 2016.

[89] H. K. Trieu, N. Kordas et W. Mokwa, «Fully CMOS Compatible Capacitive Differential Pressure Sensors with On-Chip Programmabilities and Temperature Compensation,» chez *Sensors*, Orlando, 2002.

[90] I. Bord, P. Tardy et F. Menil, «Influence of the electrodes configuration on a differential capacitive rain sensor performances,» *Sensors and Actuators,* vol. B, n° %1114, pp. 640-645, 2006.

[91] H. K. Trieu, N. Kordas et W. Mokwa, «Fully CMOS compatible capacitive differential pressure sensors with on-chip programmabilities and temperature compensation,» chez *IEEE Sensors*, Orlando, 2002.

[92] I. Bord, P. Tardy et F. Menil, «Influence of the electrodes configuration on a differential capacitive rain sensor performances,» *Sensors and Actuators,* vol. B, n° %1114, pp. 640-645, 2005.

[93] A. H. Frid, L. J. Hirsch, A. R. Menchior, D. R. Morel et K. W. Strauss, «Worldwide Injection Technique QuestionnaireStudy: Injecting Complications and the Role ofthe Professional,» *Mayo Clinic Proceedings,* vol. 91, n° %19, pp. 1224-1230, 2015.

[94] A. Friedrichs, N. Basso et S. Adler, «Dose accuracy of the ClickSTAR,NovoPen 4, and Luxura Insulin Pens: Results of laboratory and field studies,» *Journal of Diabetes science and technology,* vol. 5, n° %15, pp. 1179-1184, 2011.

Curriculum Vitae

CONTACT INFORMATION

SYLVAIN JOLY

31 ROUTE DU HAMEAU

25240 BREY ET MAISON DU BOIS

FRANCE

SJOLY@VALTRONIC.COM

SYLVAIN.JOLY25@GMAIL.COM

EMPLOYMENT HISTORY

- *2016-PRESENT: VALTRONIC TECHNOLOGIES*
  - 2016-2019: RESEARCH AND DEVELOPPEMENT INGEENER IN INNOVATION GROUP: DESIGNING PROOF OF CONCEPT FOR NEW TECHNOLOGIES AND/OR CONCEPT APPLIED TO THE MEDICAL FIELD
    - BIBLIOGRAPHY (SCIENTIFIC PUBLICATION AND PATENTS)
    - DESIGN OF PROOF-OF-CONCEPT DEVICES
    - DESIGN OF EXPERIMENTS
  - 2019-NOWADAY: ELECTRONIC ENGINEER IN THE RESEACH AND DEVELOPMENT GROUP: SUPPORT THE CLIENT TO THE TRANSFERT OF PROOF OF CONCEPT OR DESIGN ALMOST FREEZE INTO INDUSTRIAL MANUFACTURING
    - REQUIREMENTS MANAGEMENT (ELECTRONIC PARTS)
    - DESIGN FOR PROTOTYPING (V-CYCLE, RISK ANALYSIS, APPLIED STANDARDS…)
    - DESIGN FOR MANUFACTURING (SUPPORT PRODUCTION, DOCUMENTATION, RETURN OF EXPERIENCE…)
- 2014-2015: RESEARCH ENGINEER: FINISH THE DEVELOPMENT OF DEVICE WHICH ALLOW TO DO EXTENSOMETER TEST ON *"IN VIVO"* SKIN
  - DESIGN ELECTRONIC PART OF THE PROTOTYPE
  - DATA EXCTRACTION
  - SCIENTIFIC SUPPORT (WORK PRESENTATION AT CONFERENCE AND POSTER)

EDUCATION

- 2017- PRESENT: PHD STUDENT AT EPFL
- 2013-2014: MASTER MECATRONIC, MICROSYSTEM AND EMBEDDED ELECTRONIC AT UNIVERSITÉ DE BOURGOGNE-FRANCHE COMTÉ
- 2011-2014: BIOMEDICAL ENGINEER AT ISIFC
- 2009-2011: DUT GENIE ELECTRONIQUE ET INFORMATIQUE INDUSTRIEL
- 2007-2009: BAC STI GENIE ELECTRONIQUE

PROFESSIONAL QUALIFICATIONS

- SOFTWARE
  - SCHEMATIC & LAYOUT: ALTIUM, KICAD
  - SIMUATION : LT-SPICE, FEMM, CADFEM
  - MATHEMATIC: OCTAVE, MATLAB, EXCEL, IGOR
- OTHERS
  - PROGRAMMING LANGAGE :
    - WELL KNOW : PYTHON, C, VBA
    - NOTION : ASSEMBLY, C++, PHP
  - LANGAGE
    - FRENCH : NATIVE
    - ENGLISH: MEDIUM LEVEL, READING, WRITING AND SPEAKING

PUBLICATIONS

FIRST AUTHOR

S. JOLY, A. LEPPLE-WIENHUES AND C. DEHOLLAIN, "ELECTRONIC SOLUTION TO COMPENSATE THE EFFECTS OF THE TEMPERATURE AND THE HUMIDITY ON THE MEASUREMENTS OF A CAPACITIVE SENSOR DEDICATED TO AN INJECTION INSULIN PEN" *2021 18TH CONFERENCE ON PH.D. RESEARCH IN MICROELECTRONICS AND ELECTRONICS (PRIME)*, 2021 [WILL BE PUBLIED SOON]

S. JOLY, A. LEPPLE-WIENHUES AND C. DEHOLLAIN, "MODELING OF A CAPACITIVE SENSOR DEDICATED TO DRUG INJECTION," *2018 14TH CONFERENCE ON PH.D. RESEARCH IN MICROELECTRONICS AND ELECTRONICS (PRIME)*, 2018, PP. 217-220, DOI: 10.1109/PRIME.2018.8430369.

S. JOLY, A. LEPPLE-WIENHUES AND C. DEHOLLAIN, "CAPACITANCE MEASUREMENT APPLIED TO THE MEDICAL INJECTION PEN," *2017 13TH CONFERENCE ON PH.D. RESEARCH IN MICROELECTRONICS AND ELECTRONICS (PRIME)*, 2017, PP. 317-320, DOI: 10.1109/PRIME.2017.7974171.

OTHER

M. PAUN, A. SCHNEGG, S. JOLY, J. ORHAN, A. LEPPLE-WIENHUES AND C. DEHOLLAIN, "THREE-DIMENSIONAL MODEL AND EVALUATION OF AN INSULIN INJECTION PEN FOR PRECISE DOSE CAPACITIVE MEASUREMENT," IN *IEEE ACCESS*, VOL. 7, PP. 117426-117435, 2019, DOI: 10.1109/ACCESS.2019.2936290.

F. GAUGAZ, F. KRUMMENACHER, F. GAUGAZ, M. KAYAL, S. JOLY, A. LEPPLE-WIENHUES & J. B. ORHAN, "A HIGH SENSITIVITY LOW-POWER CAPACITIVE FRONT-END FOR INSULIN INJECTION PENS" IN. *MICROELECTRONICS JOURNAL*, *85*, 129-134, 2019.

INTERESTS

- PLAY MUSIC: KEYBOARD AND GUITAR
- RENOVATION OF JUKBOX, FLIPPER, CITROEN 2CV, RENAULT 4L
- SPORT: JUDO

Appendix: Conformal mapping Script

```
clear all
close all
clc

          ###################################################################
                                VARIABLE DECLARATION
          ###################################################################
Samples = 1000           # Size of vectors

eps  = 8.8541878128E-12 # Absolute electric permittivity [F/m]
epsA = 1*eps            # Electric permittivity of air [F/m]
epsW = 80.4*eps         # Electric permittivity of water [F/m]
epsP = 2.5*eps          # Electric permittivity of plastic [F/m]
epsG = 4*eps            # Electric permittivity of glass [F/m]

L       = 0.023         # Lenght of the system [m]
EAngle  = 160           # Angulare width of the electrode []
SAngle  = (180-EAngle)/2# Start angle of the electrode []
FAngle  = 180-SAngle    # Final angle of the electrode []

# Electrode 1 angle vector
theta1  = deg2rad(linspace(SAngle,FAngle,Samples));
# Electrode 2 angle vector
theta2  = deg2rad(linspace(SAngle+180,FAngle+180,Samples));
# Angle vector of the device
theta   = deg2rad(linspace(0,360,Samples));

r       = 0.0075  # Radius of the electrode
rd      = 0.00475 # Inner radius of the cartridge (drug limit)
rc      = 0.00575 # Outer radius of the cartridge (glass limit)
ra      = 0.00625 # Inner radius of the cartridge Holder (intern air limit)
rh      = 0.00725 # Outer radius of the cartridge Holder (plastic limit)

        ###################################################################
                              CREATION OF THE DEVICE

        ###################################################################

z1=r*exp(i*theta1); # Electrode 1
z2=r*exp(i*theta2); # Electrode 2
zd=rd*exp(i*theta); # Drug compartiment
zc=rc*exp(i*theta); # Cartridge
za=ra*exp(i*theta); # Gap between cartridge and cartridge holder
zh=rh*exp(i*theta); # Cartridge holder


# Creation of a grid 50 x 50

lx=linspace(-r,r,50)'+linspace(-r,r,50)*i;
```

```
ly=linspace(-r,r,50)+linspace(-r,r,50)'*i;

#### PLOT OF THE DEVICE GEOMETRY
figure(1)
plot(real(lx),imag(lx),"color",[0.6 0.6 0.6],real(ly),imag(ly),"color",[0.6 0.6
0.6],...
  real(z1),imag(z1),'b',real(z2),imag(z2),'r',real(zd),imag(zd),'m',...
  real(zc),imag(zc),'c',real(za),imag(za),'g',real(zh),imag(zh),'k')
  axis("square")
  xlabel("X-axis [mm]","fontsize",16)
  ylabel("Y-axis [mm]","fontsize",16)
  xlim([-0.0075 0.0075])
  ylim([-0.0075 0.0075])

            ########################################################
                              MÖBIUS MAPPING

            ########################################################

w1=(r+z1)./(r-z1);  # Electrode 1
w2=(r+z2)./(r-z2);  # Electrode 2
wd=(r+zd)./(r-zd);  # Drug compartiment
wc=(r+zc)./(r-zc);  # Cartridge
wa=(r+za)./(r-za);  # Gap between Cartridge and cartridge Holder
wh=(r+zh)./(r-zh);  # Cartridge holder

# Grid  Ms mapping
wx=(r+lx)./(r-lx);
wy=(r+ly)./(r-ly);

#### PLOT THE MıIUS MAPPING OF THE DEVICE
figure(2)
plot(real(wx),imag(wx),"color",[0.6 0.6 0.6],real(wy),imag(wy),"color",[0.6 0.6
0.6],...
  real(w1),imag(w1),'b',real(w2),imag(w2),'r',real(wd),imag(wd),'m',...
  real(wc),imag(wc),'c',real(wa),imag(wa),'g',real(wh),imag(wh),'k')
  axis("square")
  xlabel("u-axis [mm]","fontsize",16)
  ylabel("v-axis [mm]","fontsize",16)

               ################################################
                              FOLD BACK MAPPING
               ################################################

u1    = log((w1));  # Electrode 1
u2    = log((w2));  # Electrode 2
ud    = log((wd));  # Drug compartiment
uc    = log((wc));  # Cartridge
ua    = log((wa));  # Gap between Cartridge and cartridge Holder
uh    = log((wh));  # Holder

# Grid fold back mapping
ux   = log((wx));
uy   = log((wy));

#### PLOT THE FOLD BACK MAPPING OF THE DEVICE
figure(3)
plot(real(ux),imag(ux),"color",[0.6 0.6 0.6],real(uy),imag(uy),"color",[0.6 0.6
0.6],...
  real(u1),imag(u1),'b',real(u2),imag(u2),'r',real(ud),imag(ud),'m',...
  real(uc),imag(uc),'c',real(ua),imag(ua),'g',real(uh),imag(uh),'k')
```

```
  axis("square")
  xlabel("u-axis [mm]","fontsize",16)
  ylabel("v-axis [mm]","fontsize",16)
  xlim([min(real(u1)) max(real(u1))])
  ylim([-pi/2 pi/2])

            ########################################################
                        CAPACITANCE MATHS - Discret methods
            ########################################################
A=170 # End electrode angle
# Definition of only a quarter of the devices
Th  = linspace(deg2rad(90),deg2rad(A),Samples); ## 179.9 instead of 180 to avoid
infinity in air domain
    A =  170
# Update the mapping with only quarter of the device

Ud  = log((r+rd.*exp(i.*Th))./(r-rd.*exp(i.*Th)));
Uc  = log((r+rc.*exp(i.*Th))./(r-rc.*exp(i.*Th)));
Ua  = log((r+ra.*exp(i.*Th))./(r-ra.*exp(i.*Th)));
Uh  = log((r+rh.*exp(i.*Th))./(r-rh.*exp(i.*Th)));
U   = log((r+r.*exp(i.*Th))./(r-r.*exp(i.*Th)));

X1  = real(-U); ## U is the electrode, therefore real is electrode width
# Pythagoras to find the distance from u-axis of each domain

Dd  = real(sqrt((abs(Ud)).^2-X1.^2));
Dc  = real(sqrt((abs(Uc)).^2-X1.^2));
Da  = real(sqrt((abs(Ua)).^2-X1.^2));
Dh  = real(sqrt((abs(Uh)).^2-X1.^2));
D   = real(sqrt((abs(U)).^2-X1.^2));
#### PLOT OF THE DISTANCE FROM u-axis FOR ALL DOMAIN

figure(4)
plot(X1,Dd,'m',X1,Dc,'c',X1,Da,'g',X1,Dh,'k',X1,D,'b')
  axis("square")
  xlabel("u-axis","fontsize",16)
  ylabel("v-axis","fontsize",16)


# Thickness of all materials along u-axis

Td  = Dd;
Tc  = Dc-Dd;
Ta  = Da-Dc;
Th  = Dh-Da;
T   = D-Dh;


#### PLOT OF THE THICKNESS ALONG u-axis FOR ALL DOMAIN

figure(5)
plot(X1,Td,'m',X1,Tc,'c',X1,Ta,'g',X1,Th,'k',X1,T,'b')
  axis("square")
  xlabel("u-axis","fontsize",16)
  ylabel("v-axis","fontsize",16)
  xlim([0 max(real(u1))])

# Width of partial electrode depending of u-axis
dx=diff(linspace(0,max(X1),Samples+1));
Cf  = L.*dx./(Td./epsW+Tc./epsG+Ta./epsA+Th./epsP+T./epsA); # Full pen capa vec-
tor
```

```
Ce  = L.*dx./(Td./epsA+Tc./epsG+Ta./epsA+Th./epsP+T./epsA); # Empty pen capa
vector
#### PLOT OF THE FULL AND EMPTY CAPACITANCE ALONG u-axis

figure(6)
plot(X1,Cf,'r',X1,Ce,'b')
  axis("square")
  xlabel("u-axis","fontsize",16)
  ylabel("v-axis","fontsize",16)
  xlim([0 max(real(u1))])

CF  = sum(Cf)*1E15  # Result of the Full capacitance
CE  = sum(Ce)*1E15  # Result of the Empty capacitance
S1  = (CF-CE)/1630  # Sensitivity (considered volume 1630uL)

            ########################################################
                  CAPACITANCE MATHS - Integral methods
            ########################################################

A=170 # End electrode angle
  Cdf = L.*integral(@(TH)1./(...
    real(sqrt((abs(log((r+rd.*exp(i.*TH))./(r-rd.*exp(i.*TH))))).^2-
(real(log((r+r.*exp(i.*(pi/2)))./(r-r.*exp(i.*(pi/2)))))).^2))./epsW+...
    (real(sqrt((abs(log((r+rc.*exp(i.*TH))./(r-rc.*exp(i.*TH))))).^2-
(real(log((r+r.*exp(i.*(pi/2)))./(r-r.*exp(i.*(pi/2)))))).^2))-...
    real(sqrt((abs(log((r+rd.*exp(i.*TH))./(r-rd.*exp(i.*TH))))).^2-
(real(log((r+r.*exp(i.*(pi/2)))./(r-r.*exp(i.*(pi/2)))))).^2)))./epsG+...
    (real(sqrt((abs(log((r+ra.*exp(i.*TH))./(r-ra.*exp(i.*TH))))).^2-
(real(log((r+r.*exp(i.*(pi/2)))./(r-r.*exp(i.*(pi/2)))))).^2))-...
    real(sqrt((abs(log((r+rc.*exp(i.*TH))./(r-rc.*exp(i.*TH))))).^2-
(real(log((r+r.*exp(i.*(pi/2)))./(r-r.*exp(i.*(pi/2)))))).^2)))./epsA+...
    (real(sqrt((abs(log((r+rh.*exp(i.*TH))./(r-rh.*exp(i.*TH))))).^2-
(real(log((r+r.*exp(i.*(pi/2)))./(r-r.*exp(i.*(pi/2)))))).^2))-...
    real(sqrt((abs(log((r+ra.*exp(i.*TH))./(r-ra.*exp(i.*TH))))).^2-
(real(log((r+r.*exp(i.*(pi/2)))./(r-r.*exp(i.*(pi/2)))))).^2)))./epsP+...
    (real(sqrt((abs(log((r+r.*exp(i.*TH))./(r-r.*exp(i.*TH))))).^2-
(real(log((r+r.*exp(i.*(pi/2)))./(r-r.*exp(i.*(pi/2)))))).^2))-...
    real(sqrt((abs(log((r+rh.*exp(i.*TH))./(r-rh.*exp(i.*TH))))).^2-
(real(log((r+r.*exp(i.*(pi/2)))./(r-r.*exp(i.*(pi/2)))))).^2)))./epsA),...
    deg2rad(90),deg2rad(A))*1E15

  Cde = L.*integral(@(TH)1./(...
    real(sqrt((abs(log((r+rd.*exp(i.*TH))./(r-rd.*exp(i.*TH))))).^2-
(real(log((r+r.*exp(i.*(pi/2)))./(r-r.*exp(i.*(pi/2)))))).^2))./epsA+...
    (real(sqrt((abs(log((r+rc.*exp(i.*TH))./(r-rc.*exp(i.*TH))))).^2-
(real(log((r+r.*exp(i.*(pi/2)))./(r-r.*exp(i.*(pi/2)))))).^2))-...
    real(sqrt((abs(log((r+rd.*exp(i.*TH))./(r-rd.*exp(i.*TH))))).^2-
(real(log((r+r.*exp(i.*(pi/2)))./(r-r.*exp(i.*(pi/2)))))).^2)))./epsG+...
    (real(sqrt((abs(log((r+ra.*exp(i.*TH))./(r-ra.*exp(i.*TH))))).^2-
(real(log((r+r.*exp(i.*(pi/2)))./(r-r.*exp(i.*(pi/2)))))).^2))-...
    real(sqrt((abs(log((r+rc.*exp(i.*TH))./(r-rc.*exp(i.*TH))))).^2-
(real(log((r+r.*exp(i.*(pi/2)))./(r-r.*exp(i.*(pi/2)))))).^2)))./epsA+...
    (real(sqrt((abs(log((r+rh.*exp(i.*TH))./(r-rh.*exp(i.*TH))))).^2-
(real(log((r+r.*exp(i.*(pi/2)))./(r-r.*exp(i.*(pi/2)))))).^2))-...
    real(sqrt((abs(log((r+ra.*exp(i.*TH))./(r-ra.*exp(i.*TH))))).^2-
(real(log((r+r.*exp(i.*(pi/2)))./(r-r.*exp(i.*(pi/2)))))).^2)))./epsP+...
    (real(sqrt((abs(log((r+r.*exp(i.*TH))./(r-r.*exp(i.*TH))))).^2-
(real(log((r+r.*exp(i.*(pi/2)))./(r-r.*exp(i.*(pi/2)))))).^2))-...
    real(sqrt((abs(log((r+rh.*exp(i.*TH))./(r-rh.*exp(i.*TH))))).^2-
(real(log((r+r.*exp(i.*(pi/2)))./(r-r.*exp(i.*(pi/2)))))).^2)))./epsA),...
    deg2rad(90),deg2rad(A))*1E15
```

```
S=(Cdf-Cde)/1630
  CF =  1428.2
  CE =  450.51
  S1 =  0.59979
  A =  170
  Cdf =  947.06
  Cde =  185.39
  S =  0.46728
```

Published with GNU Octave 5.1.0

Appendix: Calibration liquid/capacitance

Pre-conditions

1. Turn on the scale
2. Center the bubble on the scale (scale calibration)
3. Connect the BLE Dongle
4. Plug cap to the power supply
5. Launch the SmartCap software application
6. Connect SmartCap sample with the software application
7. Wait 10 minutes for the warm up of the cap

Protocol

1. Take a new needle and remove the protective peel off paper
2. Degassing of the pen:
    a. Hold pen tip down, snip pen with the finger to get any air bubble(s) visible at piston, if necessary, tap against the pen with the finger/ rotate pen until the smaller air bubbles merge to a bigger one
    b. Set the dose to 12.5 IU
    c. Hold pen tip up, snip pen with the finger to get air bubble below septum, press on the knob of the pen and slowly insert the needle while pressing the knob. Do not screw the needle on.
    d. Hold pen tip down, snip with finger to get air bubble to piston (visible). Check if air bubble is <1mm; if not, repeat steps a-d
    e. Remove the needle from the pen
    f. Remove any liquid on the membrane with a cotton tip.
    g. Tare the balance and record the weight of the pen (placed with the tip up) given by the balance with four digits (after stable measurement) and write it in the excel file.
3. First injection / priming of the pen:
    a. Set the dose to 25 IU
    b. Screw the needle on the pen and keep its outer protective cap for later disposal of the needle
    c. Hold the pen with the needle pointing to a beaker or tissue
    d. Expel the pre-set dose by pressing the Dose Setting Knob until reaching zero. Hold 15 seconds (TIMER!) and release the finger from the dose setting knob. Make sure the knob correctly reached zero.
    e. Rattle the pen by rapidly turning the dose dial a quarter turn forth and back 5 times.
    f. Remove the needle and absorb remaining liquid on the membrane with cotton tip
4. Put the pen inside the cap and place vertical pen tip up for the next step (measurements)
5. Take at least 2 measurements at 0°, 90°, 180° and 270° rotation clockwise (See Annex C). Click on “Add zero” button before each angular step and after the last step.
6. Remove the pen from the cap
7. Dial 62.5 IU
8. Screw the needle on the pen
9. Take the beaker and place the centered pen with needle pointing downwards above the beaker
10. Expel the pre-set dose by pressing the Dose Setting Knob until reaching zero. Hold 15 seconds (TIMER!) and release the finger from the dose setting knob. Make sure the knob correctly reached zero. Ensure remaining drop on the needle gets into the beaker.
11. Rattle the pen by rapidly turning the dose dial a quarter turn forth and back 5 times with the needle above the beaker.
12. Start timer and wait 60 seconds before performing step 15. During this time, perform the following two steps (13-14).
13. Remove the needle and absorb remaining liquid on the membrane with cotton tip
14. Tare the scale and record the weight of the expelled liquid and of the pen (placed with the tip up on the balance) with four digits after the decimal (after stable measurement) and write it in the excel file.
15. Put the pen inside the cap and place vertical pen tip up for the next step (measurements)
16. Take at least 2 measurements at 0°, 90° , 180° and 270° rotation clockwise. Click on “Add zero” button before each angular step and after the last step.
17. Repeat steps 6 to 16 until the centered pen is empty.

18. On the last step (incomplete last injection), record the value displayed in the dose window after the injection.
19. Save the log file

Appendix: Protocol Injection

Pre-conditions

- Turn on the scale
- Center the bubble on the scale (scale calibration)
- Connect the BLE Dongle
- Launch the MB01-LogSoftware on the workstation
- Connect the battery to the smart pen cap
- Connect to the smart pen cap with MB01-LogSoftware
- Pair a new SmartCap sample with the software application simulator, measure without pen and proceed only
- when temperature measurements stabilize (less than 0.5°C per 1min)
- Wait 10 minutes for the warmup of the cap (only required if the cap has been powered off before this experiment)

Protocol

1. Mark angle positions on pen (0°, 90°, 120°, 270°)
2. Prepare the pen for the injection:
   a. Take a new needle
   b. Remove the peel off paper
3. Priming:
   a. Gently turn the dose dialer clockwise until the dose window will show 25 IU
   b. Remove the outer cap and the inner shield of the needle.
   c. Dispose the peel off paper and the inner shield
   d. Keep the outer cap for later disposal of the needle
   e. Hold the pen with the needle pointing upwards
   f. Tap the injector gently so that any air bubble rise to the top
   g. Press the Knob until reaching zero. If you see a tiny drop of fluid proceed to the next step. If not: repeat a, e, f and g until you see a tiny drop of fluid (max. 5 times). If there is no drop visible after the 5th repetition discard the pen and restart the Priming.
   h. Record the number of priming for each pen.
4. Degasing
   a. Hold the pen downwards and check if bigger air bubbles are present. If yes, then proceed with the following steps:
      i. Remove needle
      ii. Turn pen downwards, tap against the pen with the finger until the smaller air bubbles merge to a bigger one
      iii. Dial 12.5 IU
      iv. Hold pen upwards, press on the knob of the pen and insert the needle while pressing the knob
      v. Hold pen upwards and check if air bubble is gone; if not, repeat steps i-iv
   b. Remove the needle from the pen
   c. Remove any liquid on the membrane with a cotton tip.
   d. Weigh the pen and wait 60 seconds
   e. Put the pen inside the cap and take 2 measurements for each angle (0°, 90°, 120°, 270°).
5. Remove the pen
6. Set the dose according to the dosing sequence on table below.
7. Tare the balance to zero.
8. Insert needle
9. Take the beaker and place the pen with needle pointing downwards above the beaker
10. Expel the pre-set dose by pressing the Dose Setting Knob until reaching zero. Hold 10 seconds and release the finger from the dose setting knob. Make sure the knob correctly reached zero. Ensure remaining drop on the needle gets into the beaker.
11. Remove the needle and remove any liquid on the membrane with a cotton tip.

12. Record the weights (dose expelled in the beaker and pen after injection) given by the balance with four digits (after stable measurement).
13. Start timer and wait 60 seconds.
14. Put the pen inside the cap and take 2 measurements for each angle (0°, 90°, 180°, 270°).
15. Repeat steps 5 to 14 for all injections as indicated in table below.
16. Repeat all steps for every new pen.

Vset Phase 1 [IU]

Perform 75 IU injections steps until pen is empty.

Vset Phase 2 [IU]

	Vset Phase 2 [IU]
Pen 1	12.5
	212.5
	237.5
	450
Pen 2	12.5
	212.5
	450
	237.5
Pen 3	237.5
	212.5
	12.5
	450
Pen 4	237.5
	450
	12.5
	12.5
Pen 5	450
	12.5
	12.5
	212.5
	237.5
Pen 6	450
	12.5
	237.5
	12.5

Estimated test duration: 240 minutes.